# Boundary Conditions for Techno-Economic Feasibility Improvement on Large-Scale SOE by Reversibility

M. Middelbos

Master of Science Thesis
Delft University of Technology

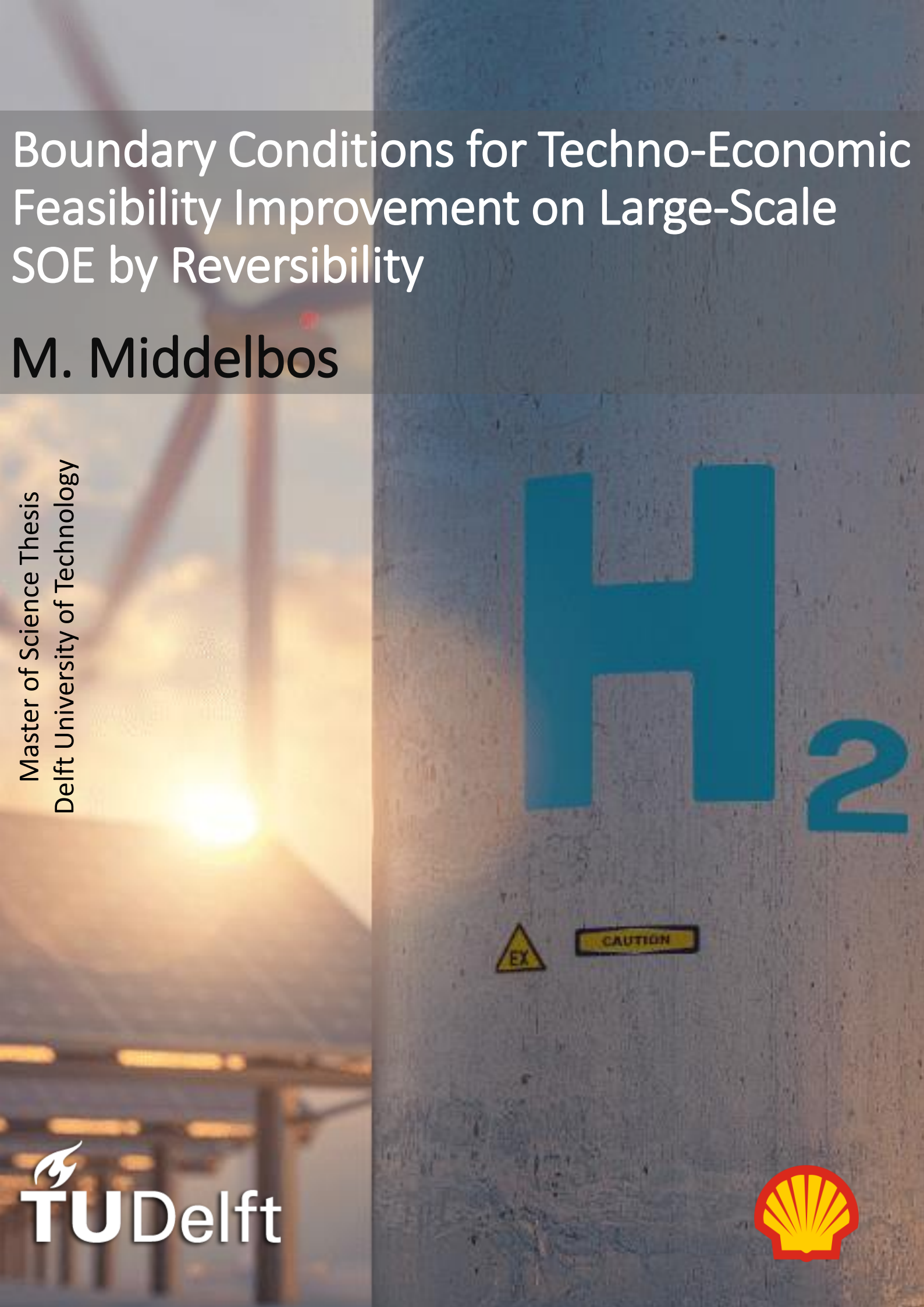


TU Delft

# Boundary Conditions for Techno-Economic Feasibility Improvement on Large-Scale SOE by Reversibility

## Master Thesis

by

M. Middelbos

to obtain the degree of Master of Science
at the Delft University of Technology,
to be defended publicly on Tuesday July 24, 2023 at 10:30 AM.


| | | |
|---|---|---|
| Student number: | 4577450 | |
| Thesis committee : | Prof. dr. ir. E. L. V. Goetheer | TU Delft (3mE) |
| | Dr. Ir. L. van Biert | TU Delft (3mE) |
| | Dr. Ir. M. Pérez-Fortes | TU Delft (TPM) |
| | Dr. Ir. S. Santhanam | Shell (Green Hydrogen) |
| Daily supervision | Ir. E. Roy | Shell (Green Hydrogen) |
| | Ir. J. C. B. Brenkman | Shell (Green Hydrogen) |

Faculty of Electrical Engineering, Mathematics and Computer Science (EEMC)
Delft University of Technology




TU Delft

# Nomenclature

## List of acronyms

| | |
|---|---|
| AE | Alkaline Electrolyser |
| aFFR | active Frequency Restoration Reserve |
| ATR | Auto-Thermal Reforming |
| BoP | Balance of Plant |
| CAPEX | Capital Expenditures |
| CE | Co-Electolysis |
| CM | Contribution Margin |
| CoGS | Costs of Goods Sold |
| CPOx | Catalytic Partial Oxidation |
| CS | Cold-Standby |
| DSU | De-sulfurisation Unit |
| E&C | Energy and Capacity Procurement |
| EC | Electrolysis |
| EHV | Extra-High-Voltage |
| EOL | End-Of-Lifetime |
| FC | Fuel Cell |
| FCR | Frequency Containment Reserve |
| G2P | Gas-to-Power |
| HS | Hot-Standby |
| HV | High-Voltage |
| KPI | Key Performance Indicator |
| LCOE | Levelised Cost of Energy |
| LCOH | Levelised Costs of Hydrogen |
| LCOSNG | Levelised costs of Synthetic Natural Gas |
| LCOX | Levelised Costs of (chemical product) X |
| LP | Low Pressure |
| MCP | Market Clearing Price |
| MCV | Market Clearing Volume |
| mFRR | manual Frequency Restoration Reserve |

OPEX Operational Expenditures

P2G Power-to-Gas

P2H Power-to-Hydrogen

P2X Power-to-X

PPA Power Purchase Agreement

PSA Pressure Swing Absorption

RES Renewable Energy Sources

rSOC reversible Solid Oxide Cell

rSOE reversible-Solid Oxide Electrolysis

rSOE (X) reversible Solid Oxide Electrolysis with fuel cell operation based on secondary feedstock X

SMR Steam Methane Reforming

SNG Synthetic Natural Gas

SOE Solid Oxide Electrolysis

SOEC Solid Oxide Electrolyser

SOFC Solid Oxide Fuel Cell

TEA Techno-Economic Analysis

TEF Techno-Economic Feasibility

TEP Techno-Economic Performance

TRL Technology Readiness Level

TSA Temperature Swing Absorber

TSO Transmission System Operator

X2P X-to-Power

# Acknowledgements

Over the past 8 months, various persons have contributed to this Master Thesis. First of all, I want to thank all the industry experts that I consulted for the interesting discussions on their expertise connected to the project. In addition, I want to thank some people in particular.

To start with, I would like to express my gratitude to Earl Goetheer and Lindert van Biert from TU Delft for their guidance throughout my thesis journey. Earl's enthusiasm, drive, and expertise have been key in shaping the direction of my research. His insightful feedback and constant support have motivated me and elevated the quality of my thesis. Similarly, Linderts' mentorship and consistent availability have been very valuable. I am truly grateful for their dedication and contributions.

Furthermore, I want to extend my appreciation to Mar Perez-Lopez for her role as a committee member. I am grateful for her interest in my research and for taking the time to assess the work.

I would also like to acknowledge Srikanth Santhanam, Esha Roy, and Jeroen Brenkman for their roles as supervisors from the Green Hydrogen team at Shell. I would like to thank Esha and Jeroen for their daily support, expertise and for connecting me to various industry experts. To Srikanth, I would like to express my gratitude for introducing me to this thesis subject, teaching me about rSOE, and providing high-level project guidance.

Lastly, I want to express my contentment with the choice for the Masters program Sustainable Energy Technology. This program has proven to be an excellent background for performing an integrated system study, as is done in this thesis. On top of that, I can honestly say that I enjoyed every bit of the program.

M.Middelbos
Delft University of Technology
July 2023

# Summary

The necessity for technology that enables affordable, scalable and transportable renewable energy storage is widely recognised in public, scientific and industrial communities. Power to Hydrogen (P2H) technologies possess the potential to fill this need. Solid Oxide Electrolysis (SOE) is a promising P2H technology that offers superior energy conversion efficiency compared to competing alternatives. However, further development and improved economic attractiveness of the technology are required, as SOE technology remains immature and costly. To overcome these challenges, reversibility, which is the ability of the electrolyser to operate as a fuel cell, could unlock economic potential and advance the development of the technology.

To assess this potential, the primary objective of this study was to determine whether reversible operation can improve the techno-economic feasibility of a large-scale open-system SOE and, if so, under what conditions. To reach this goal, a use-case was modelled, simulating reversible Solid Oxide Electrolysis (rSOE) operation in a macro system with an hourly fluctuating wind profile and power price. To assess the effect of reversibility, four plant configurations were compared: an non-reversible SOE configuration (reference case), an rSOE ($H_2$) configuration with fuel cell operation based on hydrogen, an rSOE (NG) configuration with fuel cell operation based on natural gas, and an Alkaline Electrolysis (AE) configuration (State-of-the-art case). For each of these configurations, the techno-economic feasibility was determined using three key performance indicators under baseline conditions. The relative feasibility results were analysed under changing parameters in a sensitivity analysis and for three sets of scenarios. In addition, a regret analysis was performed to deeper understand the boundary conditions of one of the most crucial parameters, the power price. Finally, by employing these analysis methods, valuable insights were gained regarding the feasibility-enhancing potential of reversibility and the specific conditions under which this improvement can be observed.

First, the results point out that reversibility can mitigate risks of regular large-scale SOE, by providing a hedge against uncertain parameters. In rSOE (Hydrogen), reversibility acts as a hedge against high power prices, low hydrogen prices, power profile inconsistency, and power price volatility, compared to regular SOE. Furthermore, the rSOE (Natural Gas) configuration exhibits similar hedges, except for the low hydrogen price hedge.

Furthermore, reversibility can significantly improve absolute techno-economic feasibility under certain internal and external boundary conditions. External conditions relate to parameters outside the system and outside the power of design, whereas internal conditions concern parameters within the power of design. The crucial external condition for feasibility improvement through reversibility lies in the requirements for a minimum ratio between the average power price and switch-price, defined as the "break-even choice ratio". This minimum ratio for hydrogen based reversibility lies at 0.66, whereas the value for Natural Gas based reversibility lies at 1.16. Crucial internal conditions entail either choosing natural gas as a secondary feedstock or meeting balancing market requirements, implying ramping to bid capacity within 10 minutes and having a response time of 30 seconds to 5 minutes, and 5 to 60 minutes for two different balancing sub-markets, respectively.

The modelled use-case, although unoptimised, proved significant potential for feasibility improvement. From a modelling perspective, the feasibility conditions established in this research can serve as a starting point for conducting a comprehensive application study, allowing to identify the most suitable technical and business applications for reversibility. Moreover, considering the techno-economic potential of reversibility, experimental research is recommended to gather knowledge on the feasibility of operational strategies and effect of reversibility on degradation.

# Contents

# 1 Introduction

For the first time in history, the Netherlands' Energy Security of Supply Standard will be exceeded in 2030, as was reported by Dutch TSO Tennet [91]. This indicates that the consequences of an energy mix with a growing installed capacity of weather-dependent, intermittent, renewable energy sources (RES) have become tangible.

These consequences are expected to become increasingly prominent as growing demand and decreasing prices for these RES are observed [61]. Further installed capacity growth is expected, resulting from a more urgent demand caused by climate targets, combined with the growing profitability of such systems [36].

An additional challenge arises from onshore RES saturation. As the Netherlands is running out of room for onshore RES, an increasing electrical supply is expected from offshore locations. According to the offshore wind strategy, the goal is to have a total installed capacity of 38-72 GW by 2050 [78]. This shall inevitably go hand in hand with electricity delivery challenges to locations further inland, for example, due to a lack of grid capacity.

To fight these challenges, scalable and transportable energy storage is necessary. Power to Gas (P2G) provides a scalable way to convert renewable electrical energy into renewable chemical energy. An example is Power to Hydrogen, which has three main applications, each solving a part of the challenge described above. Firstly, hydrogen can serve as a renewable alternative to the currently utilised fossil feedstock. Secondly, it can act as a sustainable substitute for existing fossil fuels. Lastly, it can facilitate the storage of electricity. Chemical energy storage solutions such as power to hydrogen are promising, as they can solve challenges by providing a means for long-term and large-scale energy storage, thus enabling a more stable and reliable integration of renewable energy sources into the grid. However, the well-known downsides of P2G technology are high expenses and low round-trip efficiencies [14, 35].

Solid Oxide Electrolysis (SOE) is a potent P2G technology that brings solutions to the interface of the chemical and electrical market. It uses solid oxide cells to convert electrical energy into chemical energy, like hydrogen, and vice versa. It does so by using ceramic electrolytes and high temperatures (600-1000 $^{\circ}C$)[56]. Compared to traditional electrolysis methods such as alkaline and proton exchange membrane (PEM) electrolysis, SOE potentially has superior energy conversion efficiencies [63]. Moreover, SOE technology exhibits efficient reversible operation, enabling its utilisation for both electrolysis and fuel cell applications. Consequently, the interest of this study lies in the reversibility of the SOE.

## 1.1. Hypothesis and Industrial relevance

Reversible operation of the SOE plant can generate an additional revenue stream, which is desired considering the high costs of the technology. Resulting from the challenges in the previous paragraph, the demand for flexibility in generation and consumption will increase [91]. This increased demand probably translates into an increasing reward for this flexible consumption and generation. The reward can be either passive by a more volatile electricity price or active, for example, through balancing services compensation or power purchase agreements. Reversibility answers this demand and reward for flexibility. The potential additional revenue stream from reversibility could improve the feasibility of large-scale SOE plants. Industry parties that scale up SOE technology are keen to reduce the risk of their projects. Reversibility could be an add-on that de-risks the technology and thereby accelerates its large-scale implementation. The hypothesis is that certain realistic conditions exist under which the benefits of reversibility balance out against the additional costs.

## 1.2. Research Gaps

A preparatory literature study was performed, bringing forward multiple research gaps, of which a selection is listed in the yellow text box. To get to the gaps, first a broad analysis based on the applications and the system design choices was performed, then literature was analysed on the modelling approaches, and last, methods to perform techno-economic analysis of rSOE systems were reviewed. The pre-described analysis was based on the literature in Table A.1. The research gaps are further substantiated on relevance and validity in the coming paragraphs.

**Research gaps unveiled by the Literature study**

- Techno-economic research to large-scale steam rSOE in open-system application
- Dynamic operational schedule, based on hourly fluctuating power prices and profile
- Comparison of hydrogen and natural gas as secondary feedstock for steam rSOE
- Determining the boundary conditions under which reversibility improves the feasibility of regular SOE

The first identified gap is the conduction of techno-economic analysis of open-system rSOE applications. Six of the applications listed in Table A.1 are partially open-system applications, which means they supply at least a portion of their chemical product from the SOEC mode to the market [16, 98, 74, 44, 13, 12]. Three of these open-system applications have performed an economic analysis [98, 44, 74], of which only Zhang et al. [98] models an open-system application with interaction with the chemical market. However, the focus of Zhang et al. [98] lies on comparing different primary feedstock types, which leaves a gap to put the focus somewhere else. The following paragraphs include more novelty to Zhang et al. [98].

Secondly, to assess the economic feasibility of an rSOE system, a dynamic operational schedule is required that considers various dynamic parameters. Buffo et al. [12] performed a technical, non-economic study, which bases its operational schedule on a fluctuating power profile and electricity buy price. The study examines a closed-system that aims to satisfy an urban district's hydrogen and electricity demand. There is no focus on power or chemical trade with the market. To the best of the authors' knowledge and indicated by Figure A.11, this leaves a research gap in modelling open-system rSOE applications. Namely, to model the rSOE with an operational schedule influenced by both a dynamic power profile and dynamic power sales prices.

Thirdly, a research gap exists in exploring using a different secondary feedstock than the electrolysis product. This would imply producing hydrogen through electrolysis while utilising natural gas as secondary feedstock in fuel cell operation. A rough estimation in the literature review revealed the dependency of the levelised cost of hydrogen (LCOH) on the fuel cell capacity factor, fuel price, and additional capital costs of a natural gas-based plant. An analysis comparing these fuels can determine which one is more advantageous. None of the studies included in the literature review address the differentiation between electrolysis product and fuel cell feedstock, indicating a research gap in this area.

Lastly, there is a gap in focusing on the comparison of non-reversible SOE with reversible SOE. Most studies in Table A.1 aim to demonstrate the performance of rSOE in a specific application or compare it with other storage technologies in closed-system applications. Exploring the technical and economic conditions under which rSOE offers improved feasibility over conventional SOE represents a novel area in rSOE-related research.

## 1.3. Research Objective

The research interest of this study lies in the conditions under which reversibility can bring feasibility improvement, as described in the previous paragraph. The interest of the study is translated into a research question and a set of sub-questions to approach the research question methodically.
"Can reversible operation[1] improve[3] the techno-economic feasibility[2] of a large-scale open-system SOE, and if so, under what conditions[4,5]?"

1. What and how large are the technical and economic implications of making SOE reversible?
2. What are the key performance indicators (KPIs) that measure techno-economic feasibility of large-scale open-system reversible SOE?
3. Does reversible operation, either based on hydrogen or natural gas, show improved techno-economic feasibility compared to SOE, in a baseline scenario?
4. Under what scenarios does reversibility improve techno-economic feasibility compared to SOE?
5. Under what parameter deviations does reversibility improve techno-economic feasibility compared to SOE?

## 1.4. Methodology and Scope

To answer the questions a use-case was modelled to simulate an rSOE plant in a macro system. The macro system components are a wind farm, wholesale day-ahead power market, steam source and hydrogen backbone. The use-case location is the Port of Rotterdam, as several factors are believed to be advantageous for rSOE deployment, such as proximity to offshore wind, grid balancing needs, hydrogen customers, hydrogen infrastructure and steam source availability. The focus lies on an open-system, hydrogen-producing rSOE system, built for operation in 2035. Open-system is defined as having a net hydrogen flux from the system to the chemical market.

The model simulates hourly operation and performance of the rSOE plant in the macro system. A scope choice is that the plant is a hydrogen-producing facility, implying that if there is a possibility, the plant produces hydrogen in electrolysis (EC) mode. In the absence of sufficient wind, fuel cell (FC) operation is considered by comparing the hourly day-ahead power price to a switch-price, based on hydrogen and standby cost. If the electricity price is higher than the switch-price, the fuel cell operates. If that is not the case, it goes into hot standby (HS) mode.

Using the pre-described model, the lifetime economic performance of four configurations is compared based on three KPIs. The selected KPIs, introduced in section 3.2, result from the literature study. The preparatory analyses for the selection of the KPIs is added in section A.5. The four compared cases consist of a non-reversible SOE configuration (reference case), an rSOE configuration with FC-mode based on hydrogen, an rSOE configuration with FC-mode based on natural gas, and an Alkaline Electrolysis (AE) configuration (State-of-the-art case). The performance of the four cases is compared under three sets of scenarios in the scenario analysis. An in-depth analysis on power price dependency is performed using regret analysis [80, 6, 47]. Lastly, a sensitivity analysis is performed to quantify the sensitivity of the KPIs to parameter changes.

## 1.5. Structure

The study is structured as follows. The required theoretical and practical background on the subject is discussed in chapter 2, already touching on the first sub-question. As explained in the previous paragraph, a model was built to simulate rSOE operation and measure system performance under various scenarios and parameters. Both the model and the analysis methodology are described in chapter 3. To serve as a background for answering the research question, the results are presented and discussed in chapter 4. Finally, the conclusions on the research question and recommendations for follow-up research are provided in chapter 5.

# 2
# Background

This chapter provides theoretical and practical background information concerning rSOE. Firstly, the potential of rSOE (reversible solid oxide electrolysis) is explored in section 2.1. Next, in section 2.2, the fundamental principles of rSOE are examined to establish a solid knowledge base. Regarding practical background, section 2.3 delves into various system definitions, offering clarity and context for the Methodology. Furthermore, this chapter covers the technical implications of reversibility in section 2.4, as well as its economic implications in section 2.5, which addresses the first sub-question. Lastly, section 2.6 offers background information on several macro system components required later in the study.

## 2.1. Potential of rSOE

As mentioned in the introduction, producing chemicals from electricity is a promising way to deal with the intermittency of renewable energy sources by providing a scalable and transportable storage solution. The chemical produced to store energy can be used as a fuel, feedstock, or to generate electricity again. The conversion process to produce chemicals from electricity is abbreviated, Power-to-X (P2X) or Power-to-Gas (P2G). This reversed process is called X-to-Power (X2P) or Gas-to-Power (G2P). Green hydrogen is produced via electrolysis, a P2X technology, and can be turned into electricity using a fuel cell, X2P. Both electrolyser and fuel cell technology are based on cells containing a certain electrolyte, most commonly proton exchange membrane (PEM) and Alkaline electrolytes.

Less mature than PEM and Alkaline Electrolysis (AE) is Solid Oxide Electrolysis (SOE). However, the technology can offer superior energy conversion efficiencies in electrolysis and fuel cell applications. SOE uses ceramic electrolytes and produces hydrogen at high temperatures (600-1000 °C) [56]. This high-temperature operation brings along advantages as well as disadvantages. In Table 2.1, results of a comparison between the different electrolyte technologies are listed.

The main advantage of SOE compared to PEM and AE is the low specific energy consumption of SOE. On the other hand, an important disadvantage is that SOE is less mature and more costly. To mitigate these disadvantages reversibility can play a role. Due to two identical electrodes, high efficiency, and oxygen conductivity SOE has superior reversible functionalities compared to AE and PEM. Reversibility can contribute to de-risk SOE technology compared to the state-of-the-art, by increasing the capacity factor of the SOE, which is defined as the ratio between actual production over a given period and the theoretical maximum production in that same period. A large-scale electrolyser powered completely by renewable assets, without electricity storage, follows the capacity factor of its connected asset [77]. This means that an electrolyser would stand idle or at partial load for a significant time of the year, as solar and wind energy capacity factors are usually below respectively, 35% and 60%. Thanks to its reversibility, an rSOE can produce hydrogen in electrolysis (EC) mode when electricity is available but can also operate in fuel cell (FC) mode, when it is not. This way, the capacity factor of such an electrolyser can increase significantly. Additionally, standby-costs are reduced by operating in standby-hours. The combined reversibility and low specific energy consumption of rSOE, could strongly lower hydrogen costs, which could further improve feasibility compared to PEM and AE.

Table 2.1: Comparison of electrolyser and fuel cell performance of systems based on three different electrolytes: Alkaline, PEM and Solid oxide

| Electrolyte | Alkaline | PEM | Solid oxide |
|---|---|---|---|
| Operating temperature | <100 °C [35, 14] | <140 °C [35, 14] | 600-1000 °C [35, 14] |
| Electrolysis efficiency LHV | 43-67% [35, 14] | 40-67% [35, 14] | 63-82% [35, 14] |
| Specific energy consumption [63] | 55-65kWh/kg [$H_2$] | 55-65 kWh/kg [$H_2$] | 37-42 kWh/kg [$H_2$] [Ex steam gen]<br>45-50 kWh/kg [$H_2$] [Inc steam gen] |
| Fuel cell efficiency | 45-60% [35] | 45-50% [35] | 35-63% [35, 65] |
| Start-up time | Cold: 15 min [35]<br>Warm: 1-5min [35, 14] | Cold : <15min [35, 14]<br>Warm: seconds [35, 14] | Cold: hours [35]<br>From hot standby: minutes [14] |
| Dynamics and flexibility | Min partial load 10-40% [35] | Suitable for partial load and variable load [35] | Min partial load 20-40% [35, 83] |
| Main advantages | Maturity ; Reliability ; Safety ; Lifetime | High purity hydrogen ; Preferred for fuel cell operation | Superior efficiency ; Waste heat can boost efficiency ; Flexible fuel choice ; Possibility of reversible operation |
| Main challenges | Inferior dynamic response to PEM ; Corrosive electrolyte | Expensive membranes and catalyst materials ; Less scalable than AE | Immaturity ; High degradation in SOEC ; Higher temperature operation brings challenging thermal management |
| System costs | €700-1500 [35] ; €1000-1200 [82] €800-1500 [14] kW | €800-€2300 [35] ; €1860-2320 [82] €1400-2100[14] | >€2000 kW [14] ; With a potential reduction to €760 kW [82] |

## 2.2. Fundamentals of rSOE

Basic knowledge on the reversible solid oxide cell (rSOC) is required as a basis for the rest of the thesis and is discussed in this section. A more elaborate background is displayed in Appendix A.1.1.

### 2.2.1. Cell Basics

A solid oxide cell (SOC) consists of three solid layers, as indicated in Figure 2.1: two porous electrodes and a single, dense electrolyte. The electrolyte is typically ceramic, yttria-stabilised zirconia, YSZ. The two porous electrodes are typically named after their reactant inlet or product outlet, as the terms cathode and anode are interchanged depending on the mode of operation. In this study, the electrodes are referred to as the fuel and oxygen electrodes. Other terminology may be used in the literature. As seen in Figure 2.1, electrolysis of steam and carbondioxide is possible in SOC. As it is the focus of this thesis, steam electrolysis is taken as an example.
The half-reactions taking place in electrolysis EC and FC mode are displayed respectively on the top and bottom of Figure 2.1. In EC, the oxygen ion passes through the electrolyte from the cathode side (fuel or hydrogen electrode) to the anode (oxygen electrode). An externally provided electrical current drives the reaction. In order to become sufficiently ion conductive, the solid electrolyte separating the hydrogen and oxygen sides needs to be operated at a high temperature, 600-1000 $°C$ [14]. In reversed, FC mode, $H_2$ is oxidised along the same dynamics.

### 2.2.2. Thermodynamics

The reduced specific energy consumption is the main advantage of high-temperature electrolysis and rests on the thermodynamic behavior depicted in Figure 2.2. For an electrolysis reaction to take place, the Gibbs free energy $\Delta G$ has to be supplied in the form of electricity. Additionally, an amount of energy in the form of heat ($T\Delta S$) has to be supplied because electrolysis is an endothermic process, meaning it consumes energy. Therefore, the total energy demand for electrolysis is the sum of the Gibbs free energy and the heat demand, called the enthalpy ($\Delta H$). During low-temperature electrolysis the $T\Delta S$ is usually supplied by electrical heat. At 100°C a discontinuity is observed, leading to a drop in enthalpy, $\Delta H$. At higher temperatures, one can observe that the enthalpy remains fairly constant for both $CO_2$

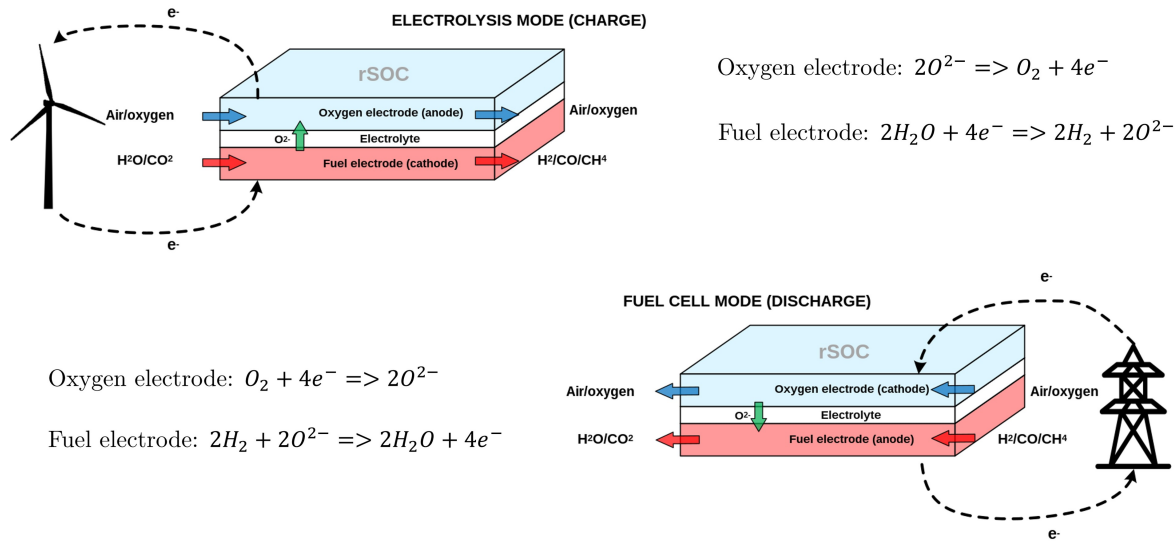


Figure 2.1: A schematic of an SOC in electrolysis mode and fuel cell mode. Figure based on Macrofici [52].

and $H_2O$ electrolysis, but that the electrical demand ($\Delta G$) shows a decrease and the heat demand ($T\Delta S$) an increase. This significantly reduces the required electrical demand and thus the specific energy consumption for high-temperature electrolysis, typically operating in the range of 600-1000°C.

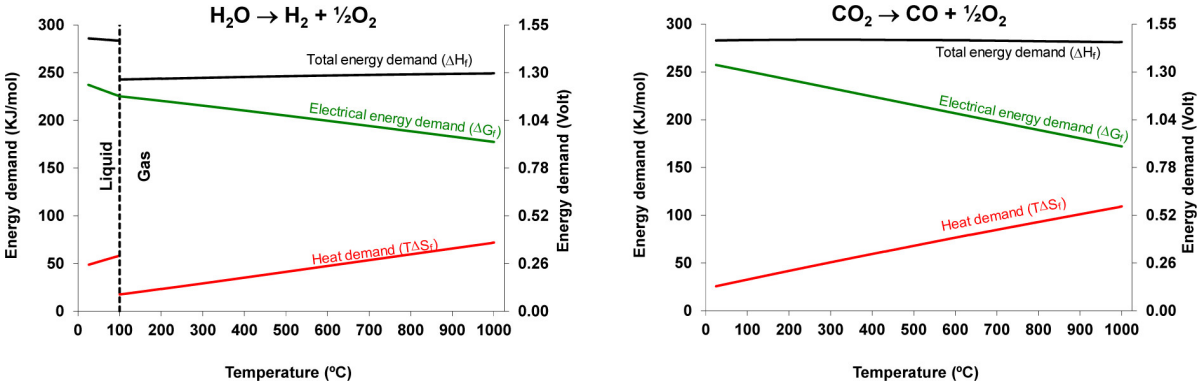


Figure 2.2: Thermodynamic properties of $H_2O$ (left) and $CO_2$ (right) electrolysis at atmospheric pressure [24]

### 2.2.3. Cell Operation

The polarisation curve (Figure 2.3) shows the relation between the applied cell voltage and the current density. The reversible cell voltage or open circuit voltage is the applied voltage with zero net fuel production. An over-potential results in electrolysis, while an under-potential leads to exothermic fuel cell reaction. Electrolysis is endothermic when the potential is under the thermoneutral voltage and exothermic when it is above. Operating at the thermoneutral voltage is desired, as no cooling or heating is required. The trade-off having higher production rates, is that higher losses occur, leading to increased specific energy consumption. These losses occurring at higher voltage explain the shape of the polarisation curve. Keeping in mind the macro system scope of this study, these losses will not be handled in further detail.

Taking into account the over- and under-potential in EC and FC mode, the reference voltage of the electrolyser should be about double that of the fuel cell in the rSOC [19]. This explains that the EC capacity is minimal, two times as large as the FC capacity. In practice, EC capacity is three to five times larger than FC capacity, due to additional losses, apart from those indicated by the polarisation curve [68, 55, 59, 66].

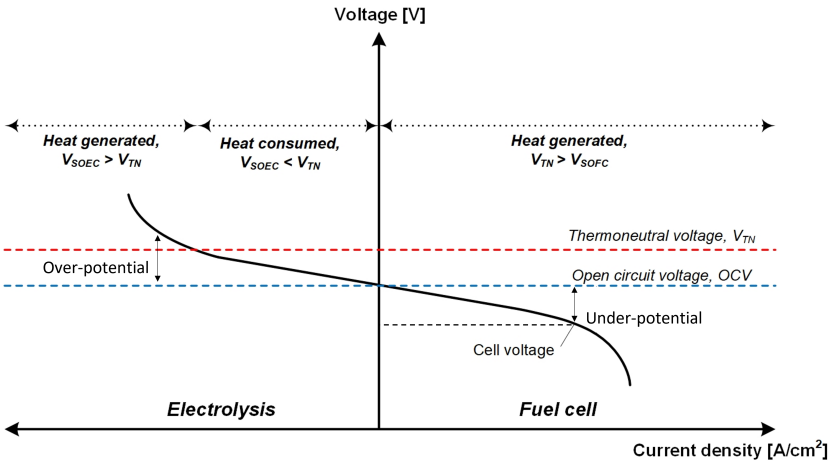


Figure 2.3: The polarisation curve of an rSOC, showing the relation between applied cell voltage and current density [53]

### 2.2.4. Degradation

Over time, the performance of the electrochemical cell degrades. A differentiation can be made between degradation in fuel cell and electrolysis mode. Exact behavior needs further research, as studies make opposing claims. Namely, Hutty et al. [35] remarks that degradation is found to be greatest in electrolysis mode. On the other hand, Nuggehalli Sampathkumar et al. [62] reports degradation to be higher in FC than in EC, respectively 1.64% and 0.65% voltage degradation per thousand hours. A real-life experiment in Salzgitter showed a voltage degradation of 0.8% per thousand hours in EC mode [68]. The study also indicates that degradation rates under hot standby (HS) are quite similar to operation. Lastly, a study by [97] even showed negative degradation in one of their stacks by reversing operation. Degradation measurements seem to be very dependent on the measuring method, as also pointed out by [56]. As results are not unanimous, linear voltage degradation shall be assumed in the Methodology.

## 2.3. System Definitions

Having covered the fundamentals of the solid oxide cell, this chapter zooms out to the broader scope of this research. This broad scope includes looking at rSOE performance in a broad system influenced by a chemical and power system. To help keep track, a few system definitions are proposed: Macro system, Balance of Plant (BoP), Balance of System (BoS), Module, Stack and Cell. Also, the definitions of an open- and closed-system application are addressed.

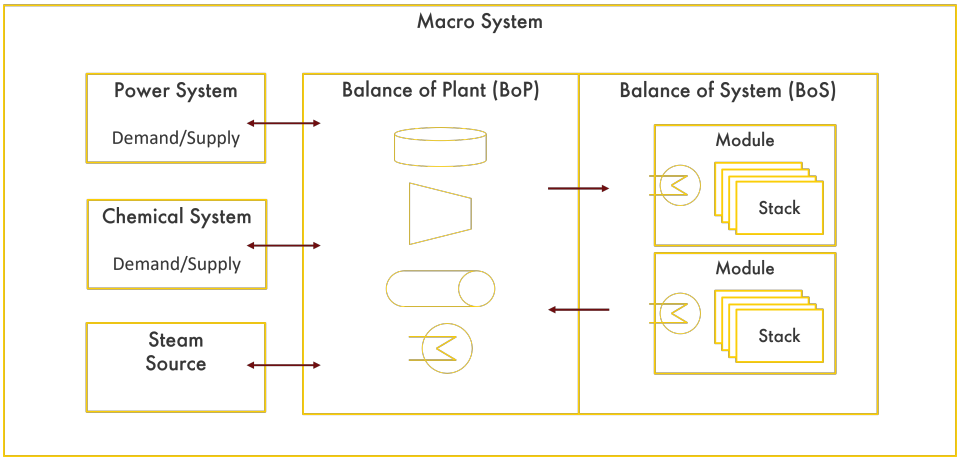


Figure 2.4: Schematic to visualise the system component definitions used along the thesis

A schematic representation of the system component definitions can be seen in section 2.3. The electrochemical reactions in EC and FC mode occur in the cell, as discussed in subsection 2.2.1.

Several cells stacked together are called a stack. Various stacks packed together, including auxiliary components inside a thermally insulated hot-box are defined as a Module. Multiple modules make up the BoS. The BoP serves as a conversion and transportation bridge between the macro system components and the BoS. Components included in the BoP are for example, storage, compression, piping, electronics and heatexchangers.

rSOE can be used in various applications. A distinction between open and closed applications can be made, as schematically represented by Figure 2.5. In this study, a closed system is defined as a system in which the product produced in electrolysis mode is utilised internally. Such a closed system is denoted Power-2-X-2-Power (P2X2P), the chemical X is used as a storage medium for electricity. An open-system application is defined as a system in which the product produced in EC mode interacts with the chemical market. In such a P2X(2P) application, a part or all of the chemical product X is transferred out of the system (P2X), in addition, externally imported or partly internally stored chemical X is converted to electricity (X2P). As the number of chemicals produced and used is not necessarily equal in an open-system, this is denoted at P2X(2P). Also, the chemical product does not have to be similar to the chemical fuel in an open-system.

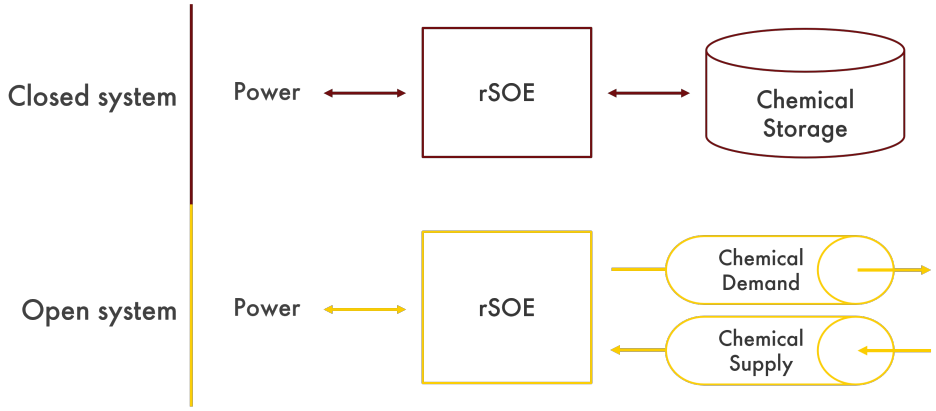


Figure 2.5: A conceptual schematic displaying the definition of an open- and closed-system

## 2.4. Technical Implications of Reversibility

The main interest of this study is based on reversibility. In order to answer the research question, several subquestions were defined in chapter 1. One of which reads: "What and how large are the technical and economic implications of making an SOE reversible?". This section addresses the technical implications of reversibility.

### 2.4.1. Modes of Operation

Four modes operation exist in reversible SOE: EC, FC, hot-standby (HS), cold-standby (CS). In EC, hydrogen is produced, while in FC electricity is produced. The system goes in standby if neither the requirements for EC mode nore FC mode are met. CS is generally not desired, as heating up the system to the high operating temperature costs a lot of time and energy. From HS, the system can instantly ramp up to an EC or an FC operating point. As the hot-box is insulated, HS only requires a fraction of the CS start-up energy to keep the system at operating temperature. During HS, cell chambers are filled with a nitrogen-based forming gas to protect the electrodes.

### 2.4.2. Differences in SOEC and SOFC System Built-up

A system component comparison between the steam-based SOEC process and the hydrogen-based SOFC process leads to the conclusion that the BoP and BoS show many resemblances [64, 93, 79]. In the literature review, the SOEC and SOFC process is described on a high level, from a chemical, thermal and electrical perspective subsection A.2.1. The findings are summarised below, and if desired the two process flow diagrams depicted in Figure 3.6 and Figure B.5 can be consulted as support.

As the electrolysis system inserts hydrogen into the macro system at a certain pressure, a compressor is required, whereas this is not the case in SOFC operation. Furthermore, the TSA used in EC mode is

not necessary in FC mode. Additionally, compared to SOEC, in SOFC an extra hydrogen recirculation loop is added from the water knock out to the secondary feedstock input.

As was described in subsection A.1.3 only 1/3 to 1/5 of the nominal capacity of the SOEC is produced in SOFC mode. Smaller but more inverters would be required for a reversible system, as operating high-capacity inverters at low operating points negatively influence efficiency. The electronics should be able to convert AC to DC and visa versa.

### 2.4.3. Additional Differences in Natural Gas-based SOFC

The use of natural gas as secondary feedstock comes with some additional components compared to hydrogen-based SOFC, as described in the last paragraph of subsection A.2.1. Compared to a hydrogen-based SOFC, natural gas-based SOFC requires an additional pre-reformer, De-sulfurisation Unit (DSU) and Afterburner [8]. The pre-reformer converts a part of the natural gas to syngas, for which three technologies are considered: Steam methane reforming (SMR), Catalytic partial oxidation (CPOx) and Auto-thermal reforming (ATR). These three are discussed in more detail in subsection A.2.3. The off-gas that remains after FC operation is usually used for heat production in an afterburner in case of SMR, or purified with a Pressure Swing Absorption (PSA) unit in case of CPOx and ATR.

When transitioning from FC to EC mode, the initial batch of hydrogen produced may be contaminated with FC feedstock and product gases. To address this issue, three options can be considered. The first option is to discard the initial batch of hydrogen altogether. The second option involves purifying the hydrogen stream, which can be achieved, for instance, by utilising a PSA process. The last option is to flush the system prior to EC operation, which introduces an additional flushing time to the overall switching process. This flushing time can vary, depending on the required purity of the hydrogen in EC mode.

## 2.5. Economic Implications of Reversibility

As explained in section 2.4 certain technical additions are required for the system to be reversible. These additions bring additional CAPEX requirements. This section outlines estimations (2.5.1) and projections (2.5.2) for these requirements for four technologies: SOE, rSOE ($H_2$), rSOE (NG) and AE. These four technologies are compared in the remainder of this study as explained in the Methodology.

### 2.5.1. CAPEX Estimations

Based on literature and industry experts, the CAPEX estimations as presented in Table 2.2 are constructed. A distinction is made between direct and service CAPEX. Direct CAPEX, is directly related to the core assets or physical infrastructure of rSOE. As definitions differ across literature [38, 46, 37], for this report, service CAPEX included all CAPEX notwithstanding the direct CAPEX. These costs are necessary for the successful execution and implementation of the project. Among the service CAPEX is engineering and design costs, permitting and regulatory compliance costs, project management costs, land acquisition costs and construction/installation costs apart from the direct asset.

Table 2.2: CAPEX estimate and increment for the four studied configurations. Underlined cells contain the assumptions that make up the table

| Type | Unit | Current price | Direct CAPEX | Service CAPEX |
|---|---|---|---|---|
| SOE | [€/ kW] | 3000 | 1375 | 1625 |
| rSOE ($H_2$) increase | | | +5 % | - |
| rSOE ($H_2$) | [€/ kW] | 3070 | 1445 | 1625 |
| rSOE (NG) increase | | | +10 % | - |
| rSOE (NG) | [€/ kW] | 3210 | 1590 | 1625 |
| AE | [€/ kW] | 2500 | 875 | 1625 |

For AE projects, the current direct costs are assumed 800-1000 euro/kW [37, 38, 46, 4]. According to these sources, the expected services costs are around 800 euros/kW, making up 40-50 % of total installed CAPEX costs. However, experience with current large-scale AE projects indicate that these costs lie significantly higher, at around 60-70% of the total system CAPEX [39, 4]. Therefore, the AE

total installed current CAPEX is estimated to be 2500 euros/kW, as shown by the underscored value in Table 2.2, which consists of 65% service CAPEX and 35% direct CAPEX.

SOE is estimated at a total installed system cost of 3000 euro/kW [79]. This total installed system cost can be divided into direct and service CAPEX. The services costs are expected to equal those of EC, around 1625 euro/kw. Resulting, current direct costs for SOE are taken to be 1375 euro/kW.

With respect to the SOE plant, the reversible SOE plant on hydrogen is expected to have a small CAPEX increase due to the electrical components required to transform and transmit produced electricity. For example, a hybrid inverter is required for AC/DC and DC/AC conversion. The power electronics, control and instrumentation components roughly contribute 30-40 % of the direct CAPEX of both SOEC and SOFC systems [9] [5]. Therefore this CAPEX increase is estimated to be 5% of the direct CAPEX.

With respect to rSOE ($H_2$), rSOE (NG) requires a reformer technology: CPOx, SMR, ATR and additionally an afterburner or PSA, as explained in subsection 2.4.3. For this research, the SMR in combination with afterburner was assumed for the rSOE (NG) scenario, which contributes roughly 5-10 % to the total system CAPEX for SOFC [5, 81]. Based on these studies, the direct CAPEX increase compared to rSOE on hydrogen is assumed to be 10%.

At stack End Of Life (EOL), replacement of the stacks is required. The stacks are estimated to contribute roughly 30% to the direct CAPEX [9, 40]. For AE systems, this accounts for only 10% of the total system CAPEX.

### 2.5.2. CAPEX Projections

The CAPEX of the pre-mentioned technologies is to develop in the future. Direct and serivce CAPEX projections for a future conservative and optimistic scenario are outlined in Table 2.3. The reasoning follows below.

Table 2.3: CAPEX projections estimations for 2035 for the two future scenarios

| Type | Conservative Direct | Conservative Service | Optimistic Direct | Optimistic Service |
|---|---|---|---|---|
| SOE | -30% | -40% | -60% | -65% |
| rSOE ($H_2$) | -30% | -40% | -60% | -65% |
| rSOE (NG) | -30% | -40% | -60% | -65% |
| AE | -20% | -40% | -40% | -65% |

For AE systems a CAPEX decrease is expected in the coming years. Direct costs can be estimated to decline with 40% up to 2035 [37, 38, 46]. This 40% is taken as the optimistic scenario, where 20% reduction is assumed for the conservative scenario. Service costs can be expected to decrease significantly with respect to the Shell number. In a conservative scenario, equal to the current projections of ISPT [38], service costs are expected to decrease to 1000 euro/kw (-40%). For an optimistic case a decrease to 600 euros/kW (-65%) is taken into account [38].

For Solid Oxide Technologies a similar service cost reduction is expected. With the development of SOE technology, direct CAPEX are expected to decrease more steeply than AE in the future. The direct CAPEX is projected to decrease with 30% in a Conservative and with 60% in an optimistic scenario.

These CAPEX projections are in line with the literature, from which a range of future price estimates are expected, which are mainly based on yearly manufacturing capacity increase [3, 51, 90, 5, 33]. A detailed bottom-up study for 100MW produced SOEC capacity arrives at a range 380-727 euros per kw after sensitivity analysis [3]. In a conservative scenario in subsection 2.5.2 the direct costs would come down 30% to around 950 euro/kW, which is on the high side of bottom-up CAPEX estimations [3, 90, 33]. In an optimistic scenario, the direct costs would decrease even further, with 60% to around 550 euro/kW, being more on the lower side of bottom-up CAPEX estimations [3, 51].

## 2.6. Macro System Background

Apart from the rSOE, the macro system contains various other system components, which are discussed in section 3.1. Some theory on the hydrogen backbone and electricity system is discussed in this section as a background for assumptions made in the Methodology.

### 2.6.1. Hydrogen Backbone

According to the Dutch government, 21GW of wind turbines are planned for instalations on the North Sea by 2030 [30]. Grid congestion and cost considerations currently favor electric transmission over hydrogen, but this may change as transmission component costs decline [20]. Hydrogen is seen as a potential industry feedstock, transport energy carrier, and storage medium. The The hydrogen strategy of the Dutch government assumes transmission through the existing gas grid [23]. However, the feasibility of a hydrogen grid remains challenging [32, 18]. If realised, the hydrogen grid is expected to be operated at 30-100 bar [34, 22, 18].

The grid operator determines the quality requirements of the hydrogen on the hydrogen backbone. According to Hillen [34], quality requirements for the future backbone of the Netherlands are still under debate, however a general feeling can be gained from conventional hydrogen quality standards. Hydrogen purity can be classified in different standards and grades. For example, according to [96] Industrial Qualified hydrogen contains >99% hydrogen. Hydrogen for PEM and fuel cell electric vehicles must be >99.97 % pure. The exact purity requirements differ per country and industry.

A step deeper, there also exist requirements on the allowed contaminants. Important for electrolysis is the allowed water content in the produced hydrogen. The water content allowed in hydrogen to be used in industry can be expressed in minimum dewpoint. The dewpoint is defined at atmospheric pressure as the temperature at which the relative humidity is 100%, which means that the hydrogen cannot hold more water in the gas form. Dewpoint requirements for industrial hydrogen at Pernis Refinery are -20°$C$ [1], but can differ per industry application. Depending on the outlet temperature and pressure of the hydrogen, most of the free water is filtered out by repetitive compression and cooling. To remove remaining water, an absorbing bed, such as a Temperature Swing Absorber (TSA), can be used.

### 2.6.2. Electricity System

An important macro system component for reversible operation is the electricity system. First, this subsection describes various channels through which electricity can be traded. Furthermore, to be connected to the grid, certain tariffs and regulations apply. The second part of this subsection touches on future developments and regulations concerning grid connection.

#### Electricity Trading Methods

As the EU electricity industry undergoes progressive liberalisation, power markets are adopting similar organisational structures. These markets typically consist of four types of power market relevant to this study: Over-the-counter (OTC), day-ahead market, intraday market, and balancing market.

- OTC or Bilateral electricity trade: Direct trading between two parties. Green Power Purchase Agreements (PPA) in which a certain supply and demand of green electricity power is guaranteed at a certain price, is a type of OTC trading [27, 43]
- The Day-ahead market: Operated through a blind auction taking place a day ahead of the traded day. Electricity is traded for all 24 hours of the next day, in hourly time slots [27].
- The Intraday market: A market on which participants can continuously trade electricity with delivery on the same day. Contracts are traded up to a maximum of 5 minutes before delivery and can be hourly, half-hourly, or quarterly. The intraday market is meant for participants to make last-minute adjustments and to balance their positions closer to real-time [27].
- Balancing market: This market entails energy trade between the transmission system operator (TSO) and parties offering or acquiring electricity [84]. A party can sell its flexibility to the TSO through the Frequency Containment Reserve (FCR), active Frequency Restoration Reserves (aFFR) or the manual Frequency Restoration Reserves (mFRR), and works as depicted in Figure 2.6. The FCR is the first response of the TSO to restore the frequency. In the Netherlands, this is usually done by using AC international interconnects, resulting in a smaller FCR need than in the UK, which is an islanded system. In the aFFR is the second line of defense. Parties offer their flexible capacity as a bid and the price is determined through market clearing. The TSO determines which assets are to be operated. The mFFR also works via market clearing, but the TSO contacts parties to operate their assets.

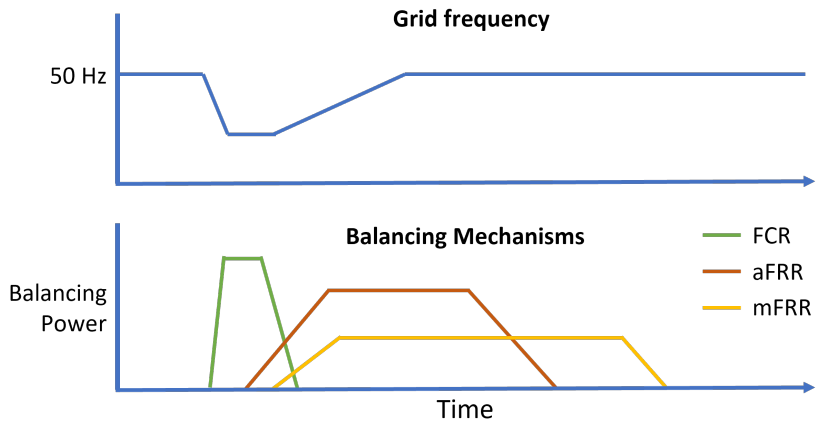


Figure 2.6: A schematic showing the defense mechanisms of a TSO to balance the grid frequency: FCR, aFFR, mFFR. Figure based on Tennet [84]

The last three markets work according to a market clearing mechanism, which is explained by Figure 2.7. Buyers and sellers of electricity must submit their bids before the order book closes, for the day-ahead market, at 12:00. A bid, or order, consists of a market participant sending their minimum and maximum willingness to buy or sell, in volume, per time period. A demand curve is constructed from all the buy orders and a supply curve is constructed from all the sell orders, as is depicted in Figure 2.7. The point where these curves intersect is the market clearing price (MCP) and market clearing volume (MCV). At that point, legally binding agreements between buyers and sellers of electricity are determined at the MCP. A buyer of electricity will never be forced to buy electricity above their willingness to pay. Likewise, a seller of electricity will never be forced to sell electricity below their willingness to pay. Electricity prices are the same for all buyers and sellers, creating a level playing field.

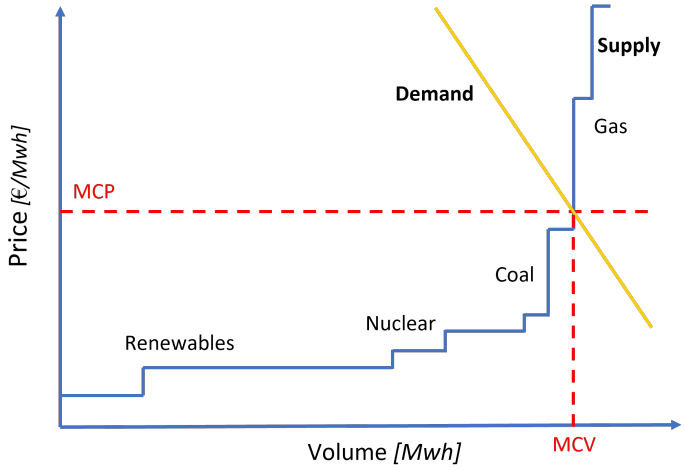


Figure 2.7: A schematic showing the supply and demand curves intersecting at the Market Clearing Price (MCP) and Market Clearing Volume (MCV). Figure based on [43]

### Grid Connection

In most countries, a TSO is responsible for balancing supply and demand and sustaining a stable grid frequency. The cost of maintaining a stable grid is distributed over the users connected to the grid. One thing included in the tariffs is the energy and capacity procurement (E&C) costs, which consist of re-dispatch, purchasing grid losses, reactive power, and contracting balancing capacity (FCR, aFRR, mFRR). Furthermore, other statutory duties, including investments in the national high-voltage grid, are included in the tariffs.

In the Netherlands, these tariffs are charged through a yearly capacity-dependent fee and a monthly peak-capacity-dependent fee, which have strongly risen in the past years. This is related to the increased energy and capacity procurement costs in 2022 [87]. The tariffs for 2024 have been announced by Tennet [87], to rise by around 80%-90% (for high-voltage (HV) customers) and 120%-135% (for extra-high-voltage (EHV) customers) compared to 2023. In absolute numbers, for EHV customers, that will amount to 0.14 million per year per MW grid connection, at an average peak consumption of 95%.

Tennet [87] also claims that, at constant E&C costs, transmission tariffs will likely continue to rise, around 15% in 2025 and 2026. If electricity prices increase again, further growth in transmission tariffs is expected, although the growth in percentage terms is expected to be substantially smaller than in 2023 and 2024. If electricity prices fall sharply, tariffs are expected to fall again. However, developments in the electricity market are so uncertain that no further statements can be made about tariffs for 2025 and 2026.

Policy and regulations around large-scale electrolysis have been and will be in flux along with further development of the hydrogen economy. In current offshore wind and onshore-electrolysis projects in The Netherlands, electricity transmission from the wind farm to the electrolyser, through the national grid is required. This on-grid system brings along yearly capacity-dependent grid fees. In the Policy for Offshore Wind 2040 by [69], Guidehouse advises the Ministry of EZK of the Netherlands to investigate a hybrid model between off-grid and on-grid. In this situation, an electrolyser is connected directly to a wind farm, possibly reducing the required grid connection of the electrolyser to the grid to a small share of the electrolyser capacity. A smaller grid connection is likely still required for auxiliary systems and to balance the frequency on this line. The reduced required grid connection would proportionally cut grid fees. This suggestion is incorporated in the Methodology subsection 3.4.2 about grid fee scenarios.

# 3 Methodology

This chapter outlines the methodology followed to answer the remaining unanswered sub-questions posed in section 1.3. To summarise, the Methodology serves to identify if and under which conditions reversibility brings improved techno-economic feasibility to large-scale SOE by evaluating performance under different scenarios and parameter deviations. The Methodology consists of five main parts (Figure 3.1) that also form the outline of this chapter.

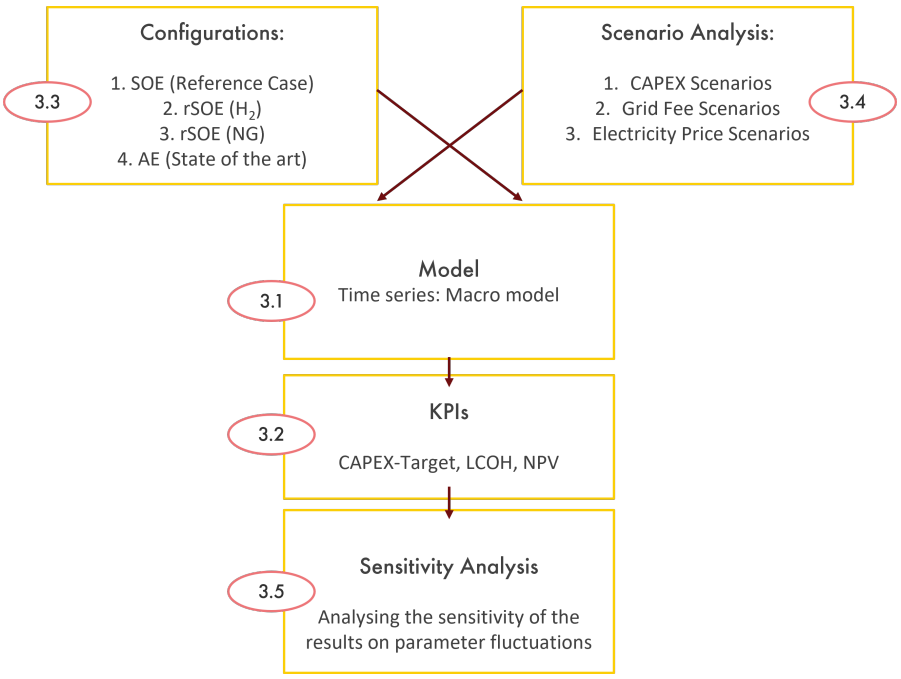


Figure 3.1: Structure followed by the Methodology

A model simulates rSOE operation in a macro system and analyses the performance. In section 3.1, the modelling methods and assumptions for each macro system component are described. The system performance is quantified using three economic KPIs introduced in section 3.2. Based on these KPIs, four configurations are analysed, which are introduced in section 3.3. As mentioned in the Introduction, these four cases consist of a non-reversible SOE configuration (reference case), an rSOE configuration with FC-mode based on hydrogen, an rSOE configuration with FC-mode based on natural gas, and an Alkaline Electrolysis (AE) configuration (State-of-the-art case). The performance of the four configurations is evaluated under three sets of scenarios in the scenario analysis explained in section 3.4. Lastly, a sensitivity analysis is performed to quantify the sensitivity of the KPIs to parameter changes, which is addressed in section 3.5. Lastly, for clarity, baseline conditions are defined in section 3.6, as various scenario- and parameter-deviations are used for this analysis.

## 3.1. Modelling the Macro System

A use-case is modelled, in which several choices on macro system components are made, as seen in Figure 3.2. These choices address the research gaps described in section 1.2. The modelling methods and assumptions for each building block are described in subsections 3.1.3 -3.1.6, as indicated by the Figure. The technical performance is converted to economic performance using the definitions described in the Economics section(3.1.7).

**Key readers instruction**

The parameters used to model the system are introduced in subsections (3.1.3 -3.1.7). The assumptions corresponding to these parameters are listed in Table 3.1.

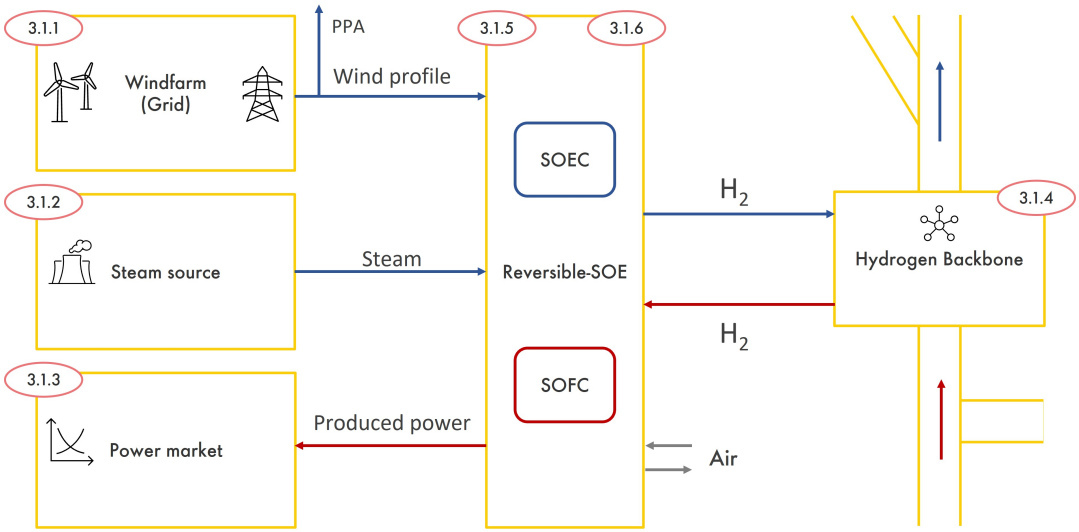


Figure 3.2: A schematic representation of the modelled macro system use-case. The blue lines represent Solid Oxide Electrolyser (SOEC), and the red lines the Solid Oxide Fuel Cell (SOFC) operation. An explanation of the macro system components can be found in the subsection numbers indicated in the red ovals.

### 3.1.1. Windfarm

Different modes of operation demand a different kind of interaction with the power system. There are three modes of operation of which the abbreviations are repeated for clarity: electrolysis (EC), fuel cell (FC), and hot-standby (HS). In EC mode this study specifically focuses on electricity available from a renewable electricity source. As renewable electricity source, a windfarm of capacity $P_{nom,wind}$ is connected to the system. Historic (2022) hourly wind data from windfarm location Borssele, is retrieved from Renewable Ninja [73]. The wind year is matched to the power price year to incorporate the correlation between the two. The dataset consists of the hourly capacity factor $C_f$ indicating the share of generated power compared to the nominal power of the windfarm. The wind power is supplied at $\theta_{LCOE,buy}$, estimated at an LCOE projection of offshore windfarms in 2035 [61]. A certain amount of the wind power profile is delivered to a client according to a power purchase agreement (PPA) of height $P_{ppa}$. As shown in Figure 3.3, the bottom part of the profile is cut off, leaving a less consistent power profile. Covering the PPA when the wind power is below $P_{PPA}$ is assumed to be unnecessary.

### 3.1.2. Steam Source

Steam is the feedstock for electrolysis operation. In the modelled use-case proximity to a steam source is assumed, supplying Low Pressure (LP) steam at temperature $T_{steam}$ and pressure $p_{steam}$. Ramping this steam supply is assumed to be possible on the hourly timescale [31]. Large industrial sites like the

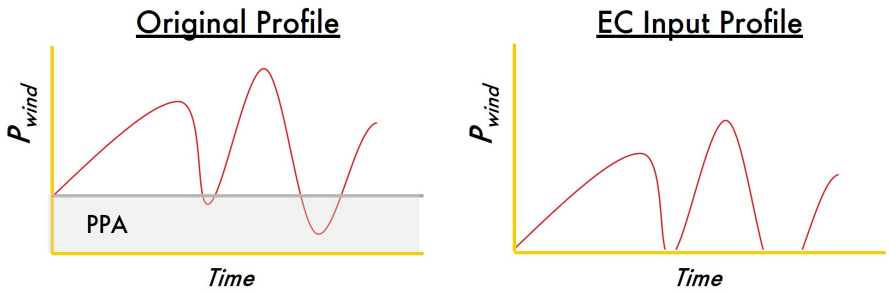


Figure 3.3: Schematic of the cut-off windprofile fed to the rSOE plant, as result of the PPA

Pernis refinery use high-volume steam networks. In the specific case of the Pernis refinery adding up to 800 tonnes per hour. This is more than tenfold the maximum steam demand of a 200MW rSOE, approximately 60 tonnes per hour (Figure B.1). Therefore, ramping on the hourly timescale of this study is assumed possible. A constant steam price $\Theta_{steam}$ is assumed for rest-steam costs [79]. If a dedicated steam-producing asset has to be built, steam costs could rise up to 135 euro per tonne [31], which is considered a sensitivity parameter.

### 3.1.3. Power Market

In FC operation, produced electricity is sold through the market, and in HS mode, electricity is bought from the market. Assumptions for this power market interaction are discussed in this subsection.

As mentioned in subsection 2.6.2, various options exist to monetise an electricity-producing asset. This study focuses on electricity trade through the day-ahead market, modelled by hourly whole sale prices. These hourly prices are denoted as $\theta_{el,sell}$. These same prices are used for systems electricity demand in hot-standby. Different power price scenarios are used based on characteristics of various historical years, which is further explained in subsection 3.4.3. All hourly power price datasets are retrieved from EMBER Climate [26].

### 3.1.4. Hydrogen Backbone

The hydrogen-producing asset is connected to the chemical system via a hydrogen backbone. It is assumed that the produced or required hydrogen can be exchanged with the backbone without flowrate limitations. However, as discussed in subsection 2.6.1, hydrogen must be supplied to the backbone at certain pressure $p_{backbone}$ and purity. These are considered in the steady state rSOE plant model by adding a compressor and TSA, described in subsection 3.1.6. To model the economics, a constant hydrogen sell price $\theta_{H_2,sell}$ and a hydrogen sell to buy ratio $Ratio_{H_2,sell/buy}$ were assumed, as was done by Zhang et al. [98]. The hydrogen sell to buy ratio describes the price difference at which hydrogen can be sold to, or bought from the backbone.

### 3.1.5. rSOE Plant: Operational Strategy

The centre component of the macro system is the rSOE plant. The two most important characteristics to model are: 1) the plant performance and 2) the plant operational strategy. The operational strategy is discussed in this section, whereas the plant performance map is discussed in the next subsection 3.1.6. The degradation of the system is modelled based on the end-of-lifetime (EOL) definition, which represents the point at which the stacks have degraded to a level that requires their replacement. The degradation profile is explained in subsection B.5.6.

The plant is operated based on an operational strategy. The main assumption is that the plant is a hydrogen-producing facility, implying that if there is a possibility, the plant will produce hydrogen. On an hourly basis, the operational strategy will work as depicted in Figure 3.4, leading to a desired and realistic schedule.

#### Desired Schedule

The top part of the strategy schematic (3.4) represents the desired schedule and explains the basic control logic of the reversible SOE. Hence, the switch-price is determined as the intersect of the hourly contribution margin curves in FC and HS mode as presented in Figure 3.5. The contribution margin is

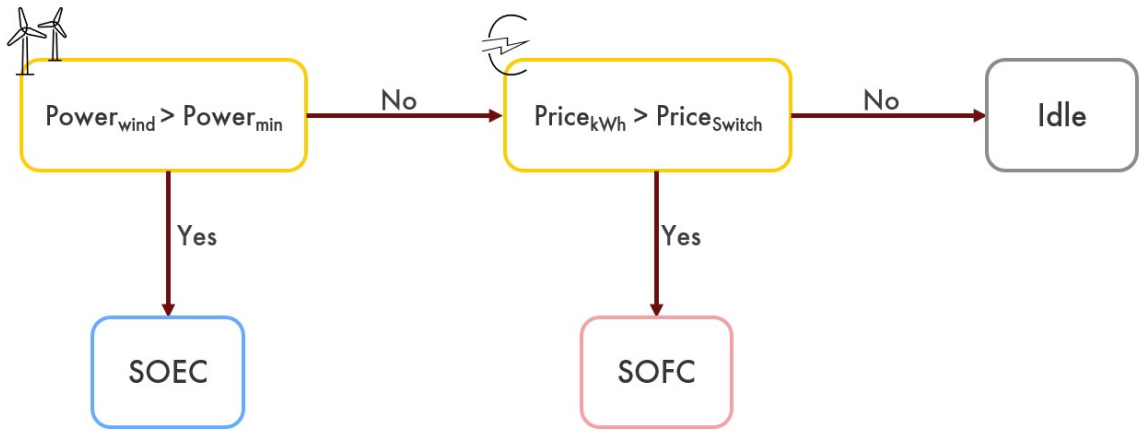


Figure 3.4: The control logic of the operational strategy followed to establish the desired schedule and the realistic schedule. The desired schedule is transformed to a realistic schedule using ramping and switching constraints

the profit or loss of operation. In other words, the revenues minus the variable costs directly related to making those revenues. In formulas the contributions margin curves yield,

$$CM_{FC,t} = Y_{el,t}\theta_{el,t} - U_{el,t}\Theta_{H_2,buy} \tag{3.1}$$

and

$$CM_{HS,t} = 0 - \theta_{el,t} f_{HS} P_{max,EC}. \tag{3.2}$$

Figure 3.5 depicts three switching prices, indicated by the red dashed lines pointing out the intersect between the HS (Blue) and FC (Green) lines. Equating these contribution margin curves leads to a definition for the switch-price

$$\theta_{switch,t} = \frac{U_{H_2,t}\theta_{H_2,buy}}{Y_{el,t} + f_{HS}U_{el,max,EC}}, \tag{3.3}$$

with $f_{HS}$, a percentage that indicates the fraction of nominal electrolyser consumption $U_{el,max,EC}$ required to heat the system during HS. In this context, $Y_{el,t}$ represents the electricity generated in hour $t$, and $U_{H_2,t}$ represents the corresponding amount of hydrogen required. As introduced $\theta_{H_2,buy}$ represents a constant the hydrogen buy price in euros per kg. The units for $U_{el,max,EC}$ and $Y_{el,t}$ are in MWh, while $U_{H_2,t}$ is measured in kilograms. The switch-price is a time-dependent parameter, as it depends on the time-dependent operating point and efficiency, through $U_{H_2}$ and $Y_{el}$.

It is important that the HS costs and time dependency of the switch-price are considered. Not considering the HS costs would result in higher switch-price, resulting in moments of HS operation, where FC operation would have been more favourable. A constant efficiency in $U_{H_2,t}$, would either result in loss-making instances when switch-price was underestimated or missed profits in case of an overestimated switch-price.

### Realistic Schedule

Certain physical constraints limit the practicability of the desired schedule, which must be modified to be realistic. The realistic schedule takes into transition constraints between operating points in consecutive hours. The pace at which the system can transition from one operating point to another is determined by Ramp rates $R_{up,EC}$, $R_{down,EC}$ ,$R_{up,FC}$ and $R_{down,FC}$, represented in MW per hour. The up or down ramp rate for either FC or EC operation is calculated as

$$R_{up/down,FC/EC} = 60\, r_{up/down,FC/EC} P_{nom,FC/EC}, \tag{3.4}$$

in which $r_{up/down,FC/EC}$ is the ramp rate in % per minute, of the nominal FC or EC capacity $P_{nom,FC/EC}$ in MW. Additionally, extra time for switching between operating modes is considered. The time required

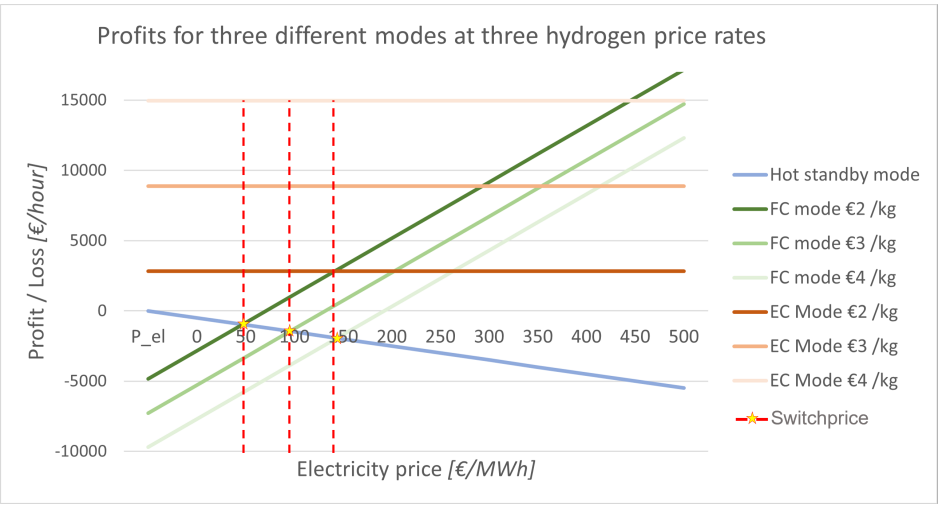


Figure 3.5: A plot of the hourly contributions margins making up the switch-price at the intersect of the CM of FC and HS mode. Plotting against electricity price and hydrogen price indicates switch-price dependency on these parameters. For this switch-price example the assumptions were as in Table 3.1 and $\eta_{FC,LHV}$=50% ,$\eta_{EC,LHV}$=80% , $\theta_{el,buy}$=46 euros per Mwh

for switching consists of a switching time $t_{switch}$ and a flushing time $t_{flush}$. The flushing time is only relevant for rSOE (NG) when switching from FC to EC mode [79]. This flushing time can vary depending on the required purity of the hydrogen in EC mode. The time required for a transition is,

$$t_{transition,t} = (P_{disered,t} - P_{t-1})R_{up/down,FC/EC} + t_{switch,t} + t_{flush,t} + t_{rest,t} \tag{3.5}$$

The realistic schedule is acquired by following the control schematic depicted in the bottom half of Figure 3.4. If the transition time is lower than an hour, reaching the desired operating point is feasible. If the transition time is larger than one hour, the operating point is constrained by the ramping rate and switching time, leaving a residual transition time $t_{rest,(t+1)}$, which will be added to the transition time in the next step.

### 3.1.6. rSOE Plant: Performance Map

The previous paragraph described how the hourly operating point is determined. A Steady State Performance Map is used for every FC and EC operating point to determine the mass and power fluxes in that hour. This map is based on Shell Internal module performance data [83]. This subsection describes the method used to make the Steady State Performance Map. The eventual map is displayed in Appendix B.1, which is made using three steps:

- First, the complete system is schematically represented in two process flow diagrams: The SOEC in Figure 3.6 and the SOFC in Appendix B.5. The module, depicted in the orange box in Figure 3.6, includes stacks, water removal, heat exchange, and power conversion. Apart from the module, the system contains additional components. For the SOEC, the additional system components are a heat-exchanger for the exhaust air and a Temperature Swing Absorber (TSA) combined with a three-stage compressor/cooling train to reach $p_{backbone}$. The TSA was assumed to be capable of reaching industrial-grade hydrogen purity. For the SOFC, the additional components are hydrogen re-circulation equipment and a heat-exchanger for the exhaust air.

- Then, mass balances are constructed on the key locations indicated by the red numbers in the flow diagrams to determine mass fluxes. To do so, the specific energy curves (Black circles in Figure 3.7) and additional parameters displayed in Appendix Table B.1 are used [83]. The mass balances are displayed in Appendix B.5.

- Lastly, the specific energy consumption is modified to include the energy duty of the compressor. The compression train is sized to the mass flow rate of hydrogen. The energy duty calculations of the compressor are depicted in the Appendix Figure B.8 and are retrieved from expert

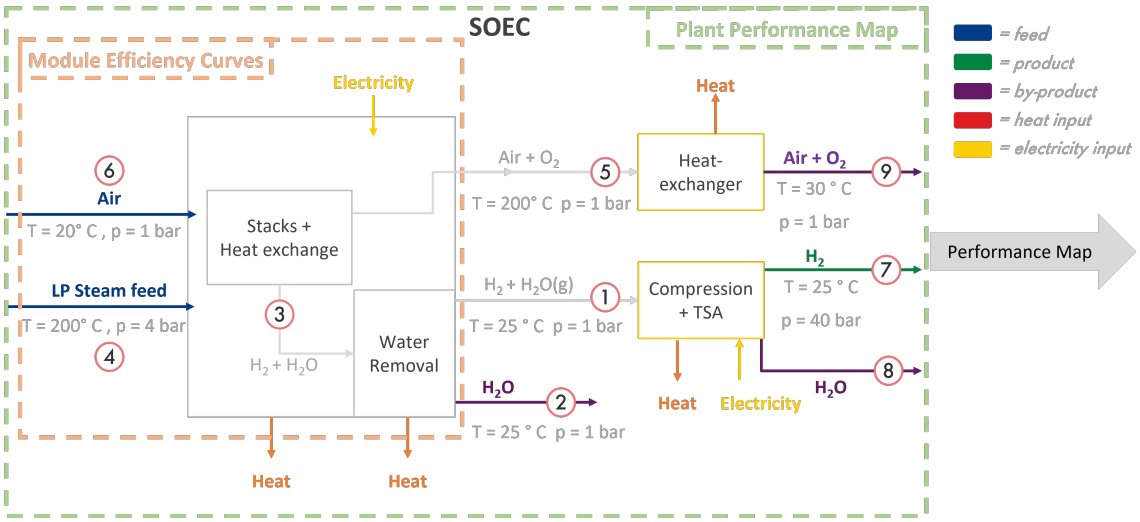


Figure 3.6: Steam SOEC process flow schematic indicating the various key process points, module scope and performance map scope. Note: Heat integration through heat exchange is included in the module. Integrating remaining heat flows (Orange arrows) is an opportunity for efficiency improvement, but are left not-optimised.

communications [11]. As it makes up a very small part of the total, the energy duty of the TSA is neglected [29, 79].

These three steps lead to the total system performance map in Appendix section B.1, including system-specific energy consumption and production, and product and feedstock mass flows. The modified system specific-energy consumption is indicated by the coloured lines in Figure 3.7.

For validation purposes, energy flows are quantified using energy balances, as displayed in Appendix B.5.4. Heat re-use through heat-exchange is incorporated in the module efficiency curves. Further heat integration, of the outgoing heat flows in the process flow diagrams, is left out of scope for this research, as the focus lies on comparing configurations. However, a Sanky diagram of the energy flows in Appendix Figure B.9 indicates the heat re-use potential.

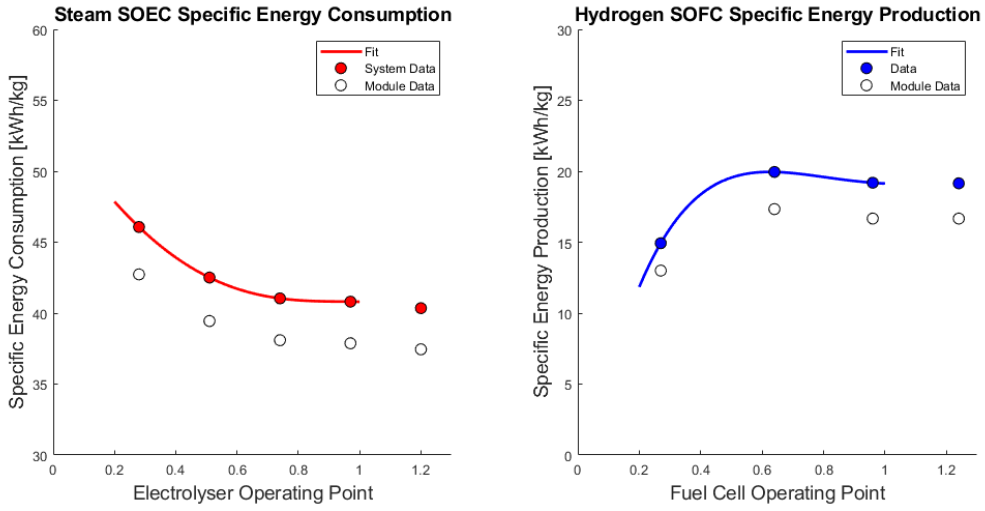


Figure 3.7: Original module- and modified system-specific energy curves for steam SOEC and hydrogen SOFC. The fit runs between the operating boundaries used in this study (20%-100%)

### 3.1.7. Economic Definitions

This paragraph outlines the economic definitions used in this study, as conventions vary across industries and disciplines. Besides that, it aims to explain how the product and feedstock of the plant

are translated into economic variables.

- This study uses the levelised system CAPEX estimations, as discussed in subsection 2.5.1. The $CAPEX_X$ is the total $CAPEX_{system}$ in euros, levelised by the nominal capacity of configuration X in kW as,

$$CAPEX_X = \frac{CAPEX_{system}}{P_{nom,EC}}. \tag{3.6}$$

- The $OPEX_{Fixed}$ are yearly costs not directly associated with the production volume. They are calculated as,

$$OPEX_{Fixed} = Ratio_{O/C} CAPEX + C_{grid}, \tag{3.7}$$

representing the sum of standard fixed project costs, such as O&M costs and grid connection fees (for the Netherlands specifically). The standard fixed project costs are assumed to be a fixed share $Ratio_{O/C}$ of the project CAPEX per year. The yearly grid fee, $C_{grid}$ is used in the grid fee scenario analysis, further explained in subsection 3.4.2.

- At EOL, the stacks require replacement. Replacement is done at a cost estimated as fixed share $Ratio_{stack/system}$ of the system CAPEX,

$$OPEX_{Stack,t} = u_t Ratio_{stack/system} CAPEX, \tag{3.8}$$

as was explained in subsection 2.5.1. $u_t$ is a discrete variable representing 1 when $t$ in years is an integer multiple of the $EOL$. As it is not a yearly cost, the stack replacement appears separately from the $OPEX_{Fixed}$ in the KPI calculations in section 3.2.

- The $OPEX_{Variable}$, are the yearly costs directly dependent on the produced volume. They consist of costs for feedstock and electricity required for EC, FC, and HS operation. The prices for this feedstock and electricity were discussed in the previous subsections and are listed in Table 3.1.

- The contribution margin, describes hourly operating profit and is defined as the hourly revenues minus the hourly variable OPEX. For the different operational modes, the contribution margin at timestep $t$ is calculated following the equations 3.1, 3.2 and

$$CM_{EC,t} = Y_{H_2,t}\theta_{H_2,sell} - U_{el,t}\theta_{LCOE} - U_{steam,t}\theta_{steam}. \tag{3.9}$$

The operational schedule outputs the operating point $P$ at every timestep $t$. The total plant input and output is calculated using the Steady State Performance Map section B.1. This input and output is the electricity use ($U_{el,t}$), hydrogen production ($Y_{H_2,t}$) , steam use ($U_{steam,t}$), electricity production ($Y_{el,t}$) and secondary feedstock use ($U_{fs,t}$). These are used to calculate the hourly contribution margin in each operational mode. The total contribution margin at timestep $t$ is defined

$$CM_t = CM_{EC,t} + CM_{FC,t} + u_{HS} CM_{HS,t}. \tag{3.10}$$

The sum of the contributions margins in each operational mode, with $u_{HS}$ a discrete variable indicating HS mode.

Table 3.1: Parameters and baseline values used for the macro system model

| Macro component | Parameter | Description | Unit | Value | Ref |
|---|---|---|---|---|---|
| rSOE | $P_{min}$ | Lower operation limit | % | 20 | [83] |
| | $P_{max}$ | Upper operation limit | % | 100 | [83] |
| | $r_{up,EC}$ | Ramping-up constraint EC | $\%/min$ | 2 | [83] |
| | $r_{down,EC}$ | Ramping-down constraint EC | $\%/min$ | -2 | [83] |
| | $r_{up,FC}$ | Ramping-up constraint FC | $\%/min$ | 2 | [83] |
| | $r_{down,FC}$ | Ramping-down constraint FC | $\%/min$ | -2 | [83] |
| | $f_{HS}$ | hot standby energy consumption | $\%/Cap_{EC}$ | 5 | [79] |
| | $t_{switch}$ | Switching time | h | 0.25 | [79] |
| | $P_{nom,EC}$ | Nominal capacity EC mode | MW | 200 | [83] |
| | $Ratio_{FC/EC}$ | Ratio between nominal capacities of FC and EC mode | (-) | $\frac{1}{4}$ | [83] |
| | $EOL$ | Stack End-of-Lifetime | years | 5 | [79] |
| Economics | $CAPEX_{rSOE}$ | Total installed system CAPEX | €/kW | 3070 | 2.2 |
| | $Ratio_{stack/system}$ | Ratio for stack replacement | (-) | 0.1 | [9, 40] |
| | $Ratio_{O/C}$ | Average project OPEX share | (-) | 0.035 | [17] |
| Project | $T$ | Project lifetime | years | 15 | [17] |
| | $r$ | Discount rate | % | 7 | [17] |
| Grid | $P_{grid}$ | Minimum required grid connection | $MW$ | 50 | none |
| | $\theta_{el,sell}$ | Time dependent wholesale market price | €/MWh | [26] | [26] |
| | $C_{Grid,month,2022}$ | Monthly Dutch Grid Fee 2023 | €/kW/year | 3.03 | [48] |
| | $C_{Grid,year,2022}$ | Yearly Dutch Grid Fee 2023 | €/kW/year | 27.98 | [48] |
| | $\pi$ | Yearly Inflation Grid fee | % | 5 | [48] |
| Hydrogen Backbone | $p_{backbone}$ | Hydrogen backbone pressure | bar | 40 | [22, 34] |
| | $\theta_{H_2,sell}$ | Constant hydrogen sell price | €/kg | 3.5 | [70] |
| | $Ratio_{H_2,sell/buy}$ | Ratio between selling and buying hydrogen | (-) | $\frac{4}{5}$ | [98] |
| Wind | $P_{nom,wind}$ | Nominal capacity of the windfarm | MW | 700 | none |
| | $P_{ppa}$ | Capacity of windenergy reserved for PPA | MW | 200 | none |
| | $Windyear$ | Year of the winddata used | (-) | 2022 | [73] |
| | $C_f$ | Hourly capacity factor of the windfarm | (-) | [73] | [73] |
| | $\theta_{LCOE,buy}$ | Constant wind energy price | €/Mwh | 46.5 | [61] |
| Steam source | $T_{steam}$ | Temperature of the low pressure steam | ℃ | 200 | [83] |
| | $p_{steam}$ | Pressure of the low pressure steam | $bar-g$ | 4 | [83] |
| | $\theta_{steam,buy}$ | Steam buy price | $€/tonne$ | 13 | [79] |

## 3.2. KPIs for Techno-Economic Feasibility

The resulting hourly economic performance from the Macro Model explained in the previous paragraph section 3.1 is used to assess the Techno-Economic Feasibility (TEF) of the various plant configurations later in the study. A distinction is made between Techno-Economic Performance (TEP) and TEF. The TEP is measured by KPIs and is used to indicate TEF, whereas TEF also includes project risks and uncertainty. This section addresses these KPIs, making up the answer to the subquestion: "What are the Key Performance Indicators that measure techno-economic feasibility of large-scale open-system reversible SOE?" The selected KPIs result from an analysis in the preparatory literature review and are the CAPEX-Target, the Levelised Cost of Hydrogen (LCOH), and the Net Present Value (NPV). The analysis is summarised below. For the full analysis, please refer to Appendix A.5.

- The CAPEX-Target resulted from the literature study as a powerful metric to indicate TEP of an immature-technology-based system, such as rSOE. Many Techno-Economic Analysis (TEA) studies base their metrics on bottum-up CAPEX estimations [19, 45, 60, 74]. However, these estimation can be unreliable for immature technologies as the components used are not necessarily off-the-shelf. Therefore, flipping this metric by determining a CAPEX-Target can better indicate the feasibility of a system [98]. The CAPEX-Target is the CAPEX per kW installed capacity for which the total project breaks even after the total project lifetime, $T$. The metric is calculated as,

$$CAPEX\ target\ = \frac{\sum_{t=1}^{T} \frac{CF_t}{(1+r)^t}}{P_{nom,EC}}, \tag{3.11}$$

  with $t$ in years, $CF_t$ the cash flow in year $t$ and $r$ the discount rate. The yearly cash flow are the yearly revenues minus the variable and fixed OPEX. In this definition, the fixed OPEX includes the yearly $OPEX_{fixed}$ and the stack replacement costs occurring at integer multiples of the EOL during the system's lifetime.

- The LCOH represents the average cost of producing hydrogen over the lifetime of a hydrogen production system. The LCOH considers all costs and is represented in euros per kilogram. The LCOH definition used in this study is slightly modified, to fit the reversible character of the system,

$$LCOH = \frac{CAPEX_{system,ann} + OPEX_{stack,ann} + OPEX_{Fixed} + OPEX_{Variable} - R_{e,ann}}{Y_{H_2,ann}}. \tag{3.12}$$

  The modification rests in the subtraction of annual revenues from electricity production $R_{e,ann}$ in the numerator. This revenue is taken as a discount on the total annual costs. $CAPEX_{system,ann}$ is calculated at the system CAPEX divided by the project lifetime. $OPEX_{stack,ann}$ is the present value of future stack investments divided by the project lifetime.

- The NPV represents the discounted cash flows minus the initial investments,

$$NPV = \sum_{t=1}^{T} \frac{CF_t}{(1+r)^t} - C_0. \tag{3.13}$$

  The discounted cash flow is the difference between the present value of cash inflows and the present value of cash outflows over a period of time. At integer multiples of the EOL, these cash flows include the investment required for stack replacement, just as in CAPEX-Target definition in Equation 3.11. $C_0$ denotes the initial CAPEX investment in year 0 and is not discounted.

## 3.3. Analysed Configurations

Based on predefined KPIs, four plant configurations were compared, a non-reversible SOE configuration (reference case), an rSOE configuration with FC-mode based on hydrogen, an rSOE configuration with FC-mode based on natural gas, and an AE configuration (State-of-the-art case). The different

configurations are modelled by adjusting certain input parameters and parts of the model compared to the described methods in subsections 3.1.5 and 3.1.6. These adjustments are discussed in the coming subsections, and parameters are displayed in Table 3.2.

Table 3.2: Parameters used in the analysed configurations. All other parameters are as displayed in Table 3.1

| Configuration | Parameter | Description | Unit | Value | Ref |
|---|---|---|---|---|---|
| SOE | $CAPEX_{SOE}$ | Total installed system CAPEX | €/ kW | 3000 | 2.5.1 |
| | $e(P)$ | Specific Energy curve SOEC | [-] | Figure 3.7 | 3.1.6 |
| rSOE ($H_2$) | $CAPEX_{rSOE,H_2}$ | Total installed system CAPEX | €/ kW | 3070 | 2.5.1 |
| | $e(P)$ | Specific Energy curves rSOE ($H_2$) | [-] | Figure 3.7 | 3.1.6 |
| rSOE (NG) | $CAPEX_{rSOE,NG}$ | Total installed system CAPEX | €/ kW | 3213 | 2.5.1 |
| | $\theta_{NG,raw}$ | Price of raw natural gas | €/ $kg$ | 0.3 | [2, 29] |
| | $\theta_{CO_2,ETS,tonne}$ | Price of $CO_2$ | €/ $tonne$ | 125 | [25, 76] |
| | $t_{flush}$ | FC to EC flushing time | $h$ | 0.25 | [79] |
| | $e(P)$ | Specific Energy curves rSOE (NG) | [-] | Figure B.2 | B.2 |
| AE | $CAPEX_{AE}$ | Total installed system CAPEX | €/ kW | 2500 | 2.5.1 |
| | $f_{s,AE}$ | standby energy consumption | % | 2.5 | [54] |
| | $EOL_{AE}$ | End of lifetime for AE system | $years$ | 8 | [54, 49] |
| | $e(P)$ | Specific Energy curve AE | [-] | Figure B.2 | 3.1.6 |
| | $r_{up/down,EC}$ | Ramping rates alkaline system | $\%/min$ | 10 | [39] |
| | $t_start$ | Start-up time | $h$ | 1 | [7, 39] |

### 3.3.1. SOE (Reference Case)

The SOE configurations is modelled as reference configuration. Compared to the rSOE ($H_2$), the SOE is modelled as follows. In terms of system performance, the specific energy curve is used as in rSOE ($H_2$), described in section B.1 [83]. The absence of FC functionality is modelled by an infinite switch-price, cutting of the FC part of the control logic in Figure 3.4. The CAPEX of SOE lay lower than for the reversible configuration. $CAPEX_{SOE}$ is taken to be the value as explained in subsection 2.5.1.

### 3.3.2. rSOE (Hydrogen)

This configuration is the base case of which the modelling is extensively described in the previous paragraph. It is worth to mention that, as a result of the additional component requirements, as described in section 2.5, rSOE has increased CAPEX compared to SOE.

### 3.3.3. rSOE (Natural Gas)

To model the rSOE (NG), the following changes to the model and to the input parameters were made, compared to rSOE ($H_2$).

The technical differences incur the following: For the rSOE (NG) case, a configuration using SMR was considered. As described in subsection 2.4.3, additional system components are required in the plant design, such as a: Pre-reformer, Desulfurisation Unit and an After-Burner. As can be seen in Figure B.2, the different secondary feedstock also has an effect on the FC specific energy production. These module specific energy curves include all the additional system components as depicted in Figure 3.8. Therefore the lines of the module and system specific energy curves overlap Figure B.2. Heat flows indicated by the orange arrows give the opportunity to increase system efficiency but remain not-optimised for this study. The last technical difference from rSOE ($H_2$) is that the LHV of methane is used instead of hydrogen.

In terms of economics, the additional system components lead to an increased CAPEX as mentioned

in subsection 2.5.1. Furthermore, the secondary feedstock costs change, taking into account the lower price of raw natural gas $\theta_{NG,raw}$, compared to hydrogen and the costs of carbon emitted per kg of natural gas used in the system. The cost of carbon emitted is determined using the costs of emitting a tonne carbondioxide $\theta_{CO_2,ETS,tonne}$ in the EU ETS [26, 76]. The costs per unit of natural gas is calculated

$$\theta_{NG,buy} = \theta_{NG,raw} + \frac{\mu_{CO_2}}{\mu_{CH_4}} \frac{\theta_{CO_2,ETS,tonne}}{1000}, \tag{3.14}$$

with $\mu_X$ the atomic mass of molecule X

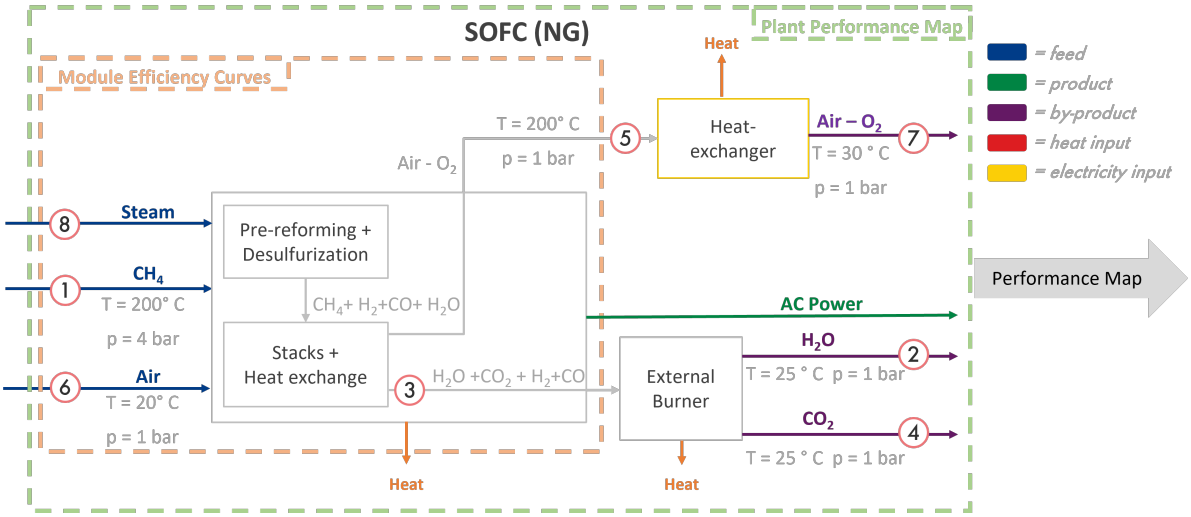


Figure 3.8: NG-based SOFC process flow schematic indicating the various key process points. Integrating remaining heat flows (Orange arrows) is an opportunity for efficiency improvement, but they are left not-optimised.

### 3.3.4. AE (State-of-the-art case)

To benchmark the results, the cases are compared to a state-of-the-art technology in the same use-case. The technology chosen to do so is Alkaline Electrolysis (AE) at atmospheric pressure, being the most frequently used technology on a commercial scale.

To mimic the AE system performance, a cell V-I curve was used to make a Steady State Performance Map [54]. In addition to the energy consumption of the cell, a constant 4 kWh / kg electricity consumption was taken into account for pumps and compressors[39]. Resulting, the specific energy curve, as displayed in Appendix Figure B.2 is used as input to the macro model. The calculation sheet is included in the Appendix B.3.

The standby energy consumption $f_{s,AE}$ is assumed to be smaller for low-temperature electrolysis and is estimated at 2.5% of the nominal capacity [54]. Furthermore, the stack EOL of AE is modelled to be longer, namely to be eight years, resulting in only one required replacement in the 15-year project time [49, 54]. A higher ramp rate $r_{up/down,EC}$ and a start-up time $t_{start}$ are assumed [7, 39]. In contrast with SOE, when the wind power is insufficient for the AE to operate at minimum power, the system must shut-down. A start-up time is required for the electrolyser to produce qualified hydrogen after shutdown. A modified total installed system CAPEX is used, as explained and displayed in subsection 2.5.1 [38, 46, 4, 37]. The installed system CAPEX is lower for AE compared to the other three cases due to a lower direct system CAPEX.

## 3.4. Scenario Analysis

Looking back at Figure 3.1, the previous sections of the Methodology described how the macro system is modelled, how the performance is measured by KPIs and for what configurations the model is used. To be able to make a well-educated comparison between the configurations, the comparison is done under several scenarios, described in this section.

### 3.4.1. CAPEX Scenarios

The performance of the four configurations is assessed under three CAPEX scenarios: a current CAPEX, future conservative CAPEX and future optimistic CAPEX. The scenarios are based on bottom-up CAPEX calculations and learning curves at different manufacturing volumes, which were outlined in Background subsection 2.5.2. In line with these projections, Table 3.3 shows the CAPEX gains for direct and service CAPEX for the scenarios.

Table 3.3: Learning rates and resulting CAPEX estimations for the three CAPEX Scenarios used for the scenario analysis

| Type | Current CAPEX [€/kW] | | | Future Conservative | | | Future Optimistic | | |
|---|---|---|---|---|---|---|---|---|---|
| | Tot | Direct | Service | Tot [€/kW] | Direct | Service | Tot [€/kW] | Direct | Service |
| SOE | 3000 | 1375 | 1625 | 1940 | -30% | -40% | 1120 | -60% | -65% |
| rSOE ($H_2$) | 3070 | 1445 | 1625 | 1985 | -30% | -40% | 1145 | -60% | -65% |
| rSOE (NG) | 3210 | 1590 | 1625 | 2090 | -30% | -40% | 1205 | -60% | -65% |
| AE | 2500 | 875 | 1625 | 1675 | -20% | -40% | 1095 | -40% | -65% |

### 3.4.2. Grid Fee Scenarios

As mentioned in Figure 2.6.2, costs for grid connections in the Netherlands have strongly increased over the past few years (Current: 2023) and have been announced to increase further in 2024. This brings along the interest to study the effect of several grid fee scenarios. As the grid fee is capacity-based, three capacity-based scenarios are defined and displayed in Table 3.4. The first is the baseline scenario with no grid fee. This scenario is taken as a baseline scenario to generalise the result, as the grid fee varies across the world. Therefore, it is important to remember that this fee is not included in the results of this thesis. Complementing the "No grid fee" scenario is the "Equal grid fee" scenario in which yearly grid fee costs for the full installed capacity are taken into account. The middle scenario is the "Differentiated grid fee" scenario, which is based on the policy and research described in Figure 2.6.2. In this scenario, only a minimal grid connection is required for electricity supplied to the grid and drawn from the grid, for example for auxiliaries, hot-standby or turndown load power. For the SOE and AE configuration, the grid connection is required for keeping the system in (hot) standby. For both reversible configurations, the required grid connection equals the FC capacity.

Table 3.4: Grid connection capacity $P_{grid}$ for the three scenarios and each configurations

| Configuration | No grid fee [MW] | Differentiated grid fee [MW] | Equal grid fee [MW] |
|---|---|---|---|
| SOE | 0 | 10 | 200 |
| rSOE ($H_2$) | 0 | 50 | 200 |
| rSOE (NG) | 0 | 50 | 200 |
| AE | 0 | 5 | 200 |

Grid costs, $C_{grid}$ is a part of the Fixed OPEX as explained in subsection 3.1.7. In the Netherlands, the grid connection fees consist of a monthly and yearly capacity-based fee, $C_{Grid,month}$ and $C_{Grid,year}$. Resulting, the yearly grid fee for 2035 is calculated using

$$C_{grid} = P_{grid}\Pi_{2035}(12C_{Grid,month,2023} + C_{Grid,year,2023}). \tag{3.15}$$

The fees for 2023 are displayed in Table 3.1. $\Pi_{2035}$ is the inflation factor

$$\Pi_{2035} = 2.3(1+\pi)^{T_{start}}, \tag{3.16}$$

which is the total inflation for the period 2023-2035. The factor 2.3 corresponds to the known rise of 130% for 2024. $T_{start}$ is 11 years as the inflation factor is determined from 2023-2035, and one year is known. A constant yearly inflation $\pi$ is assumed over these 11 years.

### 3.4.3. Power Price Scenarios

In the use-case described in section 3.1 the product of FC operation, electricity, is sold via the day-ahead market. Day-ahead market prices are represented by Dutch wholesale market prices. The effect of power

price on the TEP improvement of reversibility is studied by analysing the TEP for three artificial power price scenarios. On top of that, a regret analysis is performed to assess the effect of volatility and average power price on reversibility. The methods used for these steps are described in the coming paragraphs. However, first, the rationale for constructing artificial power price datasets, instead of using historic power price datasets, is shared.

### Rationale for Power Price Method

In this these artificial power price datasets are created by modifying the 2022 power price to a desired normalised standard deviation $\sigma_{Set}$ and average power price $\theta_{el,avg,Set}$. To do so, first the gas related volatility is filtered out. Before going deeper in the method to make these datasets, the rationale for using this method is explained.

- It allows to study the de-coupled effect of average power price and power price volatility, by the ability to construct datasets based on these parameters. This is convenient, as the power-price and -volatility is expected to change in the future as a result of increasing RES capacity. As an example, according to RVO the Dutch installed wind power capacity is to incline to 11 to 21 GW by 2030 and to 38-72 GW by 2050 [78]. This method allows to study of future power price speculations and prevents using historical prices, which are an unrealistic representation of the future.
- It allows to compare different power price scenarios based on the same wind year. To be able to compare configurations under different power price scenarios, it is important that the price scenario is based on the same wind year. This is not possible when power prices and winddata of different historic years are compared, which would give an unequal comparison.
- It allows using a constant gas price, without causing an unbalanced analysis. 2022 high gas prices have shown how rapidly electricity prices can increase. As shown in Table 3.5. The average electricity wholesale price in 2022 was 5 times as high as in 2019. This study makes use of a constant gas price and hydrogen price. If these are used in combination with a gas price-related fluctuating electricity price, the economic profit margins become unbalanced.

Table 3.5: Average electricity prices and normalised standard deviation of historic years 2018-2022 [26]

| Year | 2018 | 2019 | 2020 | 2021 | 2022 |
|---|---|---|---|---|---|
| Average electricity price [€/MWh] | 52.54 | 41.19 | 32.19 | 102.97 | 241.91 |
| Normalised standard deviation [-] | 0.29 | 0.27 | 0.47 | 0.73 | 0.54 |

### Artificial Dataset Synthesis

Artificial datasets are created based on the 2022 power price profile. First, the gas-related volatility is filtered out to justify the use of a constant gas price. This is done following the logic in

$$\theta_{el,2022,filtered}[t] = \theta_{el,2022}[t]/(\frac{\theta_{gas,weekly,2022}[t]}{\theta_{avg,gas,2022}}) \tag{3.17}$$

and

$$\theta_{el,set,filtered}[t] = \theta_{el,2022,filtered}[t]/(\frac{\theta_{avg,gas,2022}}{\theta_{avg,gas,set}}), \tag{3.18}$$

of which the result is shown in Figure 3.9. In the first equation, the gas-related volatility is filtered by dividing it by the normalised weekly gas price of 2022. In the second, the gas-related price level can be set to a desired gas price level $\theta_{gas,avg,set}$. As an example in Figure 3.9, the gas price is set to around the current (May 2023) level of 35 euro per MWh gas equivalents [95].
To artificially construct the power price datasets based on a desired normalised standard deviation and average power price, $[\sigma_{Set}, \theta_{el,avg,Set}]$, the $\theta_{el,2022,filtered}$ is further modified. The $\theta_{el,2022,filtered}$ corresponds to the second subfigure in Figure 3.9. The modification follows the following logic

$$\theta_{el,modified}[t] = (\frac{\theta_{el,2022,filtered}[t]}{\theta_{avg,2022,filtered}} - 1) \cdot (\frac{\sigma_{Set}}{\sigma_{2022,filtered}}) \cdot (\theta_{el,avg,Set}). \tag{3.19}$$


Figure 3.9: The two steps to filter gas-related volatility (first two sub-figures) and gas-related power price level (last two sub-figures) from the 2022 power price dataset. Power price data from EMBER [26] and gas price data from Yahoo Finance [95].

Three parts can be identified. The first part captures the volatility profile for the 2022 filtered dataset. The second sets the volatility size to the desired $\sigma_{set}$, and the third sets the power price level to the desired average power price $\theta_{el,avg,Set}$.

### Three Power Price Scenarios

Three power price scenarios are constructed using the previously described method: A Low, Mid and High scenario. The parameters defining the price scenarios are listed in Table 3.6. Each scenario is a modification of historic Dutch 2022 prices so that the wind power-related volatility is captured.

The High and Low scenarios are based on 2019 and 2022 prices and volatility and are used as bookmark scenarios. These are called bookmarks as they, historically, represent a very low and high price year in terms of average power price and volatility, as represented by Table 3.5. Note that in the High scenario, the difference between the normalised standard deviation in Table 3.6 and the 2022 counterpart in Table 3.5 relates to the gas volatility filter.

The Mid power price scenario is based on current (2023) average power prices. With the installed capacity of volatile RES rising, the future power price volatility can be expected to increase, as mentioned in Appendix subsection C.4.2. To capture volatility increment expectation the Mid power price scenario is set at a 0.7 normalised volatility.

A difference is made in the gas price between the scenarios. The Low and Mid scenario are set to the gas price discussed in Table 3.2. The gas price in the High power price scenario is altered proportionally to the gas price ratio between 2022 and 2023 [95].

### Regret Analysis

A regret analysis is performed to gain further knowledge on the relation of power price defining factors, $[\sigma_{Set}, \theta_{el,avg,Set}]$, to the techno-economic improvements of reversibility. The regret analysis also supports

Table 3.6: Average Electricity Prices and Standard Deviation of the three power price scenarios

| Scenario | Low | Mid | High |
|---|---|---|---|
| Average electricity price [€/MWh] | 52.54 | 90 | 241.91 |
| Normalised standard deviation [-] | 0.29 | 0.7 | 0.41 |
| Gas price [€/ kg] | 0.3 | 0.3 | 1.14 |

the usefulness of the results gained from the power price scenario analysis as it shows the overall dynamics between the power price scenarios.
Regret theory is grounded in the understanding that when a decision maker is faced with choosing between a set of prospects, they are not solely concerned with the outcome they receive from their chosen option, but they also consider the potential outcome they would have received if they had chosen differently. If the outcome of their chosen prospect is less desirable than that of the alternative option, the DM experiences the negative emotion of regret [80, 6, 47]. Under that theory, the choice with the highest regret represents the most favourable choice.

| Datasets($Avg_i$ , $Std_j$) | 1. SOE | 2. rSOE ($H_2$) | 3. rSOE (NG) | 4. Alkaline |
|---|---|---|---|---|
| Powerprice($Avg_1$ , $Std_{1)}$ | ... | ... | ... | ... |
| Regret(1,1) | ... | ... | ... | ... |
| : | | | | |
| Powerprice($Avg_i$ , $Std_{j)}$ | NPV=150 | NPV=100 | NPV=130 | NPV=50 |
| *Regret(i, j):* | *100* | *50* | *80* | *0* |
| : | | | | |
| Powerprice($Avg_x$ , $Std_{y)}$ | ... | ... | ... | ... |
| *Regret(x, y):* | ... | ... | ... | ... |
| **Total regret** | *Sum(1,regret)* | *Sum(2,regret)* | *Sum(3,regret)* | *Sum(4,regret)* |

Figure 3.10: A table explaining the method of the regret analysis

As explained in subsection 3.4.3 an hourly power price dataset can be constructed based on the standard deviation and the average power price. A power price dataset was constructed for a number $x = 15$ average power prices between $\theta_{el,avg,min} = 30$ euros per Mwh and $\theta_{el,avg,max} = 240$ euros per Mwh and a number $y = 5$ normalised standard deviation values between $\sigma_{min} = 0.4$ euros per Mwh and $\sigma_{max} = 0.7$. This leads to $x^*y = 90$ power price datasets. For these datasets, the model was used to simulate a year operation, from which the NPV is calculated per configuration. From all combinations of average power prices and standard deviations, a table is constructed with the NPV per configuration, as is done in Figure 3.10.

This table is used to calculate the regret values per power price dataset. The regret is defined as the amount of NPV that was missed for a certain configuration by choosing the least favourable configuration. For each power price scenario the smallest NPV of the four configurations is subtracted from the others, leaving 0 regret for the smallest value and a certain number as regret for the other configurations. This is seen in the sixth row of the explainer-table, Figure 3.10. For all $x$ average power prices the regrets of all$y$ normalised standard deviation options were summed, leading to a regret per configuration per average power price. The highest total regret, represents the most favourable choice under that average power price. Summing up all regrets for all $x$ power prices leads to the total regret over the complete power price uncertainty, leaving the most favourable general choice.

## 3.5. Sensitivity Analysis

A sensitivity analysis is performed to see the sensitivity of a KPI to sole parameter change. Parameters, listed in Table B.2, can willingly and unwillingly differ from the baseline parameters and influence the TEP. To gain insight into this effect two variations of sensitivity are studied for every configuration and price scenario.

- The first is a plus and minus ten percent deviation analysis. In which the percentage change of

the KPI is determined as a result of a ten percent increase and decrease of the parameter.

- The second is an expected deviation analysis. In which the absolute change of the KPI is studied as a result of an expected deviation of the studied parameter. The expected deviations for which this analysis is performed are listed as 'low' and 'high' in Table B.2. The bounds for the sensitivity analysis are shortly substantiated in Appendix B.6.

## 3.6. Overview of Baseline Conditions

As the results are analysed for different scenarios and sensitivities described above, it is important to define a baseline conditions scenario. The baseline conditions are chosen as represented in Table 3.7

Table 3.7: Baseline scenarios and parameters

| Scenario | Baseline choice |
|---|---|
| Parameters | Table 3.1 |
| CAPEX scenario | Future Conservative |
| Power Price scenario | Mid |
| Grid Fee scenario | No Grid Fee |

# 4

# Results and Discussion

This Results and Discussion chapter aims to provide the necessary background to address the research question: "Can reversible operation enhance the techno-economic feasibility of a large-scale open-system SOE, and if so, under what conditions?" To gain a comprehensive understanding of reversibility, section 4.1 presents the operational schedule and explores the factors influencing reversibility. The results of the configuration comparison under the baseline conditions are discussed in section 4.2, as outlined in the methodology. These results are evaluated across three scenarios, and the findings are presented in section 4.3. Furthermore, by conducting a sensitivity analysis, section 4.4 investigates the impact of varying parameters from their baseline values. The subsequent analysis of the scenario and sensitivity results reveals that reversibility can be a risk mitigation strategy by hedging against uncertain parameters, as discussed in section 4.5. Finally, the insights from the scenario and sensitivity analysis unveil certain external (section 4.6) and internal conditions (section 4.7) under which reversibility brings feasibility improvements compared to regular SOE.

**Key readers instructions**

- A difference is made between Techno-Economic Performance (TEP) and Techno Economic Feasibility (TEF). The TEP is measured by KPIs and is used to indicate TEF, whereas TEF also includes project risks and uncertainty.
- 'Relative feasibility' denotes the difference in feasibility between configurations, for example, between SOE and rSOE.
- 'Absolute feasibility' denotes the feasibility of configurations on themselves and is sometimes used to clarify the difference to relative feasibility.
- TEF is sometimes just denoted as 'feasibility'

## 4.1. The Operational Schedule

This study hypothesises that reversibility improves the feasibility of large-scale SOE under certain conditions. This improvement is required to de-risk the developing technology. To test this hypothesis, a model was built, described in section 3.1, as a tool to simulate rSOE in a macro system. According to an operational strategy, the model provides hourly operational schedules under varying configurations and scenarios. As a background for understanding the dynamics of the model under parameter change and different scenarios, time series graphs indicating plant operation are explained and analysed.

### 4.1.1. Dynamics of the Operational Schedule

Figure C.1 displays a three-day fragment out of the hourly schedule of a year operation. The top time series shows the hourly operating capacity, while the bottom time series shows the hourly contribution margin. This paragraph aims to explain the dynamics of the operational strategy. Under wind availability (Black line) the plant operates in EC mode at a capacity (Blue bars) capped by either the available wind power or the nominal capacity. If the wind power is insufficient to exceed the electrolysers' minimum power threshold $P_{min}$ FC operation is considered. If the electricity price (Green Stems and right y-axis) is above the switch-price (Green Dots), the plant ramps to full capacity FC mode (negative Red Bars). The operating capacity of FC mode is depicted as negative,

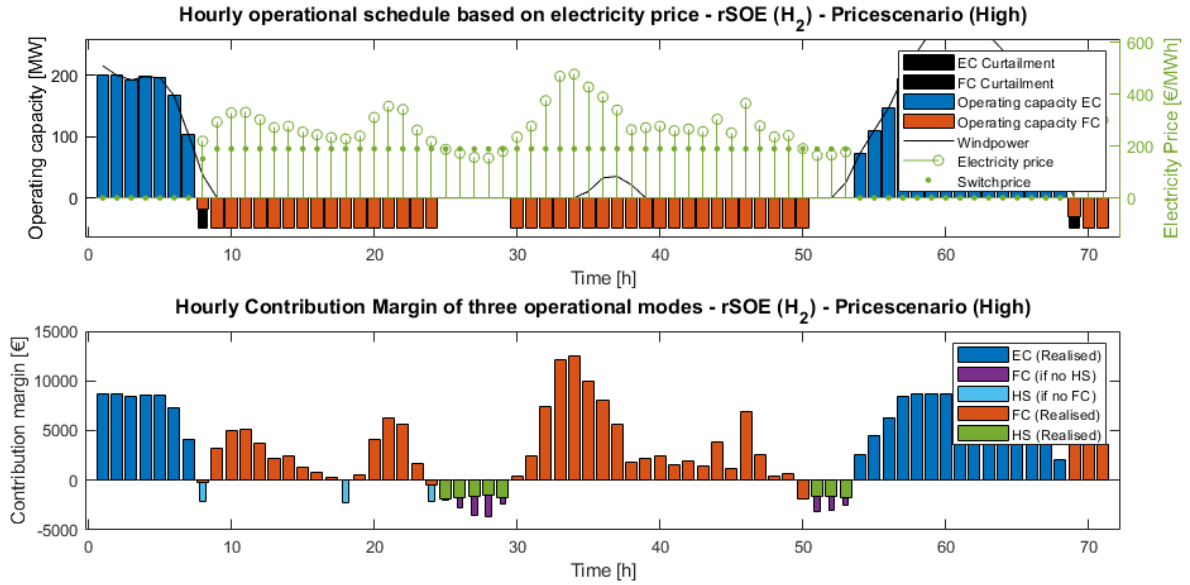


Figure 4.1: The operational schedule for a randomly selected three-day period for rSOE ($H_2$) in the High power price scenario, showing a large share of FC operation. Top graph: Hourly operating point. Bottom graph: Hourly contribution margin. Power price scenario: High. Parameters: Basis. Configuration: rSOE ($H_2$)

as electricity is exported from the plant. If the electricity price is below the switch-price the plant is operated in Hot-Standby, modelled as a fixed share of the nominal capacity, $f_{HS}$. When ramping or switching rates prevent the transition time (Equation 3.5) to be under the hour, as is seen in hour 8, the schedule is curtailed to the maximum achievable capacity. The curtailed capacity is indicated by the black bars.

The hourly operating points are translated into hourly product- and feedstock-massflows, using the steady-state performance map and, from there, resulting efficiency curves as described in subsection 3.1.6. Then, as described in subsection 3.1.7, hourly contribution margins are calculated for the three operational modes: electrolysis (EC) (Equation 3.9), fuel cell (FC) (Equation 3.1) and hot standby (HS) (Equation 3.2). The hourly contribution margins indicate the operating profit or loss from production-related revenues and costs, leaving out fixed OPEX and CAPEX. The bottom time series in Figure C.1 shows the hourly contribution margin resulting from the operational schedule (top time series). A negative bar indicates a loss, whereas a positive bar indicates a profit. A distinction can be made between full-width bars (blue, red, green) and half-width bars (cyan, purple). The full-width bars indicate realised contribution margin, whereas half-width bars indicate prevented losses by operating in the most favourable mode. As the cost of HS operation is included in the switch-price, defined in Equation 4.1, the plant prefers making a small loss in FC mode over a larger loss in HS mode, and visa versa. The cyan bars indicate the prevented HS loss and the prevented FC loss by purple bars.

Note that the switch-price is dependent on operating efficiency and thus variable across different timesteps. An example of such a time instance is at hour 8 in Figure C.1. A variable switch-price results in preventing losses in lower efficiency operating points.

### 4.1.2. Sensitivity of the Operational Schedule

From analysing the operational schedules, it can be concluded that the schedule is highly dependent on the power price, switch-price and feedstock choice and price. Figure 4.2 displays the randomly selected three-day operational schedule in three combinations of power price scenario and secondary feedstock choice. The top graph shows the schedule for rSOE ($H_2$) in the High power price scenario. By changing the power price scenario to Mid, as is done in the second schedule in Figure 4.2, the power price does not reach the switch-price for most hours, resulting in almost no FC operation. The same fragment is shown for rSOE (NG), under the Mid power price scenario to indicate how the secondary feedstock choice influences the operational schedule. As seen in the third schedule in Figure 4.2, a lower

switch-price results from the lower cost of natural gas, allowing more FC profits in no wind hours.

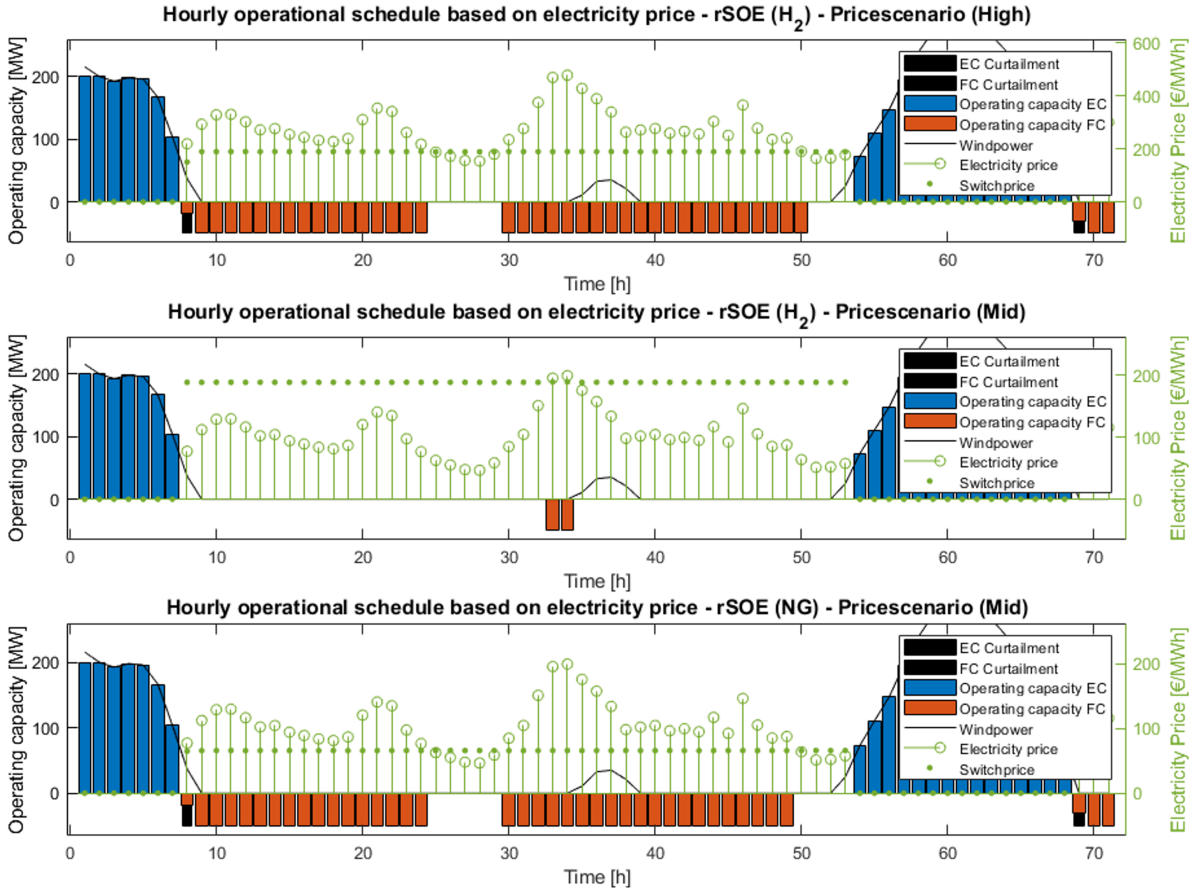


Figure 4.2: Comparison of the operational schedules of three combinations of power price scenario and secondary feedstock choice. It uncovers that the operational schedule and, implicitly, feasibility improvement by reversibility, mainly depends on power price and switch-price. Mind the right-axis-limits change in the top graph.

**Conclusions on The Operational Schedule**

- The operational schedule is strongly dependent on the power price and switch-price (And thereby on feedstock-choice and -price).
- Profit maximising logic prioritises making a small loss in FC mode over a larger loss in HS mode.

## 4.2. Baseline Conditions Analysis

The previous section introduced reversibility and its operational schedule. It introduced the dependency of reversible operation to changing modelling conditions. This section presents the performance of the four studied configurations under baseline conditions as defined in section 3.6 and aims to provide background to the subquestion: "Does reversible operation, either based on hydrogen or natural gas, show improved techno-economic feasibility compared to SOE, in a baseline scenario?".

Under baseline conditions, reversible operation does not show convincing TEP improvement compared to non-reversible SOE. This is observed in Figure 4.3, in which the LCOH of the four configurations is plotted. Two additional stacks can be observed related to reversibility in the reversible configurations. The purple being the costs of secondary feedstock for FC operation. The negative blue stack on the rSOE ($H_2$) and rSOE (NG) stacks represents the levelised revenues from FC operation. The levelised revenue discounts the LCOH by shifting the bars downwards by this amount, as was introduced by the LCOH definition in the Methodology (Equation 3.12). The LCOH of the reversible configurations does not show a reduction as the low gains of FC operation and reduced HS costs, do not match the cost of oxidised chemicals and the additional CAPEX and OPEX

In contrast to rSOE ($H_2$), rSOE (NG) does show an LCOH improvement. This can be attributed to the lower costs of secondary feedstock. On the one hand this results in a lower switch-price, causing more hours of FC operation. In addition, the lower costs cause these FC hours to be more profitable. Lastly, the hours in FC operation take the place of HS hours, reducing the costs indicated by the orange stack.

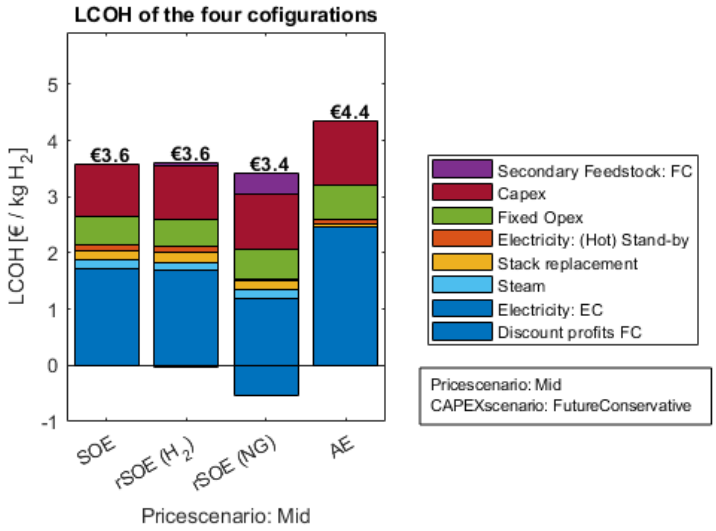


Figure 4.3: LCOH Breakdown comparing the four configurations under baseline conditions. Power price scenario: Mid; CAPEX Scenario: Future Conservative;

Comparing the four scenarios using the CAPEX-Target results in Figure 4.4. The CAPEX-Target is the levelised CAPEX [€/$kW$] at which the project breaks even. In the Figure a line indicates the normalised CAPEX-Target of each configuration. Each configuration is normalised by the Future Conservative CAPEX scenario value, which are stated in Table 3.3.

From the Figure we can observe that all CAPEX-Targets are below the projected Future Conservative CAPEX scenarios. This is the case as the normalised values are below one, which means none of the configurations breaks even under the modelled use-case in baseline conditions. As this is a non-optimised comparative study, the emphasis does not lie on the absolute results but on the relative results. The NG-based rSOE configurations' CAPEX-Target is closest to its CAPEX projection. The $H_2$ based reversible configuration is slightly further from the CAPEX projection than the SOE.

The results presented are based on baseline conditions. A more nuanced view can be established by analysing the results for different scenarios and parameter assumptions, which is done in the coming sections.

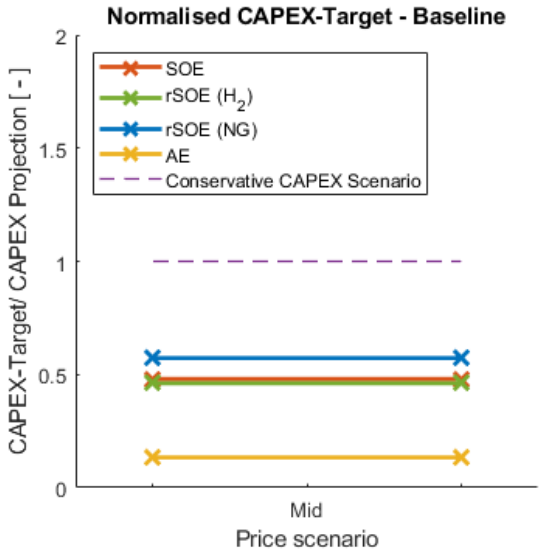


Figure 4.4: CAPEX-Target comparison of the four configurations under baseline conditions. Power price scenario: Mid; CAPEX Scenario: Future Conservative;

**Conclusions on Baseline Conditions Analysis**

- Under baseline conditions, reversibility does not bring convincing TEP improvement.
- NG-based rSOE does show reduced LCOH compared to SOE and hydrogen-based rSOE under baseline conditions.

## 4.3. Scenario Analysis

The baseline results are evaluated across three scenarios, to provide background to the sub-question: "Under what scenarios does reversibility bring improved techno-economic feasibility compared to SOE?". The finding on power price scenarios (4.3.1) and on the in-depth analysis on powerprice depenedency (4.3.2) are presented first. Then, the results from the CAPEX scenarios (4.3.3) and grid fee scenarios (4.3.4) are adressed.

### 4.3.1. Power Price Scenarios

To understand how the results from the baseline conditions relate to the power price, the use-case is modelled under three power price scenarios: Low, Mid and High. The results of the power price scenario analysis raise a demand for a more in-depth analysis of this parameter, which is discussed in the second part of this subsection. The power price scenarios are constructed according to methods described in subsection 3.4.3. The scenarios' parameters are listed in Table 3.6.

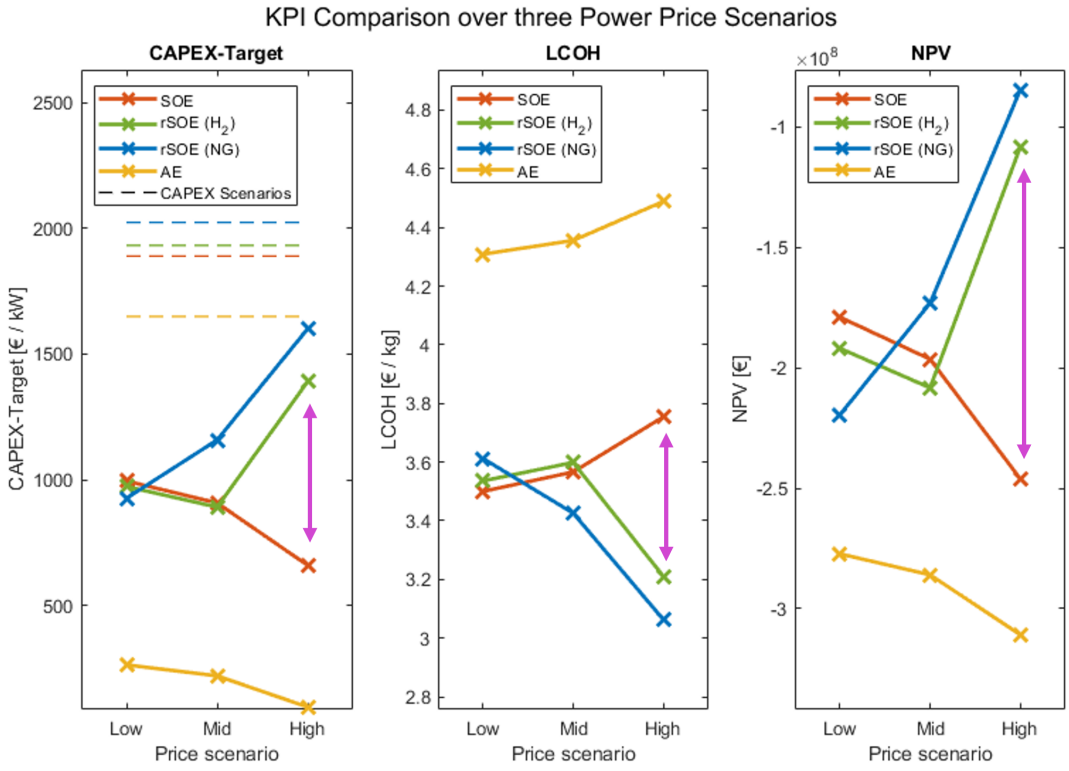


Figure 4.5: KPI plots comparing the four configurations under baseline conditions and three power price scenarios, showing large relative feasibility improvement by reversibility under higher power price scenarios. CAPEX Scenario: Future Conservative CAPEX; Power price scenarios: Table 3.6; Note: The line connecting the markers is a guide to the eye

Figure 4.5 shows that reversibility hedges non-reversible configurations against high power prices. The Figure shows the three KPIs for the three power price Scenarios. Where non-reversible systems show decreasing TEP, reversible operation results in a significant TEP increase, as indicated by the purple arrows. Consequently, the relative feasibility improvement strongly increases with power price. Analysing the LCOH, as in Figure 4.6, allows us to zoom in on the project economics dynamics. Towards higher price ranges, the electricity consumed for HS operation gets more costly, which causes a decrease in NPV for the non-reversible configurations. The reversible use-cases hedge against that occurs in two ways: 1. The higher power prices cause FC operation to be more profitable. 2. The power price is above the switch-price in more instances in the year, causing more hours of FC operation and, thus, fewer hours of HS operation.

By comparing the configurations across the power price scenarios, it is concluded that SOE is most

favourable in the Low power price scenario, rSOE (NG) shows relative improvements as of the Mid power price scenario and rSOE ($H_2$) requires the High power price scenario to show relative improvements. The hydrogen-based rSOE shows negligible LCOH improvements from the Low to Mid scenario because of the low number of FC hours, with limited margin.

Also, despite achieving substantial revenue and reduced HS costs in Mid scenario, rSOE (NG) fails to bring about convincing improvements in LCOH, thereby lacking the necessary feasibility to convincingly compete with SOE. This can be attributed to the relatively low profit margins from electricity production as the power price is just above the switch-price. Note that in the High scenario, the rSOE (NG) scenario is penalised by an increased gas price, to prevent the unrealistically high profits, as was explained in subsection 3.4.3.

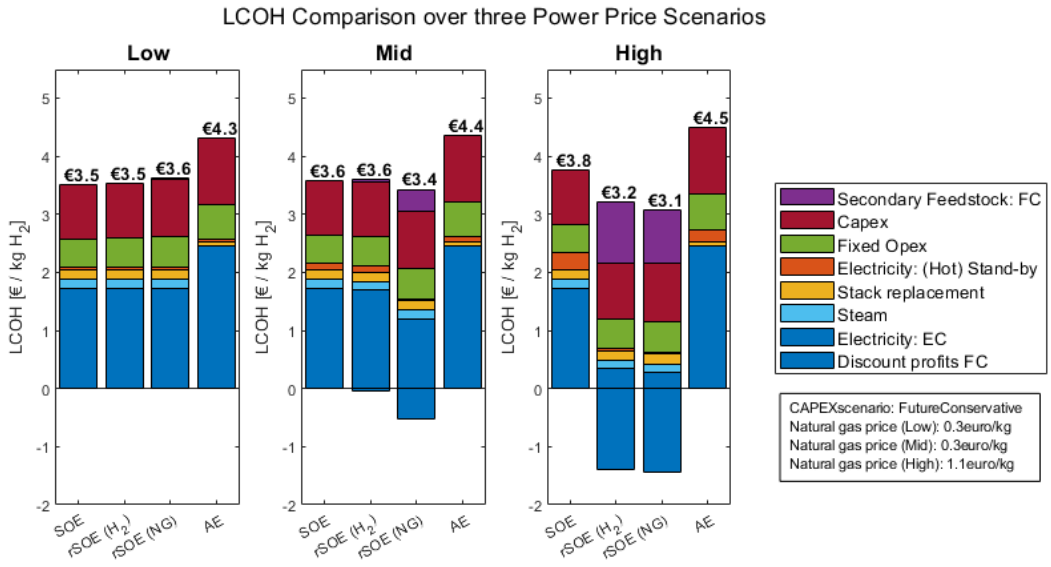


Figure 4.6: LCOH plots comparing the four configurations under baseline conditions and three power price scenarios, showing that reversibility causes a LCOH decrease under higher power price scenarios. CAPEX Scenario: Future Conservative CAPEX. Power price scenarios: Table 3.6.

In absolute feasibility terms, the modeled use-case is not under the Low, Mid and High power price scenario. None of the configurations' CAPEX-Targets reach the expected Future conservative scenario (dashed lines), as can be observed in the left-most graph in Figure 4.5. This is in line with none of the configurations crossing 0 NPV in the right-most NPV, graph. As CAPEX projections differ across configurations, it can be useful to represent the CAPEX-Target normalised by the CAPEX projection value as represented Figure C.8 from the Appendix. It measures how close the CAPEX-Target is to the expected scenario, and thereby the projects' feasibility. This enables comparing the feasibility of the configurations based on the CAPEX-Target. Nevertheless, the normalised representation does not show prominent differences to the absolute result in Figure 4.5.

### 4.3.2. In-depth Power Price Analysis

The previous paragraphs indicated the impact of power price scenarios on the outcome of the study. An in-depth analysis was performed based on regret analysis and isolines, aiming to better understand the dynamics between reversibility and power price.

#### Regret Analysis

As explained in Table 3.4.3 the regret per configuration was calculated for 90 power price data sets. Summing the regrets of all datasets with the same standard deviation $\sigma$ leads to a total regret per average power price. The highest regret represents the most favourable choice under a certain average power price. These results are plotted in Figure 4.7.

Figure 4.7 shows there exist certain "break-even power price-points" $\Theta_{el,BE,X}$ above which reversible systems, based on secondary feedstock X, become more economically attractive than regular SOE. For

this use-case $\Theta_{el,BE,NG}$ lies at 73 euro per MWh and $\Theta_{el,BE,H_2}$ at 108 euro per MWh. It is crucial to note that these absolute number "break-even power price-points" depend on the secondary feedstock price.

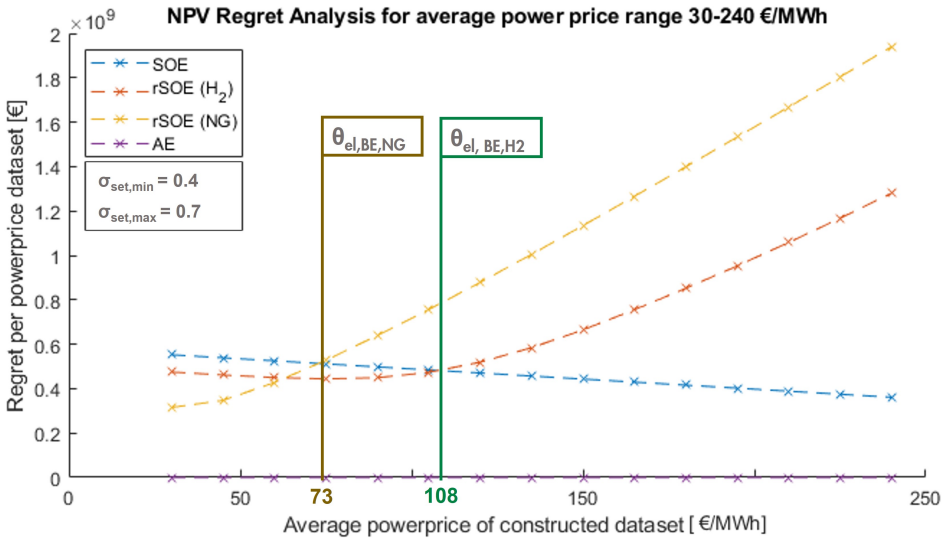


Figure 4.7: Summed up regret per average power price option for each configuration. Each cross represents the summed up the regret over the normalised standard deviation range $[_{set,min}, \sigma_{set,max}]$.

One can sum all regrets over the range $[\theta_{el,avg,min}, \theta_{el,avg,max}]$ to arrive at a total regret per configuration. This total regret can serve as a measure of the most favourable configuration choice under average power price and power price volatility uncertainty. However, by interpreting the information in Figure 4.7, it must be concluded that this total regret ranking is strongly dependent on the range chosen for the average power price $[\theta_{el,avg,min}, \theta_{el,avg,max}]$. Namely, the range shown in the graph results in the total sum in favour of rSOE (NG). However, if the maximum bound is around 70 euros per MWh, the total sum would favour SOE.

To study the dynamics between the choice of range, the total regret over a range $[\theta_{el,avg,min}, \theta_{el,avg,max}]$ is calculated for various options of maximum variable bound $\theta_{el,avg,max}$ and a fixed minimum variable bound, $\theta_{el,avg,min}$. The results are shown in Figure 4.8. From the Figure, it can be concluded that if the maximum average power price bound $\theta_{el,avg,max}$ of the analysis is set above 110 euros per Mwh the regret analysis brings forward Reversible SOE (NG) as most favourable configuration. For a maximum bound above 150 euros per Mwh, rSOE ($H_2$) is more favourable than SOE. This leaves the final conclusion on the most favourable configuration open for discussion.

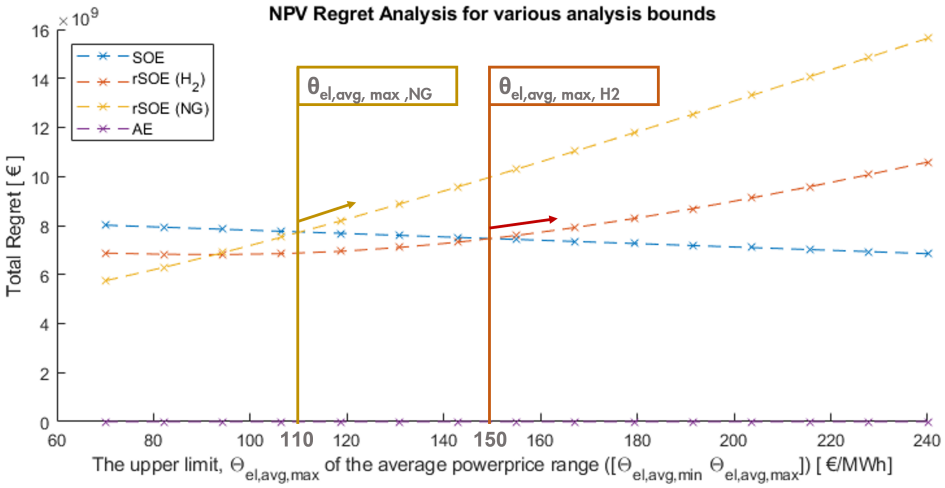


Figure 4.8: Total regret per configuration for various ranges of average power price $[\theta_{el,avg,min}, \theta_{el,avg,max}]$, varied by $\theta_{el,avg,max}$. It indicates how the final result of the regret analysis depends on analysis bounds.

### FC to EC Profit-Isolines

The power price scenarios are determined by fixed combinations of normalised standard deviation $\sigma_{Set}$ and average power price $\theta_{el,avg,set}$, as presented in Table 3.6. As reversibility is strongly influenced by power price, a deeper analysis on the parameters driving the power price scenarios is desired. The relationship between the average power price, power price volatility, and the profitability of FC operation compared to EC operation can be visualised using isolines. Figure 4.9a presents isolines for rSOE ($H_2$), whereas Figure 4.9b displays isolines for rSOE (NG). In both Figures, data from 5 historic years (Table Table 3.5) is plotted, indicating the performance based on the average power price and normalised standard deviation for those years.

The isoline plots demonstrate that higher volatility ($\sigma$) and average power price ($\theta_{el,avg}$) are beneficial for the TEF of reversible systems. By comparing the two isoline plots, it can be observed that the reward for FC operation,$\theta_{el}$, needs to be significantly higher for rSOE ($H_2$) than for rSOE (NG) to achieve the same share of FC profits. The green boxes depict this in Figure 4.9.

The difference in gradient between the two isoline figures arises from the greater impact of volatility on rSOE ($H_2$) compared to rSOE (NG) at the same price level. For hydrogen-based rSOE, the average prices plotted are mostly below the switch price of 163 euros per MWh. Therefore, volatility plays a crucial role in exceeding the switch price. In contrast, for natural gas-based rSOE, most of the isolines lie above the switch price of 63 euros per MWh, reducing the impact of volatility.

Note that the FC contribution margin in these isolines consists of the total FC benefits, including FC profits or losses and the positive effect of preventing HS loss. As a reminder, the cyan bars in Figure C.1 indicate the prevented HS loss as it is a beneficial outcome of operating FC systems even during loss-making periods.

**Conclusions on Power Price Scenario Analysis**

- Reversibility hedges against high power prices.
- SOE is most favourable in the Low power price scenario.
- rSOE (NG) shows relative improvements as of the Mid power price scenario.
- rSOE ($H_2$) requires the High power price scenario to show relative improvements.

In-depth Analysis

- There exist certain "break-even power price-points" $\Theta_{el,BE,X}$, above which rSOE (X) brings improved feasibility compared to regular SOE.
- $\Theta_{el,BE,NG}$ lies at 73 euro per MWh and $\Theta_{el,BE,H_2}$ at 108 euro per MWh
- The "break-even power price-points" are dependent on the secondary feedstock price.
- Isolines for NG and $H_2$ based rSOE show how feasibility improvement by reversibility is positively influenced by increasing price volatility and high average power prices.

## 4.3.3. CAPEX Scenarios

The configurations were compared under three CAPEX scenarios listed in Table 3.3. From the KPI plots in Figure 4.10, it can be concluded that the relative feasibility change resulting from reversibility is minimal. The difference in system CAPEX between the solid-oxide configurations is small, as presented by the values in Table 2.2. Resulting, the CAPEX scenarios have limited relative impact on the configuraitons, resulting in a small relative feasibility change.

In absolute terms, in order for the project to be profitable in this specific use-case, a Future Optimistic CAPEX scenario is required, as it leads to both normalised CAPEX-Targets larger than 1 and positive NPV. The normalised CAPEX exceeding 1 means the expected future CAPEX is lower than the CAPEX-Target. Furthermore, in the NPV plot, although small, there is an alteration in the order of configuration feasibility. This can be attributed to the steeper learning curves of solid oxide configurations, which also have a larger impact as their system CAPEX is higher.

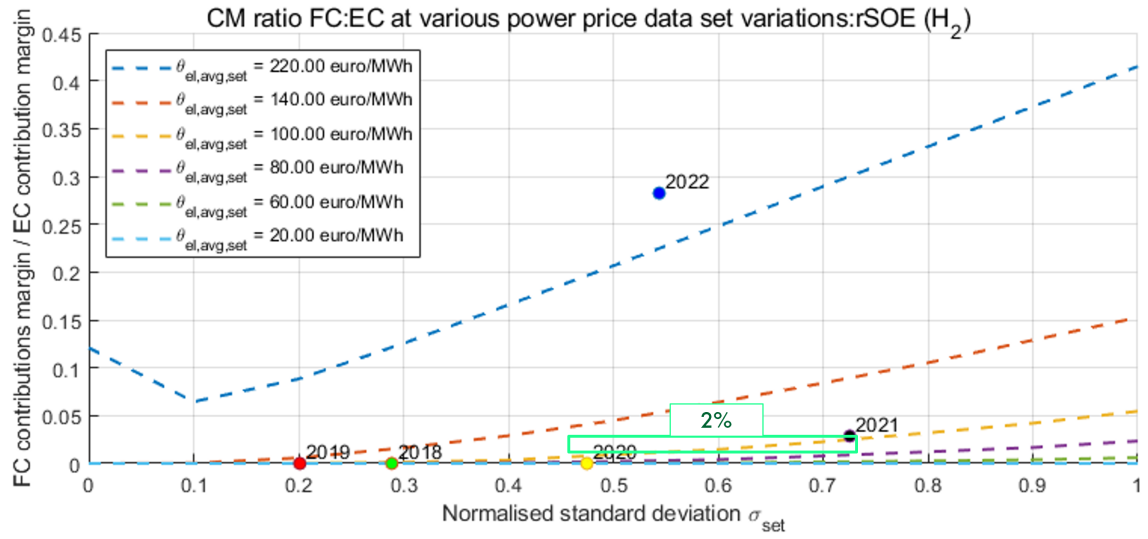


(a)

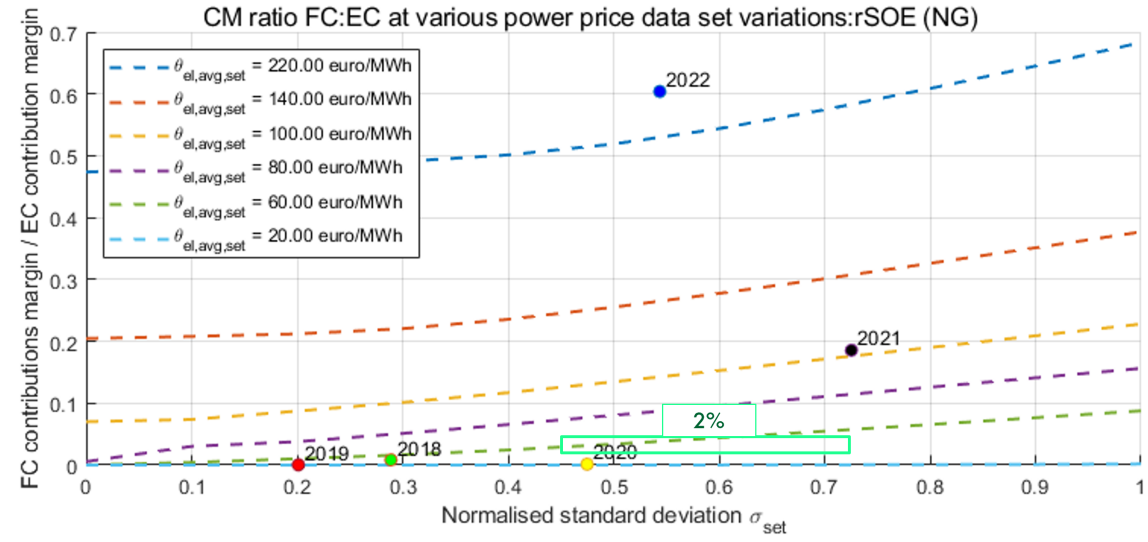


(b)

Figure 4.9: FC to EC contribution margin ratio behavior as a function of average power price and normalised standard deviation for the (a) rSOE ($H_2$) and (b) rSOE (NG) configuration. The green boxes indicate that a 2% FC profit is reached at 100 euros per MWh for $H_2$, whereas less than 60 euros per MWh is sufficient for the NG-based configuration.

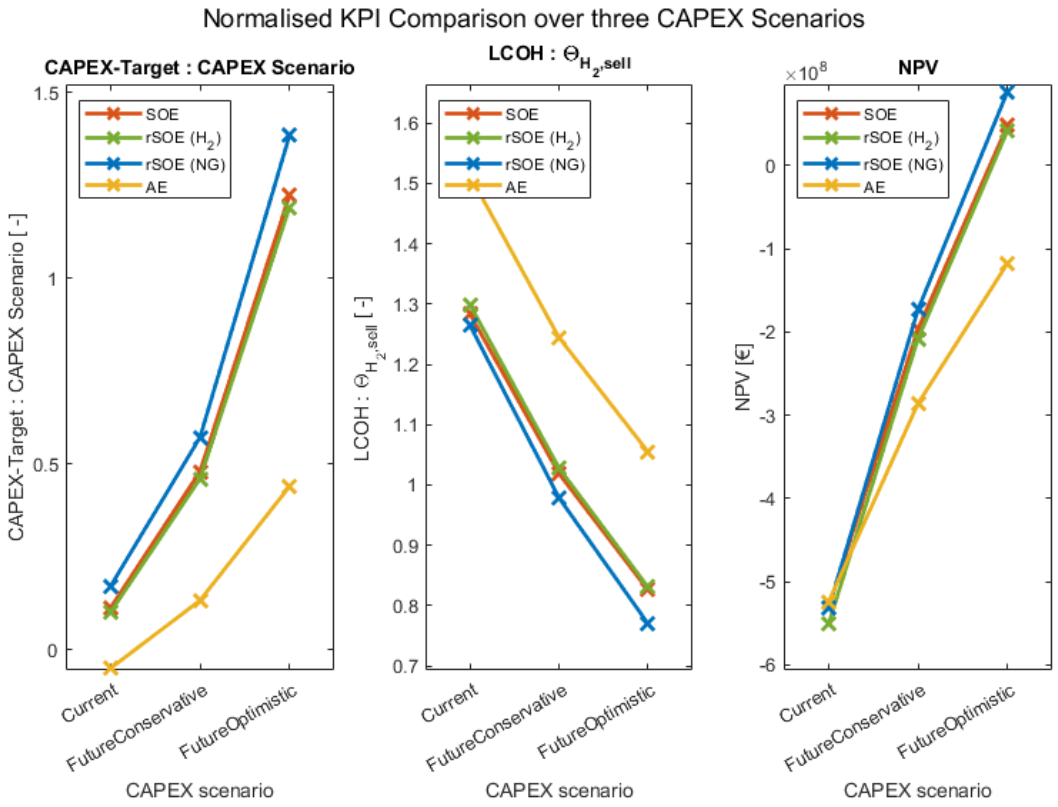


Figure 4.10: Normalised KPI-based configuration comparison for three CAPEX scenarios, showing a strong general feasibility improvement. However, relative feasibility improvements by reversibility are small. Note: The line connecting the markers is a guide to the eye

The future optimistic CAPEX scenario causes the LCOH to decrease by 36%. This brings the LCOH below the modelled hydrogen sales price, indicated by sub-one normalised LCOH values. This effect on LCOH is brought through both OPEX and CAPEX, as OPEX implicitly depends on CAPEX. More detailed LCOH representation under the CAPEX scenarios is depicted in the Appendix Figure C.6a.

**Conclusions on CAPEX Scenario Analysis**

- Relative feasibility change between configurations under CAPEX scenarios is small due to the small system CAPEX differences, as presented in Table 2.2.
- In absolute terms, the Future Optimistic CAPEX scenario results in favourable KPIs, namely a NPV larger than 0, an LCOH smaller than $\theta_{H_2,sell}$ and CAPEX-Target above the CAPEX projections from Table 2.3.
- The CAPEX reduction affects the LCOH through both the OPEX and CAPEX, leading to a total reduction of 41%.

### 4.3.4. Grid Fee Scenarios

As described in subsection 3.4.2, three grid fee scenarios were studied. The scenarios consist of different required grid connection capacities, outlined in Table 3.4. Figure 4.11 displays the normalised LCOH for all configurations under the three scenarios, with the grid fee is included in the fixed OPEX.
The differentiated grid fee scenario, which was based on a policy advisory report from Prinsen et al. [69], favours non-reversible systems. The share of fixed opex in the total LCOH, indicated by the black text in the green stacks, increases significantly more for the rSOE ($H_2$) and rSOE (NG) cases than the SOE case. In that scenario SOE has a slightly lower LCOH. It must be noted that in this stage, at least in the Netherlands, this scenario is practically unfeasible under current regulation [69, 48]

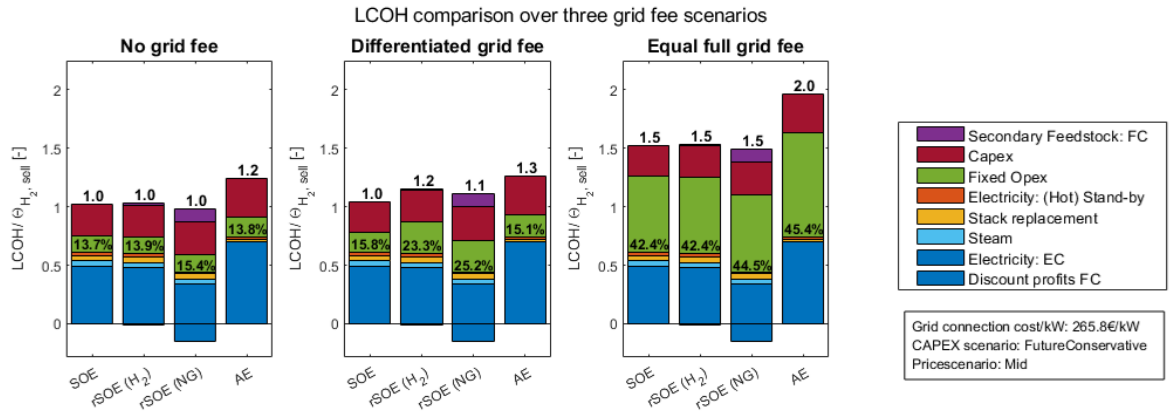


Figure 4.11: Normalised LCOH Comparison for three grid fee scenarios. LCOH values are round to one decimal.

In terms of absolute feasibility, the impact of the full grid fee scenario is enormous, increasing the total LCOH with 50% to an LCOH 1.5 times the hydrogen selling price. A normalised LCOH larger than one indicates the project is loss-making. From this scenario the general conclusion is drawn that the grid fee is a major influence on the LCOH and must be minimised for the project to be feasible.

**Results on Grid Fee Scenario Analysis**

- A differentiated grid fee favours non-reversible systems as a smaller grid connection is required.
- The grid fee is a major influence on the LCOH and must be minimised for the projects' feasibility, as the full grid fee scenario raises the LCOH from 1 to 1.5 times to hydrogen selling price.

## 4.4. Sensitivity Analysis

The previous section studied the effect of three scenarios on the feasibility change by reversibility. This section shows the sensitivity study results performed to reveal the feasibility change by reversibility under parameter change. The sensitivity analysis measured the CAPEX-Target, while thirty parameters were adjusted from their baseline values one by one. This was done for each configuration and power price scenario leading to the "Tornado Charts" displayed in the Appendix C.3. The sensitivity figures are made up of two tornado charts. The right shows the percentual deviation from the CAPEX-Target for a -10% and +10% deviation. The left shows the absolute deviations for certain expected parameter deviations, which are listed in Appendix Table B.2.

The sensitivity results can be used for two purposes. The first is to use it to measure the effect of a changing parameter on the absolute feasibility of a configuration. The second is to study the effect of the parameter change on the relative feasibility between configurations. The latter is of main interest as it aligns with the sub-question: "Under what parameter deviations does reversibility bring improved techno-economic feasibility compared to SOE?".

To answer that question, the sensitivity results from the Appendix were compared. Eleven parameters were identified as significantly impacting the relative feasibility when deviated from their baseline values. The parameters with the largest relative changes were related to electricity sell price, secondary feedstock price, and power profile volatility. As the effect of the electricity sell price $\theta_{el,sell}$ was already extensively discussed in subsection 4.3.1, subsection 4.4.1 directly moves on to the relevant parameters related to the secondary feedstock price, including $\theta_{H_2,sell}$, $\theta_{NG,buy}$, and $\theta_{CO_2,penalty}$. Then, subsection 4.4.2 addresses the findings for parameters related to power profile volatility, such as windfarm capacity and PPA windfarm. The remaining parameters with relative feasibility impact are discussed in subsection 4.4.3. Additionally, subsection 4.4.4 present the insensitivity to ramp rate and transition time deviations. Lastly, in subsection 4.4.5, there is a brief discussion on the dependency of the sensitivity results on the power price scenario.

### 4.4.1. Secondary Feedstock Price

Within expected deviations, the CAPEX-Target is most sensitive to the hydrogen sell price, as it directly impacts FC and EC profits. The parameter has a direct and indirect effect on relative feasibility. It directly affects the costs of FC operation and indirectly affects the number of FC hours due to the relation with the switch-price.

Up to a certain "break-even secondary feedstock price-point" $\Theta_{X,buy,BE}$ reversibility brings feasibility improvement compared to SOE. For the rSOE ($H_2$) configuration, this implies that the hydrogen sell price $\theta_{H_2,sell}$ must be below a certain value. As indicated in Figure 4.12, this price point lies between 1 and 3.5 euros per kg for this use-case. The break-even point is highly dependent on the power price scenario.

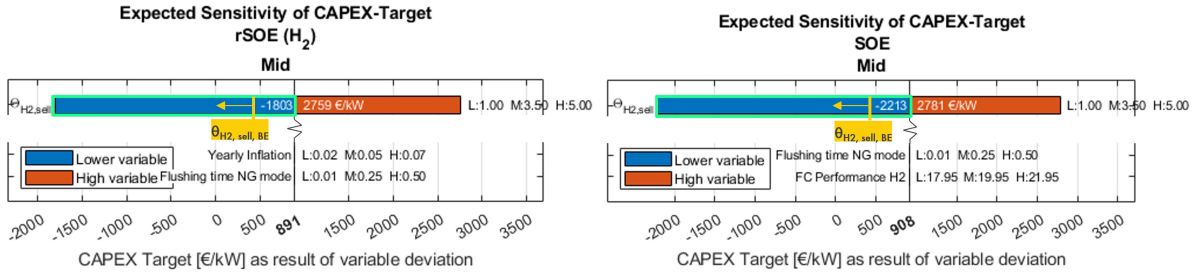


Figure 4.12: Selection of the sensitivity-analysis result-comparison for rSOE ($H_2$) and SOE under the Mid power price scenario. Indicating the "break-even hydrogen price-point" $\theta_{H_2,sell,BE}$ below which reversibility brings feasibility improvement compared to regular SOE. Spreads are rounded to multiple integers of 50.

Notwithstanding the exact break-even point, Figure 4.15 hydrogen-based rSOE hedges SOE against low hydrogen prices. The Figure compares the Tornado Chart of rSOE ($H_2$) with SOE and indicates that the negative response to hydrogen price deviation is less extreme for rSOE ($H_2$) than for SOE. This means increased FC profits due to a lower hydrogen price increasingly damp the decreasing EC profits due to that lower hydrogen price.

This damping is clearly illustrated by Figure 4.13, in which the contribution margins (CM) are

plotted for each operational mode, in each pricescenario. It can be concluded that the rSOE ($H_2$) plant in the Low scenario completely acts as a non-reversible SOE plant, as no profit is made from FC operation. The purple markings indicate how, compared to this Low scenario, reversibility can strongly increase the CAPEX Target the low hydrogen price region. This positive effect fades away with increasing hydrogen price, as can be seen by the decaying dashed line indicating CM from FC, which can be contributed to the effect of the hydrogen price on the switch-price. In the Figure, the hydrogen price-point at which the CAPEX-Targets in the Low and Mid power price scenario are equal, lies around 2 euros per kg, as marked in green.This means the positive effect of reversibility fades away after this point.

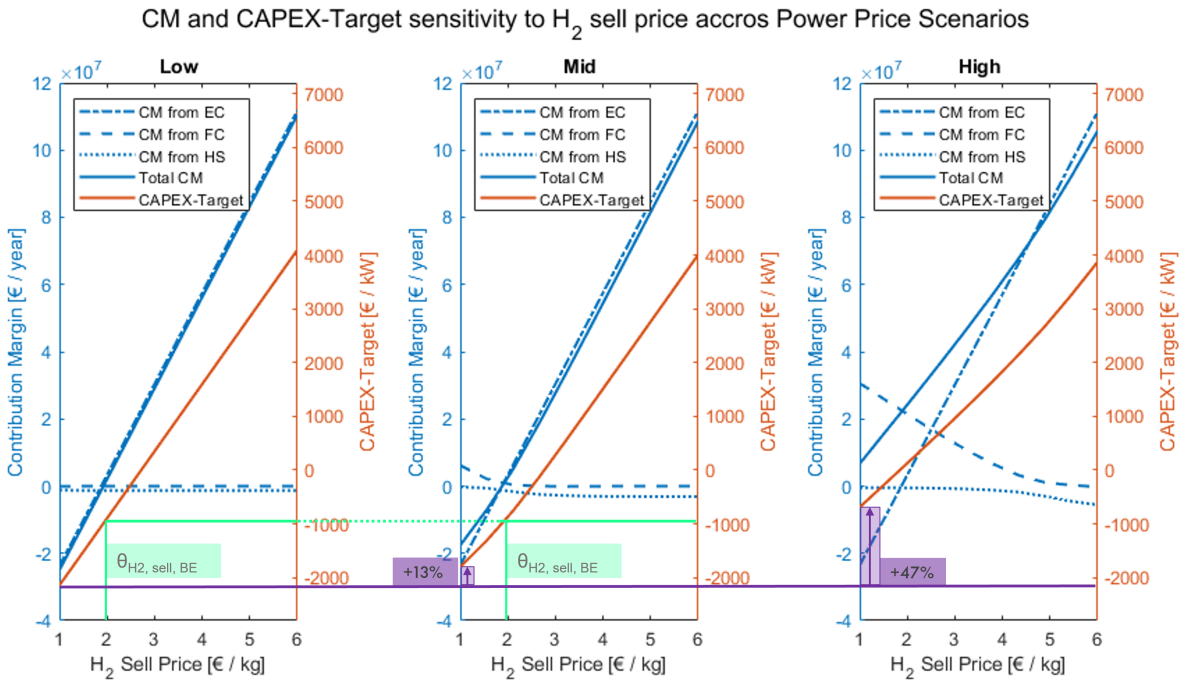


Figure 4.13: The contribution margins of the operational modes and CAPEX-Target against hydrogen price for three power price scenarios. The damping effect (Purple) of FC operation increases with lower hydrogen prices and rising electricity prices. Above a certain $\Theta_{H_2,sell,BE}$ (Green) damping effect disappears.

In NG-based rSOE, the hedging effect compared to SOE is not present as the system has no benefit from a lower hydrogen price. This implies that compared to rSOE ($H_2$), rSOE (NG) is more negatively sensitive to lower hydrogen prices as is observed in Figure 4.14. However, the comparison also shows that high hydrogen price deviations cause larger positive CAPEX-Target sensitivity for rSOE (NG) compared to rSOE ($H_2$). This is the case, because in rSOE (NG), increased hydrogen prices have a positive effect on EC profit and do not negatively affect FC profits, where in rSOE ($H_2$) high hydrogen prices do negatively affect FC profits.

### Natural Gas Price

The natural gas-based reversible configuration is sensitive to the natural gas price and carbon penalty height. Within the expected deviations, under baseline conditions, rSOE (NG) remains the preferred configuration, as can be seen by comparing (Figure C.15 and Figure C.17). However, also for natural gas, there exists a certain "break-even secondary feedstock price-point" $\Theta_{NG,buy,BE}$, outside the boundaries of this sensitivity study.

The other configurations are not sensitive to the natural gas price and carbon penalty, which increases the amount of uncertain parameters compared to other configurations. On top of that, the natural gas price is a parameter susceptible to geographic tensions. However, once more, it does not cause alarming, relative or absolute feasibility deterioration within the expected deviations.

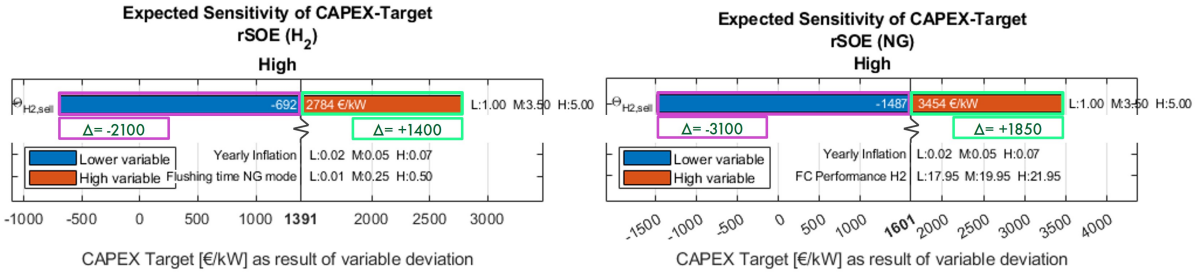


Figure 4.14: Selection of the sensitivity-analysis result-comparison for rSOE ($H_2$) and rSOE (NG) under the High price scenario, showing the low hydrogen price hedge of rSOE ($H_2$) (Purple) and the high power price hedge of rSOE (NG) (green). Spreads are rounded to multiple integers of 50

### 4.4.2. PPA and Windfarm Capacity

The sensitivity results point out that reversibility shows relative feasibility improvement for power profile inconsistency and volatility. This power profile inconsistency is indirectly indicated by the parameters PPA and windfarm capacity. An increasing PPA or decreasing windfarm capacity harms both SOE and rSOE profitability. However, the negative effect on rSOE profitability is significantly lower, especially for a High power price scenario. This can be seen by comparing the negative CAPEX sensitivities for PPA and windfarm capacity in Figure 4.15, resulting in a 45% risk reduction to the high PPA deviation in the High power price scenario.

It must be noted that this effect is not present in Low and Mid power price scenarios. However, it acknowledges the hypothesis that reversibility hedges TEP against the negative effects of volatile power profile inputs.

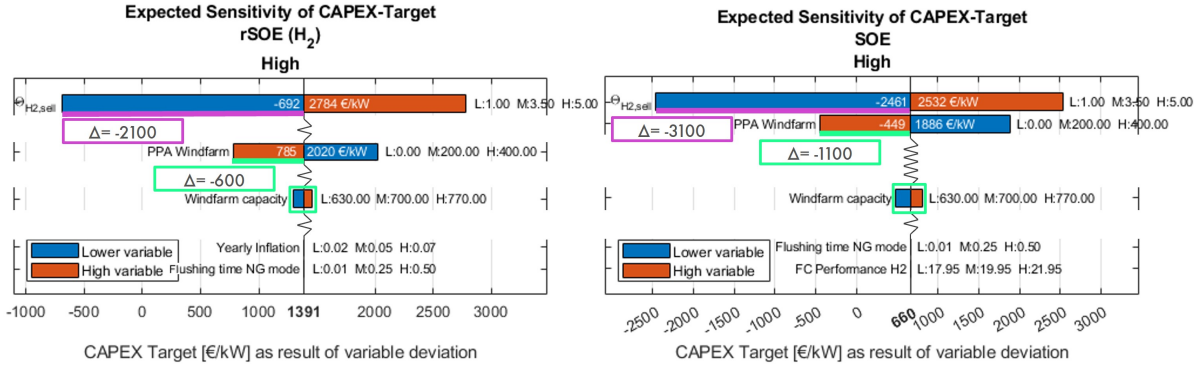


Figure 4.15: Selection of the sensitivity analysis result comparison for rSOE ($H_2$) and SOE under the high price scenario, showing reduced negative sensitivity to hydrogen price (purple) and power profile volatility (green). Spreads are rounded to multiple integers of 50.

### 4.4.3. Parameters with Small Relative Feasibility Effect

Certain parameters cause relative feasibility changes but do not change the overall feasibility order of the configurations. The effect on CAPEX-Target is small within the expected deviations of their baseline values.

#### Hot-Standby Energy Consumption

Hot-standby energy consumption $f_{HS}$ has an effect on relative feasibility. It affects feasibility directly through the HS costs and indirectly through the inverse effect on the switch-price. Reversible configurations are less sensitive to this parameter due to the reduced amount of HS hours, as can be seen by comparing (Figure C.20 vs Figure C.19). This means reversible systems are more compatible with use-cases or designs with higher hot-standby energy consumption.

#### FC/EC Ratio

The FC/EC ratio directly affects the FC capacity. Therefore, an increasing FC/EC ratio improves the power of reversibility to improve feasibility as the volumes of produced electricity increase. The effect of

the FC/EC ratio is significant in the case where the operational schedule already has a significant share of FC operation, for example, in higher price scenarios or/and an NG-based configuration Figure C.20 and Figure C.21. Within the bounds of the expected deviation, it is not a parameter that is likely to bring decision-changing effects.

#### FC Performance

The FC performance of both rSOE ($H_2$) and rSOE (NG) has a direct and indirect effect on the feasibility improvement by reversibility. The direct effect lies in the reduced costs, as less secondary feedstock is required for the same amount of power produced. The indirect effect lies in the switch-price. The equation for the switch-price was introduced in the methodology and reads

$$\theta_{switch,t} = \frac{U_{X,t}\theta_{X,buy}}{Y_{el,t} + f_{HS}U_{el,max,EC}}, \tag{4.1}$$

with

$$U_{X,t} = \frac{P_{max,FC}}{LHV_X\eta_X}, \tag{4.2}$$

the used amount of secondary feedstock X. The FC performance as is discussed in this subsection appears in Equation 4.2 as, $\eta_X$. A higher efficiency results in a lower switch-price, resulting in more hours of FC operation, benefiting reversibility. The proportional effect of the FC efficiency to the TEP can be seen from Figure C.17. The sensitivity analysis of the NG configuration in the Mid power price scenario, Figure C.17, shows that a 10% efficiency increase results in a 4% TEP increase.

#### Hydrogen Sell to Buy Ratio

Figure C.20 shows that a lower hydrogen sell to buy ratio, has a negative effect on the feasibility of the rSOE ($H_2$) configuration. Logically, the lower the hydrogen sell to buy ratio, the higher the cost of hydrogen for FC operation. The ratio depends on the hydrogen grids' transmission costs, tax, and markup. At decreasing ratios, the economics of (partly) on-site storage becomes more relevant. However, further analysis of this effect and opportunity is left out of the scope of this research.

### 4.4.4. Insensitivity to Ramp Rates and Transition Time

In all configurations, the expected deviations in ramp rates $R_{up/down,FC/EC}$, switchtime $t_{switch}$ from the baseline conditions have a limited effect on the TEP and, therefore on relative feasibility. This can be observed in Appendix Figure C.23 and is caused by the hourly time resolution of the operational strategy. The ramprates are high enough to ramp to full capacity, within the hour. To stress the insensitivity, an unrealistic 2-hour switchtime is modelled and only causes a 10% CAPEX-Target decrease, Figure C.23. The same insensitivity hold for the flushtime $t_{flush}$ in natural gas-based FC operation, Figure C.21.

For the NG-based reversible system ramp rates from EC to FC can be constaint by the ramping of the pre-reformer. A pre-reformer generally has slow ramp rates due to the required time to heat up. Therefore the system should be designed so that the pre-reforming happens inside the hot-box, which is kept at operating temperature.

For this application with an hourly resolution, the TEP is insensitive to the parameters mentioned above. However, these transition times and ramp rates may become important when stricter requirements on response and ramp-time come into play, for example on the balancing market, as discussed in subsection 4.3.2.

### 4.4.5. Power price Dependency of the Sensitivity

It must be noted that the size of the sensitivity is strongly dependent on the power price scenario. This is observed comparing rSOE ($H_2$) sensitivity versus SOE sensitivity, for the Mid (Appendix Figure C.16) and High (Appendix Figure C.20) power price scenarios. The relative feasibility effects discussed in the previous sections, are enlarged in higher power price scenarios. This effect arises from the increased number of hours in FC mode. This reinforces the conclusion made in Table 3.4.3 that a certain reward for power production is required for reversibility to benefit SOE feasibility.

Conclusions on the Sensitivity Analysis

- The price of secondary feedstock must be below a certain "break-even secondary feedstock price-point" $\Theta_{X,sell,BE}$ for reversibility to bring feasibility improvement. For rSOE $H_2$ this break-even point lies around 2 euros per kg.
- rSOE ($H_2$) hedges SOE and rSOE (NG) feasibility against low hydrogen prices as FC operation is short on hydrogen price.
- Compared to rSOE($H_2$), rSOE(NG) hedges against high hydrogen prices.
- Reversibility shows relative feasibility improvement for power profile inconsistency and volatility, though $PPA$ and windfarm capacity.
- Deviations in hot-standby energy consumption, FC/EC ratio, FC performance and hydrogen sell to buy ratio cause a small relative feasibility change.

## 4.5. Feasibility Improvement by Hedging

This study aims to answer the question: "Can Reversible operation improve the techno-economic feasibility of a large-scale open-system SOE, and if so, under what conditions?". Regardsless of the absolute KPI improvement, used to indicate techno-economic feasibility, reversibility can mitigate risks of regular large-scale SOE, by providing a hedge against uncertain parameters. The feasibility of the fuel cell and electrolyser complement each other for these parameters. rSOE ($H_2$) acted as a hedge against high power prices, low hydrogen prices, power profile inconsistency, and power price volatility when compared to regular SOE. These hedges were mentioned in the Scenario and Sensitivity Analysis and are emphasised in this section for clarity.

- The high power price hedge is visual in Figure 4.5. The SOE and rSOE ($H_2$) CAPEX-Target are roughly equal in the Mid scenario (900 euros / kW). In the High power price scenario, the rSOE ($H_2$) configurations' CAPEX-Target is 130% higher than in SOE (1400 vs 600 euros / kW). Note that, this spread would further increase in case 1) the electricity price for hydrogen production rises along with this electricity sales price or 2) FC operation can be prioritised over EC operation.
- The low hydrogen price hedge was explained by Figure 4.15, leading to a 32% risk reduction compared to SOE under the low hydrogen price deviation (Under the High power price scenario). As was shown by Figure 4.14, rSOE (NG) does not hedge against low hydrogen prices, however, it does show improved performance in high hydrogen prices, compared to rSOE ($H_2$).
- The power profile hedge was also explained by Figure 4.15, leading to a 45% risk reduction to high PPA deviation (Under the High power price scenario).
- Lastly, the hedge against power price volatility is shown in Figure 4.16. The green arrow serves as an example of the magnitude of the power price volatility dependency. For the 100 euros per Mwh isoline, a 0.3 to 0.8 normalised standard deviation increase causes a factor 25 FC profit increase.

Conclusions on Feasibility improvement by hedging

- Reversibility can mitigate risks of regular large-scale SOE, by providing a hedge against uncertain parameters.
- In rSOE ($H_2$), reversibility hedged against high power prices, low hydrogen prices, power profile inconsistency, and power price volatility compared to regular SOE.
- The rSOE (NG) configuration exhibits the same hedges, except for the low hydrogen price hedge.

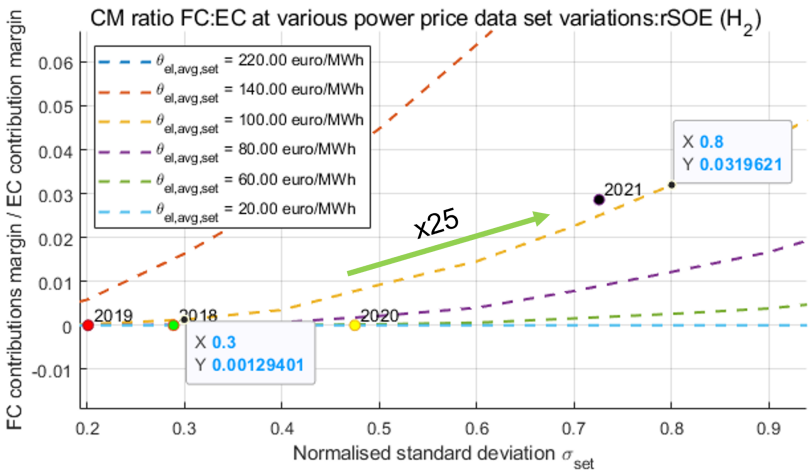


Figure 4.16: The impact of power price volatility on FC profits compared to EC profits, shown by a zoomed-in isoline plot. The green arrow indicates the magnitude of the dependency. Historic years 2018-2021 are plotted for reference.

## 4.6. Feasibility Improvement under External Conditions

Results from the Scenario and Sensitivity analysis show that reversibility can significantly improve the TEP of large-scale SOE. However, for reversibility to bring these improvements, certain crucial and beneficial external conditions were found to be essential. External conditions relate to parameters outside the system and outside the power of design. Crucial conditions can make or break the feasibility improvement by reversibility by themselves, meaning only meeting one of these conditions is necessary. Beneficial conditions only have a beneficial effect on feasibility improvement by reversibility. The crucial conditions are described in subsection 4.6.1. Beneficial external conditions impacting the relative feasibility are discussed in subsection 4.6.2.

### 4.6.1. Choice Ratio

In the power price scenario analysis, subsection 4.3.1, it was revealed that there exists a "break-even power price-point" $\Theta_{el,BE,X}$, above which reversible systems based on secondary feedstock X become more economically attractive than regular SOE. The absolute value of this point heavily depends on the switch price and, consequently, the secondary feedstock price.

Additionally, in the sensitivity analysis, section 4.4, it was found that there is a certain "break-even secondary feedstock price-point" $\Theta_{X,buy,BE}$ below which reversibility brings feasibility improvement compared to SOE. The average power price strongly influences the absolute value of this break-even point.

It is concluded that for reversibility to bring feasibility improvements, a certain relation must exist between the power price and the secondary feedstock price. The choice ratio, $R_X$, is introduced to be the ratio between the average power price of a dataset $\theta_{el,avg}$, and the switch-price $\theta_{switch,X}$. Consequently, the choice ratio describes a relation between external parameters to which the feasibility is most sensitive, power price and feedstock price.

$$R_X = \theta_{el,avg}/\theta_{switch,X} \tag{4.3}$$

The choice ratio $R_x$ must be larger than the break-even-choice ratio, $R_{BE,X}$, for reversibility to bring feasibility improvements compared to SOE. The feasibility choice ratio is defined as,

$$R_{BE,X} = \Theta_{el,BE,X}/\theta_{switch,X} \tag{4.4}$$

For the use-case studied and baseline conditions, the switch-prices, $\theta_{swtich,NG}$ and $\theta_{switch,H_2}$, are respectively 63 and 163 euros per MWh. As schematically represented in Figure 4.17, this implies that the "break-even choice ratios" $R_{BE,NG}$ and $R_{BE,H_2}$, are 1.16 and 0.66. These results follow from the regret analysis in which the analysed standard deviation range lies between 0.4 and 0.7. This means that under the uncertainty where in this range the normalised stand deviation lies, reversibility is the best choice for a choice ratio above $R_{BE,X}$.

For the hydrogen-based rSOE the average power price can be significantly lower than the switch-price, while this is not the case in the NG-based rSOE. This can be explained by the larger effect the normalised standard deviation has in higher power price regions.

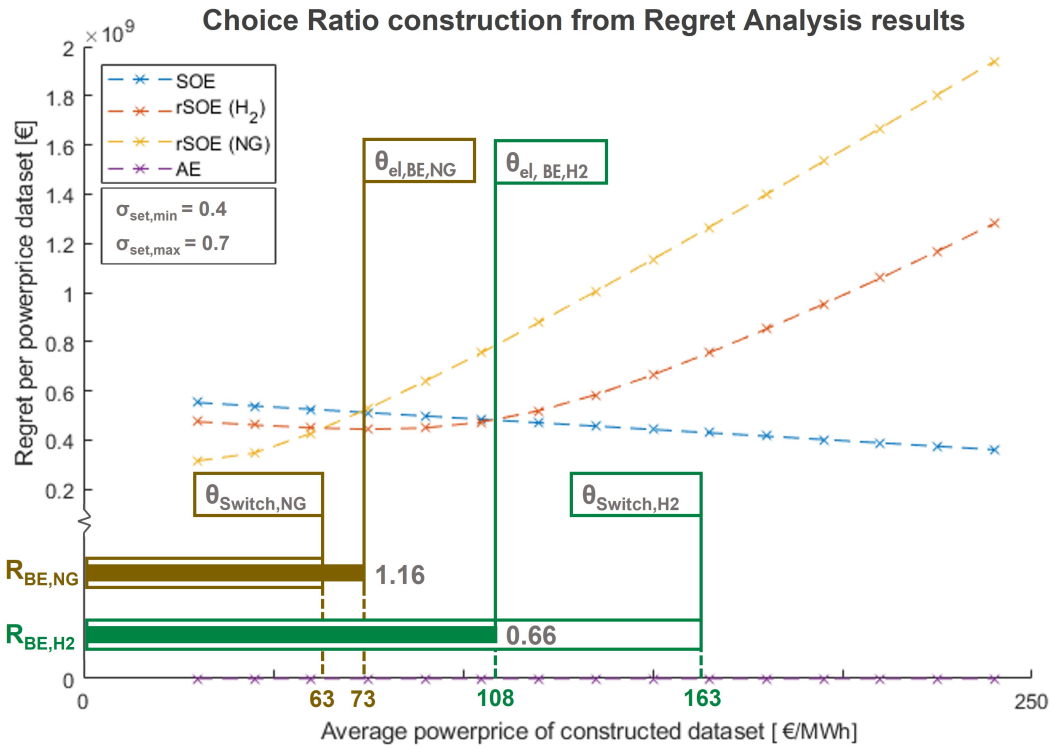


Figure 4.17: Schematic representation of the ratio between "break-even power price-point" $\Theta_{el,BE,X}$ and the switch-price $\theta_{switch,X}$, called the "break-even choice ratio" $R_{BE,X}$. A choice ratio above the $R_{BE,X}$, reversibility based on secondary feedstock X yields improved feasibility (For baseline conditions and a normalised standard deviation range [0.4 0.7])

### 4.6.2. Other Beneficial External Conditions

Other external conditions are beneficial for feasibility improvement by reversibility. Four of them are shortly touched on in the subsection.

#### Power Price Volatility

If the average power price lies below the switch-price, power price volatility is crucial for reversibility to bring improvement. Appendix subsection C.4.2 contains a brief view on future power prices. Due to increasing installed renewable capacity, power price volatility is expected to increase. This improves the position of reversibility in the future.

#### Power Profile Inconsistency

In a use-case that prioritises hydrogen production, as is studied in this thesis, power profile inconsistency is required to improve reversible configurations' relative feasibility. This was shown implicitly in the sensitivity analysis, as reduced negative sensitivity was observed for parameters PPA and windfarm capacity.

#### Grid Fee

Figure C.10 shows the major impact grid fee can potentially have on project feasibility. In a situation where differentiated grid connection is technically and legally possible, the reversible configurations have a disadvantage. In terms of general feasibility, the grid fee must be minimised to achieve project feasibility.

#### Hydrogen Sell to Buy Ratio

Logically, hydrogen-based reversible systems benefit from a high hydrogen sell to buy ratio. At a certain ratio, on-site storage for the self-produced hydrogen becomes interesting. More realistic estimation of the sell to buy ratio and determining this on-site storages' ideal scaling and benefits is recommended for further research.

**Conclusions on Feasibility Improvement under External Conditions**

- Relative feasibility is most sensitive to power and secondary feedstock prices. Certain break-even points for both parameters indicate the boundaries of feasibility improvement by reversibility: $\Theta_{el,BE,X}$ and $\Theta_{X,buy,BE}$.
- As these break-even points are interdependent, the choice ratio is defined as the ratio between average power price and switch-price, which implicitly holds the secondary feedstock price.
- The choice ratio must be above a "break-even choice ratio" $R_{BE,X}$ for reversibility to bring feasibility improvement.
- The "break-even choice ratios" $R_{BE,NG}$ and $R_{BE,H_2}$, are 1.16 and 0.66 for this use-case.

## 4.7. Feasibility Improvement under Internal Conditions

As discussed in the previous section, reversibility can improve the TEP of large-scale SOE under certain external conditions. Apart from external, certain crucial and beneficial internal conditions apply for reversibility to bring these improvements. Internal conditions relate to parameters inside the system and inside the power of design. Crucial conditions can make or break the feasibility improvement by reversibility by themselves, meaning meeting only one of these conditions is necessary. Beneficial conditions only have a beneficial effect on feasibility improvement by reversibility. These crucial conditions are described in subsection 4.7.1 and subsection 4.7.2. Other beneficial internal conditions impacting the relative feasibility are discussed in subsection 4.7.3.

### 4.7.1. Secondary Feedstock Choice

Under baseline conditions, choosing the NG-based configuration is crucial for reversibility to bring TEP improvement compared to regular SOE.It is evident from the results (Figure 4.5 and Figure 4.7) that NG-based rSOE brings more potential to make TEP improvements than hydrogen-based rSOE. Despite the increased CAPEX, in all scenarios except for the Low power price scenarios, rSOE (NG) shows superior KPIs compared to rSOE ($H_2$), SOE and AE. Furthermore, in the Low scenario, the differences are small. The reason for NG superiority lies in the low switch-price, as indicated in Figure 4.18.

Also, compared to $H_2$ based rSOE, NG-based rSOE hedges against high hydrogen prices, because FC operation based on natural gas does not require hydrogen. This hedge was indicated in Figure 4.14, in the Sensitivity Analysis. This can be beneficial at the start of the hydrogen economy when hydrogen prices are still too high to profitably produce electricity.
Despite the NG superiority in TEP, rSOE ($H_2$), brings some advantages compared to rSOE (NG).

- The TEP of Solid Oxide systems is most sensitive to the hydrogen sell price. As also shown by Figure 4.14, rSOE ($H_2$) hedges against the negative effect of low hydrogen prices, compared to SOE and rSOE(NG). This strongly reduces risks.
- The natural gas price and $CO_2$ costs bring additional uncertain parameters, which rSOE ($H_2$) does not have. However, within expected deviations, they do not cause alarming feasibility deterioration.
- rSOE ($H_2$) can be completely green, whereas NG-based rSOE uses a fossil source of energy. Electricity produced from it can not be sold as green electricity. In the study, this is only considered as the cost of Carbon. No differentiation is made between the price of green electricity and grey electricity. It should also be considered whether using the green hydrogen plant in a non-green way has implications for the "Green" or "Low-carbon" status of the hydrogen.


(a) Hydrogen

(b) Natural Gas

Figure 4.18: Back of the envelope relation of secondary feedstock prices to the switch-price, using Equation 4.1, to point out the advantage of natural gas due to switch-price. power price scenario levels are plotted for reference. Total system efficiency $\eta_{FC,H_2,LHV}$=50% , $\eta_{FC,H_2,LHV}$=60% , $\theta_{CO_2,buy}$=125 €/tonne ,$f_{HS}$=5%

- rSOE ($H_2$) has a less complicated plant design than rSOE (NG). The NG-based system must handle both hydrogen, steam, and syngas. Economically this is accounted for by the increased CAPEX. As mentioned in the steady state model methodology, subsection 3.1.6, an additional flushing time is taken into account to flush the system from FC to EC operation. As studies in the sensitivity analysis demonstrate, this additional flushing time does not result in feasibility deterioration. However, in other use-case it can bring implications, which is further discussed in subsection 4.7.2.

It can be concluded that rSOE (NG) shows superior TEP, however prominent advantages for rSOE ($H_2$) exist. A hybrid system or system designed for retrofit can capture the benefits of both secondary feedstock. It is recommended to determine the technical and economic feasibility improvement of designing such a system.

### 4.7.2. Balancing Market Conditions

Designing according to balancing market requirements is crucial for enhancing the feasibility of reversible systems. As concluded in section 4.6, the reward for FC operation must exceed a certain "break-even power price-point" $\theta_{R,X}$ to make reversibility a feasible option. As represented in the Mid power price scenario, wholesale market prices do not provide significant feasibility improvement compared to regular SOE systems. Therefore, exploring the potential of the balancing market becomes crucial.

#### Balancing Market Background

The balancing market generally consists of a subset of different markets. These different markets vary in function and, as a result of that, in requirements. As mentioned in subsection 2.6.2, the balancing market in the Netherlands is built-up out of the FCR, aFRR and mFFR. Different requirements exist to act on each submarket, as listed in Figure 4.19. The feasibility of these requirements is discussed later.

The balancing market accepts bids for both up-balancing and down-balancing. Up-balancing can be done by supplying electricity to the grid or curtailing consumption. Curtailing would mean ramping down the electrolyser, producing less hydrogen. Supplying electricity can be done using FC mode. There exist different strategies to bid on the balancing market. An option is to bid the FC capacity on the day-ahead market and, if the bid is not accepted, to bid in on the balancing market. Another option is to bid only a share of the FC capacity on the day-ahead market and hold the remaining share for the balancing market.

Down-balancing can be done by consuming electricity from the grid. For the use-case of this study, that would mean being paid to ramp up the electrolyser and produce hydrogen. As the goal of the asset in this use-case is to produce green hydrogen, the use of grid electricity for hydrogen production is left out of scope.

| Sub-market | FCR | aFRR | mFRR |
|---|---|---|---|
| Minimum bid [MW] | 1 | 1 | 10 |
| Response time | seconds | 30s-5min | 5-60min |
| Ramptime to bid capacity | < 1 min | Up: 10 min Down: 15 min | Up: 10 min Down: 15 min |

Figure 4.19: The requirements for the Dutch Balancing sub-markets [84, 42]. The Color coding indicates the feasibility of these requirements.

### Balancing Market Potential

The balancing market offers the potential to exceed the "break-even power price point" for reversible systems (X). Historical data from the balancing market demonstrates this potential. For thirteen months from May 2022 to May 2023 minute-based balancing market bids from Tennet [85] were analysed. May 2022, a representative month, shows that the average power price on the balancing market was nearly 50% higher than the average day-ahead market price. Additionally, up-balancing capacity was auctioned approximately 39% of the time. Over the 13 months, on average, the price increase lies at 53% and the required timeshare of up-balancing at 41%. Data for all months is shown in Appendix C.4.1.

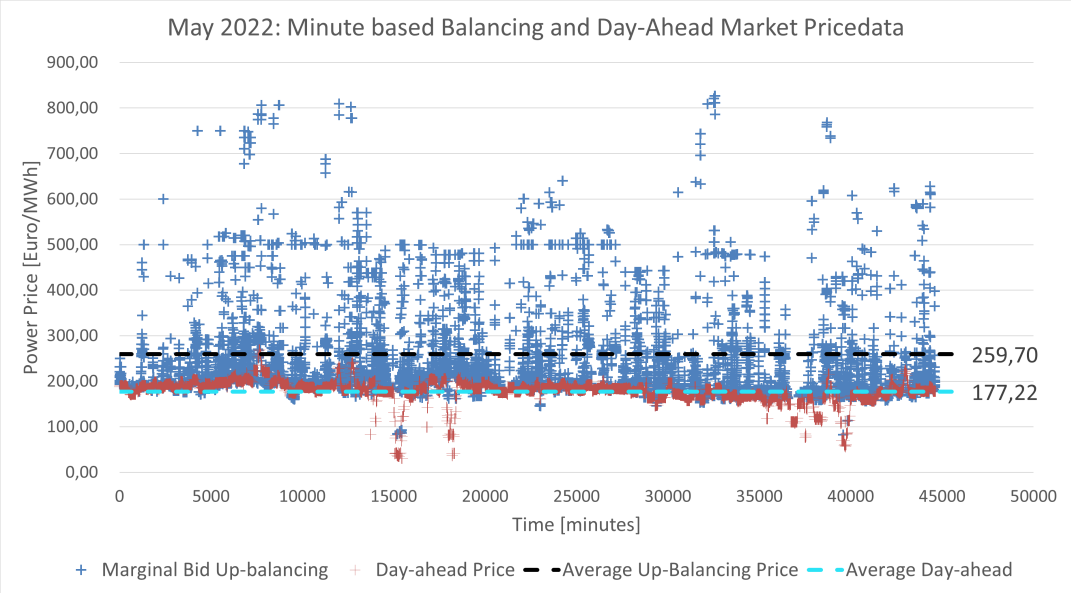


Figure 4.20: Market clearing prices of the Day-Ahead and Balancing markets for a representative month, May 2022, in the Netherlands [85]. The plot indicates the difference in average bid height

### Balancing Market Feasibility

Certain additional boundary conditions apply for balancing market operation, as listed in Figure 4.19. A short analysis leads to the impression that the requirements of the aFRR and mFRR are achievable, shown by the color coding in the figure. Firstly the minimum capacity is achievable.

Secondly, the response time depends on the transition time. As the stacks can reverse within seconds [58], this time is limited by switching the BoP to reverse mode. The aFRR and mFRR response times can be met. If the aFRR requirements must be met, the BoP should be designed to have a response time under 5 minutes.

Finally, the ramp time requirements of the aFRR and mFRR can be met in two ways. The most straightforward, by designing the system that ramps at a ramp rate reaching full capacity within the 10 minutes. Another way to meet the ramping requirements is by bidding in only a part of the nominal capacity by deploying several modules at part capacity, which logically also takes a shorter time.

Ramp rates of rSOE systems reported in the literature vary with system design. Motylinski et al. [58] reports ramp rates at 5 $A$ per minute for a 100 $A$ system with an acceptable temperature change rate, bringing no risk of damage to the elements and components in the stack. This comes down to

5 % per minute, so 20 minutes to full EC capacity. For this thesis, the assumption is that the FC capacity makes up a quarter of the EC capacity. The same ramp rate would result in 20% per minute, so 5 minutes to full FC capacity. Based on this study, ramping at 10% per minute FC capacity seems achievable. A workaround, as explained in the previous paragraph, is bidding a lower volume than full capacity, as a lower bid decreases the ramp time to reach that bid.

Flushing time in NG-based FC operation delays the switch from FC to EC. This does not hamper balancing market applicability as it does not delay power supply or demand. However, the increased ramping rates caused by pre-reformer ramp rates could prevent the NG-based rSOE configuration from applicable to the balancing market. A design requirement is to include the pre-reformer in the hot-box to prevent low ramp rates.

### 4.7.3. Other Beneficial Internal Conditions

Other internal conditions are beneficial for feasibility improvement by reversibility. Three of them are shortly touched on in the subsection.

#### Intermittent or Volatile Power Supply

Intermittent or volatile power profile design is beneficial for feasibility improvement by reversibility. Compared to SOE, reversibility shows improved TEF in more volatile and inconsistent power profile scenarios, as implicitly shown by the PPA and windfarm capacity in subsection 4.4.2. The use-case can be designed such that the power profile is inconsistent, to exploit the potential of reversibility. For example as is done by the PPA in this study, by using the consistent part of the profile for a more profitable purpose and the more inconsistent low value part for hydrogen production.

#### Thermal Design Optimisation

The Sensitivity study shows that increasing the FC performance contributes to feasibility improvement by reversibility. The FC performance should be optimised to exploit the potential of reversibility. As SOFC technology has been under development for quite some time, stack efficiency is not expected to increase with more than 10 percent in the near future[79]. However, compared to the plant design used in this study, system efficiency improvements can be made by integrating residue heat flows as explained in subsection 3.1.6. This would improve the position of reversibility compared to non-reversible systems.

#### Module-Based Schedule Optimisation

A large-scale rSOE or SOE consists of multiple modules. This study allows the full plant to be in one mode:EC, FC or HS. However, the plant can be designed such that each module can be operated in an operational mode separately. Optimising this unit-commitment problem can benefit the relative feasibility improvement of reversible systems. From analysing the year-based operational schedules, of which a three day subset is shown in Figure C.1, it can be concluded that the electrolyser is not operated at nominal capacity in 18% of the time. Two ways are proposed to optimise this module operation, which are depicted in subsection 4.7.3.

One way to use the optimisation is to optimally distribute the operating capacity over the modules. For example, at half the nominal capacity, by operating half of the modules at full capacity, or by operating all modules at half capacity. Factors determining these operating point-choices are the specific energy curves (Figure 3.7), the degradation rate in various modes and the thermal balance.

Another way to use the optimisation is to maximise profits by additional operation. The left-over capacity that is in HS could be be operated in FC mode, if power prices are favourable to do so.

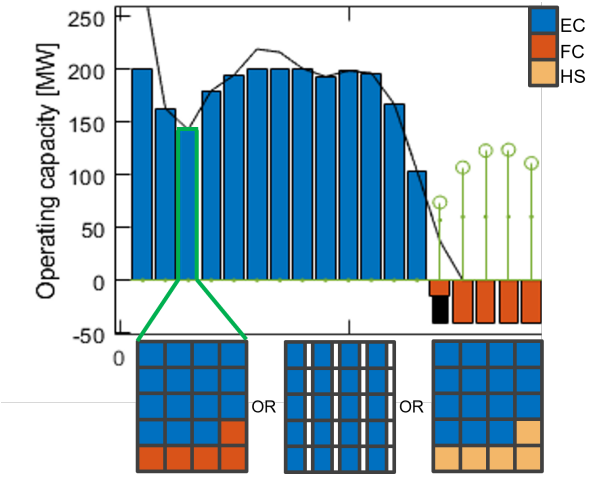


Figure 4.21: Schematic displaying the proposed module-based operation strategy. The plant operation is broken down into 20 modules operating at a desired operating point in a desired mode.

**Conclusions on Feasibility Improvement under External Conditions**

- Under baseline conditions, designing the system for NG as secondary feedstock is crucial. Of the two secondary feedstock choices, NG-based rSOE brings most potential to make TEP improvements. However, a hybrid[a] system can capture the benefits to TEF of both secondary feedstock.
- Design according to balancing market requirements is crucial for feasibility improvement by reversibility, as it has the potential to exceed "break-even power price points"

[a] A hybrid rSOE is defined as a plant designed for the use of both NG and $H_2$ as secondary feedstock. This can either mean that it can instantly switch to the other feedstock or that it can be retrofitted to do so

# 5

# Conclusions and Recommendations

## 5.1. Conclusions

This study aims to answer the question: "Can reversible operation improve the techno-economic feasibility of a large-scale open-system SOE, and if so, under what conditions?"

Firstly it is concluded that reversibility can improve the feasibility through risk mitigation in view of uncertain future conditions. As the techno-economic performance of fuel cell (FC) mode and electrolysis (EC) mode complement each other, reversibility based on hydrogen can hedge SOE against uncertain and unfavourable parameters, such as low hydrogen prices, high power prices, power profile inconsistency, and power price volatility. The dynamics of these hedges are best explained by the low hydrogen price hedge; Low hydrogen prices negatively affect the techno-economic performance of SOE and rSOE, as it reduces EC profits. However, the negative effect is significantly smaller for rSOE ($H_2$) than for SOE. A low hydrogen price causes a reduced switch-price, which is the power price at which it is economically advantageous to run in FC mode compared to hot-standby (HS) mode. Consequently, when the plant would normally be in HS, it now operates in FC mode. In terms of performance improvement, this cuts two ways. Firstly, the FC makes additional profits from selling electricity. Secondly, the HS energy costs are reduced as the plant is operated more productively. The same dynamics result in the three other hedges mentioned above. Compared to rSOE ($H_2$)[1], the rSOE (NG)[1] configuration exhibits the same hedges, except for the low hydrogen price hedge.

On top of feasibility improvement by hedging, reversibility can improve techno-economic performance significantly under certain boundary conditions. A distinction is made between crucial and beneficial external conditions and crucial and beneficial internal conditions. The external conditions relate to parameters outside of the system and outside the power of design, while the internal conditions lie inside the system and within the power of design. Crucial conditions can make or break the feasibility improvement by reversibility by themselves, meaning meeting only one of these conditions is necessary, while beneficial conditions only have a beneficial effect on feasibility improvement by reversibility. Recognising the significance of these conditions is essential, as under baseline conditions, improvement was found to be unconvincing.

- External Crucial Conditions: A minimum ratio between power and secondary feedstock price is crucial for feasibility improvement by reversibility. From scenario analysis, it can be concluded that rSOE (NG) improves the feasibility of SOE in the Mid power price scenario, while rSOE ($H_2$) does so in the High power price scenario. A regret analysis shows there exist certain "break-even power price-points" $\Theta_{el,BE,X}$ above which rSOE (X) brings improved feasibility compared to regular SOE. For this study, $\Theta_{el,BE,NG}$ lies at 73 euro per MWh and $\Theta_{el,BE,H_2}$ at 108 euro per MWh. The "break-even power price-points" are dependent on the secondary feedstock price.

  From sensitivity analysis, it is concluded that there are certain "break-even secondary feedstock price-poins" $\Theta_{X,buy,BE}$ below which reversibility brings feasibility improvement compared to SOE. The absolute value of this point is strongly influenced by the average power price. For rSOE ($H_2$), the break-even point lies at a buy price of 2 euros per kilogram.

  To conclude, the two crucial external conditions are interdependent and can be coupled in one condition. The choice ratio $R_X$ is introduced to be the ratio between the average power price of a dataset and the switch-price, which yields

[1] rSOE (X) reversible Solid Oxide Electrolysis with fuel cell operation based on secondary feedstock X

$$R_X = \theta_{el,avg}/\theta_{switch,X}. \tag{5.1}$$

The choice ratio $R_x$ must be larger than the "break-even choice ratio", $R_{BE,X}$, for reversibility to bring feasibility improvements compared to SOE. The "break-even choice ratio" is defined as,

$$R_{BE,X} = \Theta_{el,BE,X}/\theta_{switch,X}. \tag{5.2}$$

For the use-case studied and baseline conditions, the switch-prices, $\theta_{swtich,NG}$ and $\theta_{switch,H_2}$, are 63 and 163 euros per MWh respectively. This implies that the "break-even choice ratios" $R_{BE,NG}$ and $R_{BE,H_2}$, are 1.16 and 0.66.

- External Beneficial Conditions: Two important beneficial external conditions are the power profile and power price volatility. If the average power price is below the switch-price, power price volatility becomes essential for reversibility to have a positive impact. The expected increase in power price volatility due to the growing renewable energy capacity improves the position of reversibility in the future. Additionally, in a hydrogen production prioritising use-case, power profile inconsistency is necessary to benefit from the relative feasibility improvement of reversible configurations, as demonstrated in the sensitivity analysis.

- Internal Crucial Conditions: The secondary feedstock choice is identified as a crucial internal condition, as the choice can result in feasibility improvement compared to SOE. Under baseline conditions, designing the system for NG as secondary feedstock is crucial. Of the two secondary feedstock choices, NG-based rSOE brings the most potential for feasibility improvements. However, a hybrid[2] system can capture the benefits of both secondary feedstock.

  Besides the secondary feedstock choice, ramp rate and transition-time design according to balancing market requirements can be crucial for feasibility improvement by reversibility. A balancing market analysis shows a potential 50% power price increase, potentially bringing rewards above the previously stated crucial "break-even power price-points". Acting on the balancing market poses strict requirements on ramp rate and transition time, where hourly day-ahead-market time-resolution, which was the baseline of this study, showed economic insensitivity to these parameters. For two balancing sub-markets called the aFRR[3] and mFRR[4] the asset must respond within 30 seconds to 5 minutes and 5 to 60 minutes, respectively. After that, it should ramp up to the bid capacity in 10 minutes.

- Internal Beneficial Conditions: An inconsistent power profile design is beneficial for feasibility improvement through reversibility. By designing the use-case to benefit from this character, the consistent part of the profile can be used for a more profitable purpose, while the more inconsistent low-value part can be used for hydrogen production. In this way, these use-cases can benefit from reversibility as a facilitator of feasibility.

  The final internal beneficial condition is to use the plant to its maximum potential. This condition entails increasing FC performance through heat integration and module-based optimisation of the operating strategy.

In summary, this study shows that reversibility can significantly improve the techno-economic feasibility of a large-scale SOE. Reversibility mitigates risks of regular large-scale SOE by providing a hedge against uncertain parameters. At the same time, reversibility vastly improves techno-economic performance under the aforementioned crucial conditions.

[2] A hybrid rSOE is defined as a plant designed for the use of both NG and $H_2$ as secondary feedstock. This can either mean that it can instantly switch to the other feedstock or that it can be retrofitted to do so

[3] A balancing sub-market called the active Frequency Restoration Reserve

[4] A balancing sub-market called the manual Frequency Restoration Reserve

## 5.2. Recommendations for Further Research

This study clearly proves the potential of reversibility, which should be further substantiated and realised by further research. Both the results and limitations can serve as a starting point for future studies, as outlined in this section.

### Practical Implications of Reversibility

To validate the demonstrated potential of reversibility, further experimentally exploring the practical implications on design, operation, and costs, is recommended. Key questions arise regarding the impact of switching on degradation, the optimal operating duration, the required additional components, and the associated additional CAPEX. Additionally, as the potential of the balancing market is identified, further research should focus on the feasibility of system design according to balancing market requirements.

### Optimise Operational Strategy

Analysing the optimal operational strategy, such as utilising a module-based approach, is crucial to unlocking the full potential of reversible systems. This approach enables the operation mode selection for each module at each time step, optimising total system performance. Employing linear optimisation programs can effectively help optimise the ideal mode and optimal operating point.

### Optimal Use-Case and Business Model

The feasibility conditions established in this research can serve as a starting point for conducting a comprehensive application study to find the most suitable technical and business applications for reversibility. Where this study focused on an operational strategy based on wind profiles and wholesale power prices, alternative operational strategies or business cases may be more suitable for reversibility. The study on the balancing market is an example, showing increased potential. Therefore, it is recommended to explore alternative options, such as basing strategies on power prices or optimising the business case specifically for reversible systems.

### Plantmodel Efficiency Enhancement

To further enhance the relative improvement by reversibility, the overall efficiency of the FC can be increased by employing a more realistic and detailed plant model. The current study utilised a scaled version of the rSOE module without further heat integration. By integrating residue heat flows into the system design, efficiency improvements can be achieved, further enhancing the advantages of reversibility compared to non-reversible systems.

### Improve Power and Chemical Market Assumptions

To enhance the accuracy of the study, it is crucial to consider more realistic power and chemical price scenarios. The power price scenarios used in this research were based on historical data, which imposes limitations, particularly in projecting future prices. It is recommended to develop models that simulate future power prices based on projected installed energy capacity and cost assumptions. Utilising linear programming software, such as Linny-R, one can create a power market model that uses merit-order-based clearing. This approach allows for determining hourly electricity prices, thereby assessing the feasibility of reversible systems under different capacity scenarios. Additionally, modelling the chemical market with fluctuating values would better reflect real-world conditions.

### Differentiate Grey and Green Electricity

This study did not consider the differentiation between grey and green electricity in power price assessments, despite the price difference on the current market. Incorporating this distinction would improve the accuracy of the comparison between hydrogen and natural gas. Furthermore, exploring the implications and benefits of utilising bio-gas as a replacement for natural gas presents an intriguing avenue for further investigation.

### Extend the Comparison

Lastly, the comparison used in this study aims to uncover the feasibility improvement by reversibility on SOE. It is recommended to extend this comparison to other promising storage technologies with a low Technology Readiness Level (TRL) to uncover a more comprehensive view of the feasibility improving potential of reversibility.

# A

# Appendix: Literature Review

This Appendix section includes certain parts of the literature study performed preparatory to the Master Thesis. The content serves as background to methods, assumptions, KPIs and scope choices used in the thesis. Specific sections are referred to throughout the thesis when required. The goal of the literature research was to identify relevant research gaps and suitable research methods in rSOC application-based research. First some theory on rSOE is provided, first on the cell fundamentals in section A.1 and then on the rSOE process and system built up in section A.2. Literature was analysed based on application, techno-economic analysis method and modelling method. The findings of these analysis can respectively be found in section A.3, section A.4 and section A.5. Lastly, conclusions on research gaps are discussed in section A.6.

## A.1. Fundamentals of rSOC

Basic knowledge on the reversible solid oxide cell (rSOC) is required as a basis for the rest of the thesis. This section discusses the built up, thermodynamics, operation and degradation of the cell.

### A.1.1. Cell Basics

A solid oxide cell consists of three solid layers, as indicated in Figure A.1: two porous electrodes and a single, dense electrolyte. The electrolyte is typically ceramic, yttria-stabilised zirconia, YSZ. The two porous electrodes are typically named after their reactant inlet or product outlet, as the terms cathode and anode are interchanged depending on the mode of operation. In this study, the electrodes are referred to as the fuel electrode and the oxygen electrode. Other terminology may be used in the literature. As can be seen in Figure A.1 electrolysis of steam and carbondioxe is possible in a SOC. As it is the focus of this thesis, steam electrolyssis is taken as example.

The half reactions taking place in steam electrolysis are:

Fuel electrode: $2H_2O + 4e^- => 2H_2 + 2O^{2-}$

Oxygen electrode: $2O^{2-} => O_2 + 4e^-$ .

The oxygen ion passes through the electrolyte from the cathode side (fuel or hydrogen electrode) to the anode (oxygen electrode). An externally provided electrical current drives the reaction. In order to become sufficiently ion conductive, the solid electrolyte separating the hydrogen and oxygen sides needs to be operated at very high temperature, 600-1000 $°C$ [14].

The reactions above govern in electrolysis (EC) mode. In reversed, fuel cell (FC) mode, $H_2$ is oxidised through the half reactions below.

Fuel electrode: $2H_2 + 2O^{2-} => 2H_2O + 4e^-$

Oxygen electrode: $O_2 + 4e^- => 2O^{2-}$

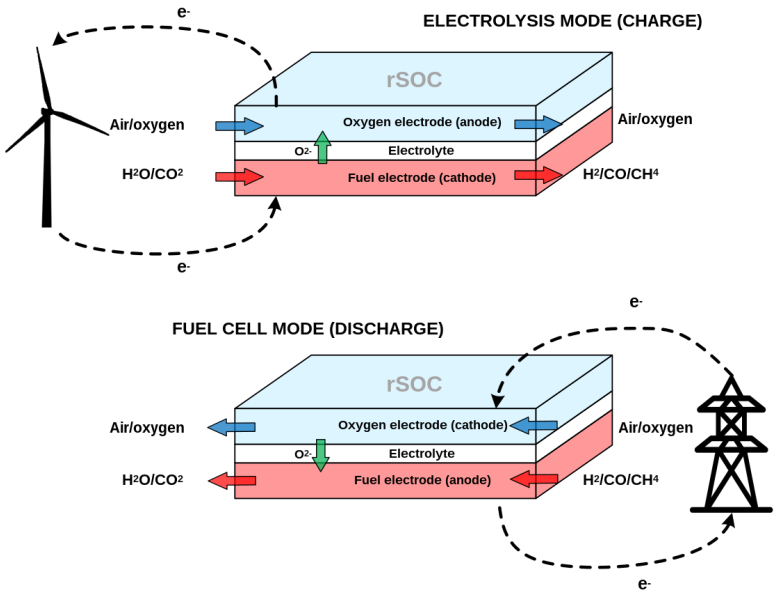


Figure A.1: A schematic of an SOC in electrolysis mode and fuel cell mode [52]

## A.1.2. Thermodynamics

For an electrolysis reaction to take place, the Gibbs free energy $\Delta G$ has to be supplied, in the form of electricity. However, an extra amount of energy in the form of heat ($T\Delta S$) has to be supplied, because electrolysis is an endothermic process, meaning it consumes energy. Therefor, the total energy demand for electrolysis is the sum of the Gibbs free energy and the heat demand, called the enthalpy ($\Delta H$).

$$\Delta H = \Delta G - T\Delta S \tag{A.1}$$

$$\Delta G = nFE_{cell} \tag{A.2}$$

with n the number of electrons transferred, and $E_{cell}$ the cell potential. So the Gibbs free energy is the minimum amount of electrical energy that needs to be supplied. Equation A.2 shows the relation of the Gibbs free energy with the minimum applied cell potential. The potential resulting precisely in the Gibbs free energy is called the reversible potential and results in net 0 fuel production. The reversible voltage is sometimes called the Open circuit voltage.

$$E_r(T,P) = \frac{\Delta G(T,P)}{nF} \tag{A.3}$$

Thermoneutral potential, is defined as the operating point where the potential is large enough to provide the whole energy demand, and thus a constant temperature could be maintained. Between $E_r$ and $E_{tn}$ the reaction occurs in an endothermic matter.

$$E_{tn}(T,P) = \frac{\Delta H(T,P)}{nF} \tag{A.4}$$

The main advantage of high temperature electrolysis, rest on the thermodynamic behaviour depicted in Figure A.2. During low temperature electrolysis the $T\Delta S$ is usually supplied by electrical heat. At 100°C a discontinuity is observed, leading to a drop in Enthalpy, $\Delta H$. At higher temperatures one can observe that the enthalpy remains fairly constant for both $CO_2$ and $H_2O$ electrolysis. On the other hand, with increasing temperature, the electrical demand ($\Delta G$) shows a decrease and the heat demand ($T\Delta S$) an increase. This results in a significant reduction of the required electrical demand, at a typical operating temperature in the range of 600-1000°C.

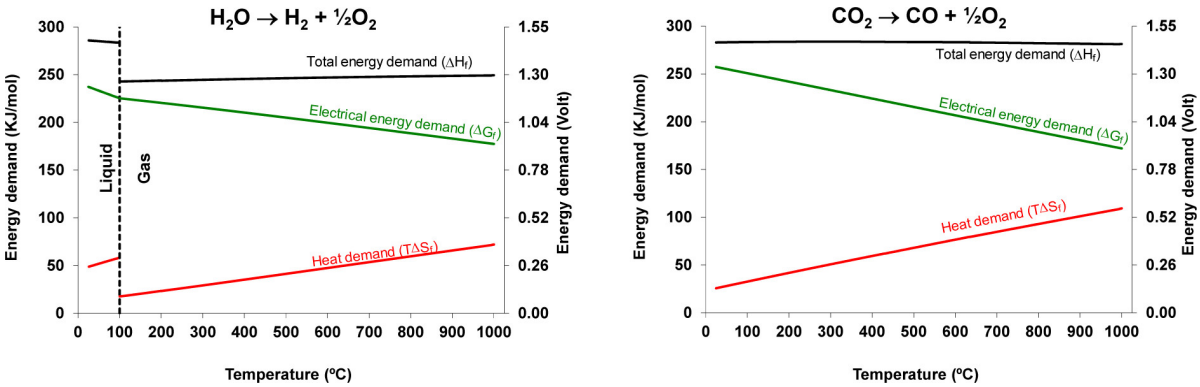


Figure A.2: Thermodynamic properties of $H_2O$ (left) and $CO_2$ electrolysis [24]

The cell efficiency is defined as the ratio between the theoretical amount of energy required for water splitting, $W_t$, and the real amount of energy consumed, $W_r$. To define efficiency, the definitions of the Higher Heating Value (HHV) and Lower Heating Value (LHV) are important. HHV is the theoretical energy needed for water splitting at atmospheric pressure and 25 °C. As the LHV is defined as the HHV minus the energy needed for evaporation of water. In high temperature electrolysis the feedstock is steam, making it common to use the LHV.

$$\eta_{cell} = \frac{W_t}{W_r} = \frac{E_{tn} I t}{E_{cell} I t} \tag{A.5}$$

### A.1.3. Cell Operation

The polarisation curve (Figure A.3) shows the relation between the applied cell voltage and the current density. For electrolysis, an operating voltage higher than the reversible cell potential, an over-potential, needs to be applied. A voltage under the reversible cell potential, underpotential, needs to be applied to operate in exothermic fuel cell mode. It even shows that the cell must be operated above the thermal equilibrium potential to achieve practical production rates. Operating between reversible potential and thermoneutral potential results in endothermic electrolysis, while operating above the thermoneutral potential results in exothermic electrolysis. The trade-off made for having practical production rates is that higher losses occur, leading to lower cell efficiencies. These losses occurring at higher voltage explain the shape of the polarisation curve. Keeping in mind the macro system scope of this literature research, these losses will not be handled into further detail.

Taking into account the over- and under-potential in EC and FC mode, the reference voltage of the electrolyser should be about double that of the fuel cell in the rSOC [19]. This explains that the electrolyser mode capacity is minimal two times as large as the fuel cell capacity. This ratio is a factor three to five in real life applications, due to additional losses, apart from those indicated by the polarisation curve [68, 55, 59, 66].

### A.1.4. Degradation

Over time, the performance of the electro-chemical cell degrades. The various degradation phenomena on cell level are deemed out of scope for this literature review. However, in a less detailed way the amount of degradation can be represented over time. A differentiation can be made between degradation in fuel cell and electrolysis mode. Exact behaviour needs further research, as studies make opposing claims. Namely, Hutty et al. [35] remarks that degradation is found to be greatest in electrolysis mode. On the other hand, Nuggehalli Sampathkumar et al. [62] reports degradation to be higher in SOFC than in SOEC, respectively 1.64% and 0.65% voltage degradation per thousand hours. Degradation measurements seem to be very dependent on the measuring method as pointed out by [56]. A real life experiment in Salzgitter showed a voltage degradation of 0.8% per thousand hours in SOEC mode [68]. The study also indicates that degradation rates under hot standby are quite similar to operation. Lastly, a study by [97] even showed negative degradation in one of their stacks by reversing operation.

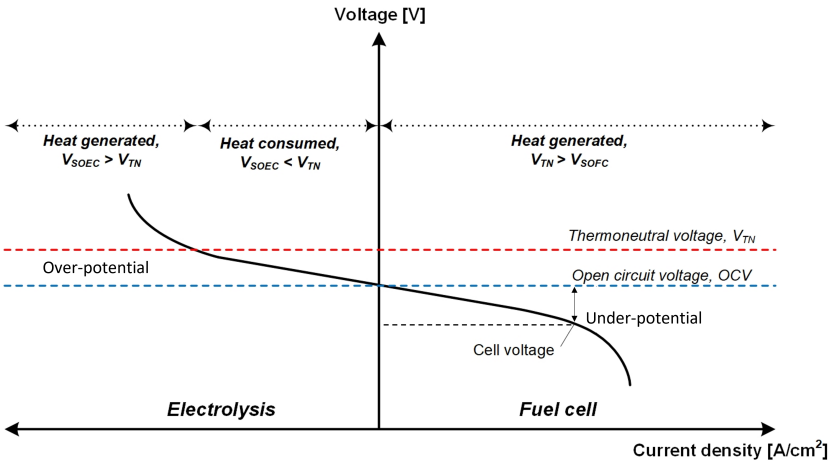


Figure A.3: The polarisation curve of an rSOC, showing the relation between applied cell voltage and current density [53]

# A.2. rSOE System Built-up

## A.2.1. BoS and BoP Components

A deeper explanation of the processes inside the system helps to understand the required components for the different system levels. Processes in a basic system are described in electrolysis and fuel cell mode. The system design as described below is conducted from steam rSOC systems described by Perna et al. [64] and Wendel et al. [93]. It must be noted that a basic system is described to compare systems in SOFC and SOEC mode.

SOEC mode

In electrolysis mode the three inputs to the BoP system are low pressure (LP) steam from a rest heat source, air feed and typically (high voltage) AC current. The BoP contains a blower, valve, piping, heatexchangers and optionally a compressor, and (trim)heater to provide low pressure (LP) steam at the right conditions as primary feedstock from the macro system to the (BoS). The right conditions consist of a certain mass flow rate, temperature and pressure. Typical temperature and pressure as input to the BoS are 150-200°C and 3 bar (g). The mass flow rate depends on the operating capacity. Likewise the BoP uses electrical components as an inverter and cables to supply DC electricity from the macro system at the right conditions to the BoS.

Inside the BoS the LP steam and air feed are heated from 150-200°C to operating temperature (600-1000°C), by heat exchange with outgoing gasses and optionally an additional heater. The steam is fed to the stack at the right mass flow rate, using a valve. Likewise, electricity from the BoP is converted to stack operating conditions. Cables and a DC-DC converter are used to control the right operating voltage.

The product gas and exhaust air are led through the heat exchanger to heat the incoming steam and air feed, as just described. Both streams are then led to the BoP to be prepared for the macro system.

Arriving in the BoP heat from the exhaust air is used in a heatexchanger after which it can be released to the environment. The product gas, containing a mixture of steam and hydrogen is processed by the BoP components to go into the macro system. A water removal component, such as a water-knock-out is used to cool the product gas and separate the majority of water from the hydrogen. Heat won in the water-knock-out is reused. To purify the hydrogen even further a Temperature Swing Absorber (TSA) is used, which absorbs the water that is left in the product gas. Finally a compressor is used to control the pressure of the hydrogen going into the macro system. A hydrogen grid proposed in Cerniauskas et al. [18] would require an input pressure of 70-100 bar.

SOFC mode : hydrogen

In fuel cell mode using hydrogen, the inputs to the BoP are fuel (secondary feedstock) and air feed. The hydrogen is preheated using a heatexchanger and optionally a (trim)heater. Hydrogen comes into

the BoP from the hydrogen grid at elevated pressures as just described. An expander and again the blower, valve, piping are used to provide the hydrogen at the right conditions from the macro system to the BoS.

Inside the BoS the secondary feedstock and air feed are heated the same way as in electrolysis mode, by heatexchange and an optional (trim)heater, but to slightly different temperatures. The temperatures of the input and output gasses can differ as different operating voltages lead to increased exothermic or endothermic cell behaviour, as explained by the polarisation curve in subsection A.1.3.

In the stack, the majority share of the hydrogen oxidises, called the fuel utilisation factor, leaving three output streams of the stack. The first two are exhaust air on the oxygen electrode side, and a the off-gas (a hydrogen-steam mixture) on the fuel electrode side. These two are led through the heat exchanger to heat the incoming hydrogen and air feed. The third is the fuel cell product, DC current. The DC-DC converter is used to increase the voltage of the electricity outputs from the stacks.

Arriving in the BoP heat from the exhaust air is used in a heatexchanger after which it is released to the environment. The off gas, is led through a water knock out system in which the steam condenses to liquid water, which is separated from the hydrogen. Heat won in the water-knock-out is reused. A TSA is not required. The hydrogen is then recirculated into the secondary feedstock stream. The water can be reused. The DC-current-streams coming out of the DC-DC converters of the various stacks, are combined and converted to AC current using a DC/AC converter. The AC current can now be exported to the macro system.

SOFC mode: methane

A more commonly used secondary feedstock or fuel in SOFCs is methane or natural gas. As compared to a hydrogen SOFC system a few extra system components are needed [8].

Arriving in de BoP from the macro system, the methane is preheated, just as hydrogen, by a heat exchanger and optionally a pre-heater. Then the methane is first brought to the right pressure using an expander. The methane is then brought together with water in a pre-steam-methane-reformer (pre-SMR), leading to a mixture of water, methane and syngas. A desulfurization unit (DSU) is used to remove sulfur dioxide from the mixture. Piping and valves are used to transport the fuel gas to the BoS.

In the BoS the fuel gas and air feed is heated in the same way, by heat-exchange and an optional (trim)heater. Internal reforming leads to the majority of the methane left in the mixture to be converted to syngas [8].

Again three output streams are left. The exhaust air and offgas release their heat to the incoming gas streams entering the BoS. The exhaust air is then released to the environment. Electricity is created and is exported to the macro system just as with hydrogen SOFC.

The offgas, mainly consisting of $CO_2$ and steam also contains hydrogen and CO. Energy is typically retrieved from this mixture in an afterburner. This heat can be reused in the pre-SMR.

### A.2.2. Differences in SOEC and SOFC System Built-up

The previous section (A.2.1) described the processes and system components needed for operating an rSOC in both SOEC and SOFC mode. It can be concluded that the BoP and BoS system for operating in SOEC mode show a lot of resemblance to operating in SOFC mode, when steam and hydrogen are used as primary and secondary feedstock [64, 93]. As the electrolysis system inserts hydrogen to the macro system and the fuel cell system retrieves hydrogen from the macro system, respectively a compressor and expander are used. Furthermore, the TSA used in SOEC mode, is not necessary in SOFC mode. Additionally, compared to SOEC, in SOFC an extra recirculation loop is added from the water-knock-out to the secondary feedstock input.

As was described in subsection A.1.3 only 1/3 to 1/5 of the electrolysis power is produced in fuel cell mode. Operating high capapcity inverters at low operating point negatively influences efficiency. Therefore an rSOC system could use multiple, but smaller inverters, where a SOE system would use a large capacity inverter.

The use of methane as secondary feedstock comes with some system additionalities as described in the last paragraph of subsection A.2.1. Compared to hydrogen based SOFC, methane based SOFC requires an additional pre-SMR, DSU and Afterburner [8].

### A.2.3. Differences in SOFC ($H_2$) and SOFC (NG) Sytem Built-up

The use of natural gas as secondary feedstock comes with some additional components compared to hydrogen based SOFC, as described in the last paragraph of subsection A.2.1. Compared to hydrogen based SOFC, natural gas-based SOFC requires an additional pre-reformer, DSU and Afterburner [8].The pre-reformer is used to convert a part of the natural gas to syngas. Three technologies are considered: SMR, CPOx and ATR.

Steam methane reforming (SMR) is a method for producing hydrogen by reacting steam and methane in the presence of a catalyst at high temperatures. This reaction produces hydrogen and carbon monoxide, syngas, which can be used in the SOFC. A downside of this process is the thermal energy required for the fuel reforming. [15]

Partial oxidation (POX) is a process for producing syngas by reacting a hydrocarbon fuel (such as natural gas) with a limited amount of oxygen in the presence of a catalyst or without the presence of a catalyst (CPOx). Partial oxidation is a more energy-efficient process than steam reforming, but it produces a smaller amount of syngas per unit of fuel.[15]

Autothermal reforming (ATR) is a process that combines partial oxidation and steam reforming in a single step. This process involves reacting natural gas with oxygen and steam at high temperatures and pressures to produce hydrogen, carbon monoxide, and a small amount of methane. [15]

The off-gas that remains after FC operation is usually used for heat production in an afterburner in case of SMR, or purified with a PSA in case of CPOx and ATR. Pressure swing adsorption (PSA) is currently the most popular method for extracting and purifying hydrogen from syngas that contains other components such as CO,$CO_2$, and $N_2$, which is the case after fuel cell operation [15].

When transitioning from FC (Fuel Cell) to EC (Electrolysis) mode, the initial batch of hydrogen produced may be contaminated with FC feedstock and product gases. To address this issue, three options can be considered. The first option is to discard the initial batch of hydrogen altogether. The second option involves purifying the hydrogen stream, which can be achieved, for instance, by utilising a PSA process. The last option is to flush the system prior to EC operation, which introduces an additional flushing time to the overall switching process. This flushing time can vary, depending on the required purity of the hydrogen in EC mode.

### A.2.4. Safety Considerations

Risk can be defined as the probability times impact. Measures should be taken into account to minimise the risk of operation. This is done by minimising the probability of an accident happening and the impact an accident might have.

The rSOC system produces or uses explosive chemicals as hydrogen and natural gas. Therefor, there is an explosive hazard. The system should be designed in such a way that these gasses are not released to the environment, minimising probability. If gasses escape to the surrounding its surroundings should be designed in such a way that the consequences of these hazards are minimised, minimising impact. A way to design areas to minimise impact is to declare an ATEX safety zone of some class. ATEX zone 0 being continuous explosive atmosphere and ATEX zone 1 being an explosive gas atmosphere likely to occur in normal operation.

On a smaller scale, SOCs must be safeguarded from pressure-induced stress by maintaining equilibrium between the pressures on the fuel and oxygen sides of the cells. To minimise the probability of pressure differences occuring in the cell, appropriate regulatory measures must be installed, as these might damage the cell. Furthermore, if pressure deviations do occur, to minimise impact some emergency safety releases should be installed to release the gases. These gasses are then released to the environment, which could cause an explosive hazard, which can be minimised by designing the area for such events to occur safely.

When hydrogen is used in both fuel cell and electrolysis operation the system can be considered airtight, on the fuel side, in the sense that no hydrogen should be released to the air, during normal operation. However, when methane is used extra caution is required as the off-gas is burned in the afterburner, of which the exhaust is connected to the environment. As these systems are widely used in industry, appropriate safety measures are available to be installed.

The system operates at very high temperatures (600-1000°C). The high temperature part of the system should be non accessable, in a hot box, to minimize the probabity of accidents occurring from these operating temperatures. To minimise the impact, measures should be installed. As an example one could think of burning risks, and a measure to minimise impact would be a medical kit, or emergency

protocol.

There are also fire hazards present. A way to minimise the probability of a fire, is to install temperature sensors, causing emergency shutdown if needed. Impact can be minimised by installing fire alarms to warn the fire department.

## A.3. Application Analysis

A literature search to rSOE-application-based studies led to the selection of papers and reports listed in Table A.1. Different types of research were gathered: Technical Analysis (TA), Techno-economic Analysis (TEA) and Experimental Research (Exp). The applications were compared per application and macro system component, resulting in research gaps displayed in section 1.2.

### A.3.1. Closed-System Application

rSOC is mostly studied in closed system applications. One application for an rSOC is electrical storage (P2X2P) for a certain electrical load. Investigating this application from an integrated system perspective is a prevalent subject in closed system research [19, 44, 45, 35, 55, 12]. In a different application, Motylinski et al. [58] specifically studies a closed-system electrical storage application for grid balancing, while Rokni [75] explored the use of rSOC as the basis for a base load power application, simultaneously using rest heat to desalinate water. Again in an electrical storage application, Wendel et al. [93] and Motylinski et al. [58] examine the thermodynamic performance of the Balance of System (BoS) in these systems. However, these studies tend to leave out macro system components, such as a fluctuating power profile. Wang et al. [92] also looked at P2X2P applications, but with a focus on comparing the Round Trip Efficiency (RTE) of different types of feedstock.

### A.3.2. Open-System Applications

In an open system application the product produced in electrolysis mode has another or added purpose than being only converted back into electricity. The six open system application studies are introduced.

Zhang et al. [98] examines a P2X(2P) configuration to compare different primary and secondary feedstock types on their thermodynamic and economic performance. Considered system product and fuel cell fuel are hydrogen, syngas, methane, methanol and ammonia. Both interaction with the chemical market P2X and the electricity market P2X2P are evaluated for the range of feedstock types. Feedstock types are compared on the minimum CAPEX per stack requirement to earn back the system over its lifetime, which will be discussed in detail in section A.5. An overview of the conceptual system is depicted in Figure A.4. It must be noted that the study provides little transparency in the actual system design choices made in the model.

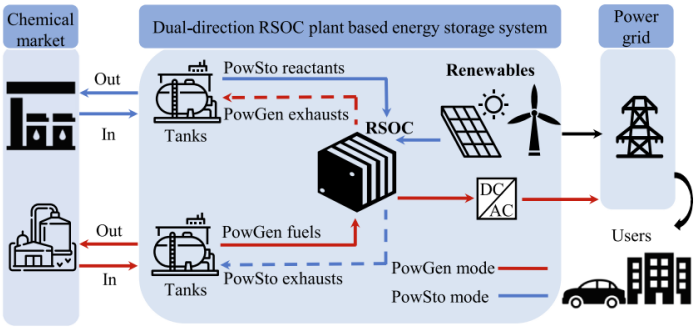


Figure A.4: The conceptual system proposed by Zhang et al. [98]

Carbone et al. [16] perform an analysis of a combined W2P2X(2P) application in Italy. The goals of the designed system is to process organic waste, balance the grid and produce renewable methane on a regional scale. The system can operate in three different modes which are depicted in Figure A.5: PowerGeneration, PowerStorage, PowerNeutral. In the PowerGen mode biomass is first converted to syngas, which is then used as a fuel to produce electricity using the rSOC. In the PowerStorage mode biomass is converted to syngas, which is then used as a feestock to produce methane using excess

Table A.1: An overview of studies focused on various rSOC system applications

| Author, Year | Type | Application | Results |
|---|---|---|---|
| Buffo et al. [12], 2020 | TA | Open/Closed: P2X(2P) 50/10MW for the power load of urban district and $H_2$ need of a mobility fleet. | For $H_2$ demand ranging 10-1000 ton/year: yearly efficiency 70-55 % ; 50-5 % emission reduction |
| Butera et al. [13], 2020 | TA | Open: P2X(2P) using pressurized rSOC producing SNG transported to the national gas grid; CO2 storage in a cavern. | DC-to-DC RTE of 80% with SNG due to net power production of the BoP in SOEC mode |
| Carbone et al. [16], 2021 | TA | Open: W2X(2P) rSOC to valorise organic rest, balance the grid and produce SNG | Requirement for deployment: Availability of 6.7MT low grade organic waste, 10 TWh of overproduction, 5 TWh of underproduction, to produce 1.4-2.4 Mt $CH_4$ |
| Lamagna et al. [44], 2022 | TEA | Open/Closed: P2X(2P) wind turbine coupled rSOC 120/21kW for auxiliary systems load. Residual load used for $H_2$ production. | Auxiliary systems can be supplied. Export strategy: yearly 15 tons hydrogen production |
| Reznicek et al. [74], 2020 | TEA | Open: P2X2P using pressurized rSOC 50MW to produce SNG; Stack and BoP focused. | SNG production: 92% purity, at $ 22.7/MMBTU and LHV efficiency of 81%. Reversible system net metering syngas: RTE of 58% with LCOE of 10.5 ¢/kWh |
| Zhang et al. [98], 2021 | TEA | Open: P2X(2P) plant design comparison 82MW/37MW between different primary and secondary feedstock types. | Hydrogen most economically feasible at 175-290 /kW stack power > syngas > $CH_4$ > $CH_3OH$ > $NH_3$ (With wind penetration (200-250%), little chemical storage need) |
| Chadly et al. [19], 2022 | TEA | Closed: P2X2P for energy storage system in green buildings, 454kW rSOC on $H_2$, comparison with PEM and Battery | LCOS PEM RFC 41.73 ¢/kWh > rSOC 28.18 ¢/kWh > LIB 27.35¢/kWh |
| Hutty et al. [35], 2020 | TA | Closed: P2X2P grid connected household agents with PV connected to a battery and rSOC, based on $H_2$ | System with 50% grid independence: at >2000/kW PBP > Lifetime; At future CAPEX > 760/kW PBP of 20 years |
| Lamagna et al. [45], 2021 | TEA | Closed: P2X2P energy storage system for commercial public buildings (Hotel/Hospital/Office/Smart district), based on 40.8kW rSOC using $H_2$ | Energy self-sufficiency increase of 29-58%, PBP equal to lifetime at 7843/kW rSOC. PBP decrease to 3 years at target CAPEX (undefined) |
| Motylinski et al. [58], 2021 | TA | Closed: P2X2P 1MW grid integration for power balancing, comparing switching dynamics to experimental cell data, based on $H_2$ | rSOC model shows that energy balancing can be implemented on continuous basis. Model is validated with experimental data. |
| Rokni [75], 2019 | TA | Closed: P2X2P Integrated system using rSOC to deliver a base load, 500kW power output while also desalinizing water, based on $H_2$ | Hydrogen production of 2200 kg/day. $H_2$ production efficiency: 39% (74% if free heat assumed). Plant efficiency 47% (100% if free heat assumed) |
| Wang et al. [92], 2020 | TA | Closed: P2X2P plant design focussed study, comparing thermodynamic performance of feedstock types | RTE $CH_4$ (47.5%) > Syngas (43.3%) > hydrogen (42.6%) > methanol (40.7%) > ammonia (38.6%) |
| Wendel et al. [93], 2016 | TA | Closed: P2X2P technical model testing to BoP configurations on thermodynamic performance | RTE of respectively 74% and 68% for the stored water-vapour system and the condensed water system. |
| Mermelstein et al. [55], 2017 | Exp | Real life : report on 50/120kW pilot project, at Huntingdon Beach facility in California, by Boing and Sunfire | Efficiency SOEC 60% ; SOFC 49% ; RTE 30% |
| Mouginn et al. [59], 2021 | Exp | Real life : report on 120kW, (unfinished) pilot project, REFLEX smart energy hub, at the Envipark in Turin, with Elcogen stacks. | No results, targets defined in Mouginn et al. [59] |
| Peters et al. [65], 2021 | Exp | Real life: report on 5/15kW pilot project at Forschungzentrum Julich GmbH | Voltage degradation: 0.6%/1000h (SOEC) ; Efficiency SOEC 70% ; SOFC 62.7% |
| Posdziech et al. [68], 2019 | Exp | Real life: report on 30/150kW pilot project, Green Industrial $H_2$, in Salzgitter, by Sunfire | Voltage degradation: 0.8%/1000h (SOEC). No efficiency loss up to 50-40% (SOEC-SOFC) partial load. |

electricity with the rSOC in SOEC mode. In the PowerNeutral mode one rSOC is operated as SOFC to produce electricity from syngas. This electricity is utilised to power electrolysis of syngas to methane in the second rSOC. The study quantifies the residual loads and biomass availability in various regions to determine the highest potential use-case location.

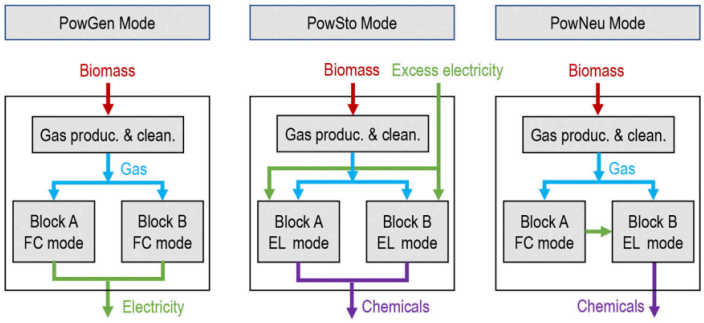


Figure A.5: The three different modes of operation in the system design proposed by [16]

Reznicek et al. [74] and Butera et al. [13] both study an SNG producing application connected to the natural gas grid and respectively a $CO_2$ pipeline and a $CO_2$ storage cavern.

Performing a more technical study of the plant, Butera et al. [13] is built on the work of Jensen et al. [41] and Monti et al. [57], achieving a high enough methane content for the system to be connected to the natural gas grid. The system uses pressurised rSOC, combined with catalytic reactors to reversibly convert $CO_2$ rich gas and electricity into SNG. The optimal RTE of this set-up was reported to be 80 %. Despite being depicted as a integrated system model, the study is focused at the stack and BoP operation. In that respect, external influences, such as a fluctuating power profile, electricity price or SNG price are not taken into account.

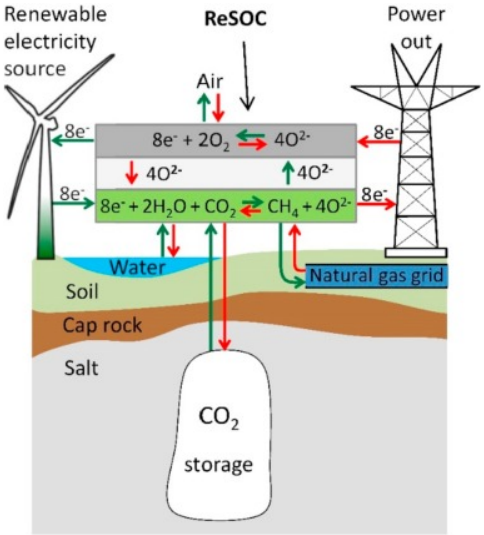


Figure A.6: The conceptual SNG based rSOC system proposed by Butera et al. [13]

Reznicek et al. [74] analyses both technical and economic features of the plant. The proposed integrated system, as depicted in Figure A.7, raises the expectation that the study is focused at various influences of the macro system components. However, this study is also mainly focused on Balance of System operation. Shortly summarising the results, P2X/X2P mode LHV efficiencies of 84 % and 69 %, respectively, were reported for the 50 MWe plant. Mainly because of assuming economies of scale and the lack of expensive storage tanks, the economic outlook for mature rSOC systems are found to be competitive with current energy storage technologies and natural gas peaker plants.

Buffo et al. [12] examine a 10MW P2X(2P) application of rSOC for an urban district. The goal of the application is to deliver hydrogen for public transportation and to satisfy the electrical load of

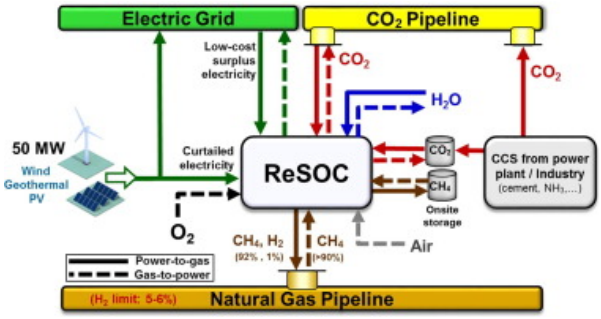


Figure A.7: The conceptual SNG based rSOC system proposed by Reznicek et al. [74]

the urban district with a high share of renewable electricity. The mode of operation depends on a predetermined constant switching price in a fluctuating electricity price system. Hydrogen is produced at prices below the switching price. Hydrogen is stored as compressed gas and is used for either public transportation or electricity production in peak hours, when the electricity price is above the switching price. Although the system is considered as an open system due to the hydrogen public transportation demand, it does operate according to a schedule suiting an electrical load.

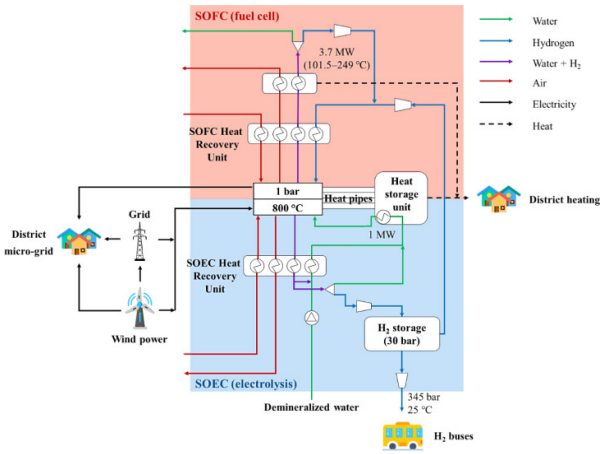


Figure A.8: The hydrogen based rSOC system proposed by Buffo et al. [12]

Lamagna et al. [44] models rSOC primarily as an electricity storage application (closed) at an offshore wind turbine, to supply electricity to its auxiliary systems when wind-energy is not directly available. Residual power is transported as electricity. A second strategy (open) models a hydrogen export strategy that uses the residual power to produce hydrogen, which is exported through compressed gas pipelines. Connected to the system is a desalination system, supplying desalinated water for electrolysis.

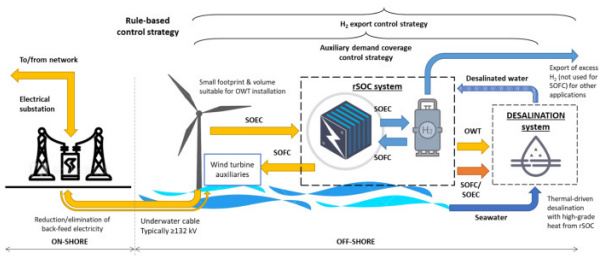


Figure A.9: The hydrogen based rSOC system proposed by Lamagna et al. [44]

## A.4. Modelling Approach Analysis

A means to study the technical or economical performance of a system is to perform real-life experiments [55, 59, 65, 68]. Prior to real-life experiments, models are made to predict system behaviour. A broad range of modelling approaches exists, from very specific to general models, from very detailed to highly simplified. This chapter temps to lay out insights about the modelling methods seen in literature, to serve as a (non-exhaustive) overview of approaches. Also, the applicability of the observed methods on the overarching research shall be discussed. The modelling approach analysis is done from small to large scale: First concerning the stack (A.4.1), then the BoS and BoP (A.4.2), to wrap up with the macro system A.4.3. The last section shall also discuss a modelling research gap.

### A.4.1. Stack Modelling

Dimensions Modelling the behaviour of electrochemical stacks can consider both temporal and spatial dimensions. Modelling can be done up to a certain depth, serving the envisioned outcomes of the model. 0D, 1D and 0.5D models are discussed. The dimension of modelling is discussed on the basis of stack modelling, but its applicability also holds for modelling systems at different scales, as BoS and BoP.

A zero-dimensional (0D) model is the simplest type of model and is only dependent on time. These models are typically described by a set of ordinary differential equations and can provide insight into the temporal dynamics of the system, such as the rate of charge and discharge, but also overall energy density and fuel utilisation. They do not take into account any spatial dependencies within the stack. Steady-state stack simulations or stack experimental data can be used to create a map of operating points for rSOC operation [12, 44].

In contrast, one-dimensional (1D) models include one spatial dimension, such as x, y, or z. These models are also time-dependent and can provide additional insight into the spatial distribution of variables within the system, such as the distribution of active material and current density. The evolution of 1D models can be either transient or steady-state, depending on the specific application. These models can be useful for understanding the performance of electrochemical stacks under different operating conditions and for identifying potential limitations or areas for improvement. Reznicek et al. [74], Butera et al. [13] and Wendel et al. [93] use a one-dimensional, steady-state rSOC model published by Wendel et al. [94]. Aspen Hysys software contains a quasi-1D rSOC model used by Motylinski et al. [58]

Half-dimensional models (also known as "0.5D" models) are a combination of 0D and 1D models, they include both temporal and spatial dimensions, but with reduced complexity compared to full 1D models. These models are typically used to capture the essential physics of the system while minimising the computational demands. Half-dimensional models can be obtained by assuming symmetry in the system, hence reducing the number of variables that need to be solved. As an example, Nami et al. [60] uses a 0.5 D steady-state model to evaluate the polarisation (I-V) characteristics of its SOEC.

From the analysis described above, it can be concluded that higher dimension modelling is used for stack or system dynamics performance improvement. In terms of the system definitions proposed in section 2.3, the studies using higher dimensional models are not aimed at the Macro system scale, but rather on the Stack or BoP scale, which is not the purpose of the overarching research. In a Macro system study, a high quality low fidelity 0D model is deemed sufficient to represent stack or even BoS operation.

Degradation To incorporate degradation in a model various methods are used, by the studies listed in Table A.1.The study by Chadly et al. [19] assumes a linear voltage degradation, independent of switching, amounting 10 $\mu$V per hour. This corresponds to the voltage degradation of 0.8% per thousand hours as observed in SOEC mode by the real life experiment in Salzgitter [68].

A different approach to model degradation is to determine a certain stack End of Life (EOL), after which replacement is required, as proposed in Zhang et al. [98]. The study takes a replacement time of 5 years. This stack replacement can be incorporated into the Fixed OPEX when performing a techno-economic analysis.

Lastly, it is worth noting that various studies put degradation out of scope in their models [74, 12, 45, 98, 35].

Based on the theory described in subsection 2.2.1, it can be concluded that cell degradation is a significant phenomenon that is worth taking into account. Using the degradation rate seen in [68], a

full year operation results in a 7% voltage degradation. In the authors opinion, only taking into account a system lifetime does not suffice as the yearly effect is so significant. It is clear that there exists a difference in degradation for SOFC and SOEC operation (2.2.1) [35, 62]. However, further research is needed to come to a definite answer to use in a model. Therefore, taking into account a linear degradation, based on pilot experiment results, as is done by Chadly et al. [19] is deemed sufficient as a modelling starting point.

## A.4.2. BoS and BoP Modelling

The design of the BoS and BoP is an important aspect of chemical process engineering and can be achieved through the use of various chemical process design programs. The definitions and processes in the BoS and BoP were described in subsection A.2.1. Some studies explicitly mention BoP modelling [12, 58, 93, 74, 75], while other studies do not [45, 44, 35].

Figure A.10 shows a detailed BoP design, for a power-to-methane plant mentioned in a study by Reznicek et al. [74]. The goal of showing the design is not go into the details of the operation, but to give an example what a such a system looks like. Often schematic BoP representations show mass and heat-transferring BoP components. It is important to realise that electrical components and components that do not transfer mass, heat or electrons, like isolation are also part of the Balance of Plant.

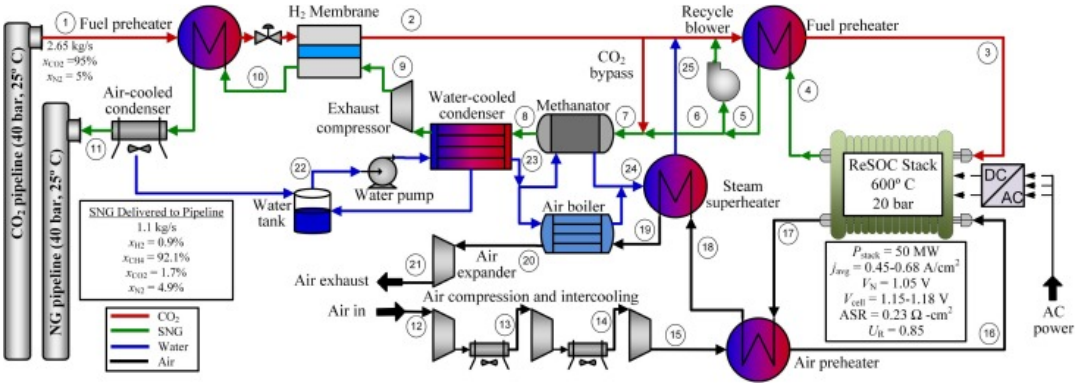


Figure A.10: An example BoP schematic of an rSOC system in power-to-methane mode[74]

The primary objectives of creating a detailed BoP design include to asses and improving thermodynamic system performance, comparing BoP designs for different plant configurations (such as the use of methane or hydrogen as secondary feedstock). For mature technologies, a detailed BoP design also aids in estimating the total system CAPEX.

For an immature technology as rSOC, a detailed BoP design does not necessarily lead to a more accurate CAPEX estimation. Since, this mainly holds when components used in the design are off-the-shelf products, with a known price. An example of assuming the system CAPEX via the BoP is Reznicek et al. [74], of which the method to determine the CAPEX is further discussed in section A.5.

If the purpose of a research does not require detailed BoP or BoS modelling, one could choose to model the BoS or BoP as a 0D unit based model, meaning not every single component of the BoP is modelled. The balance of stack is then usually modelled using a high-quality performance curve or performance map from literature or a commercial vendor [12]. This method would be a good starting point for the model of the overarching research.

## A.4.3. Macro System Modelling

In order to model the macro system, one can choose to create either a static or a time-dependent model. For the purpose of analysing the operational performance and value of a rSOC in an integrated application, a time-dependent model is preferred.

An analysis (A.4.3 on dynamic modelling approaches in open system rSOC applications, led to a relevant research gap. Sections A.4.3 and A.4.3 show methods found by further analysis of Table A.1, on respectively reducing computational time and optimising system design.

Dynamic modelling gap Of the applications listed in Table A.1, six are (partly) open system applications, which is defined as a system supplying at least a part of its chemical product, from

SOEC mode to the market [16, 98, 74, 44, 13, 12]. The realistic operation of an rSOC in an open system application depends on both influences from the chemical and power market. A short review on the modelling approach used by the open application studies is given below. To assist this review a schematic of the parameters influencing the operational schedule of the six open system applications is provided, Figure A.11.

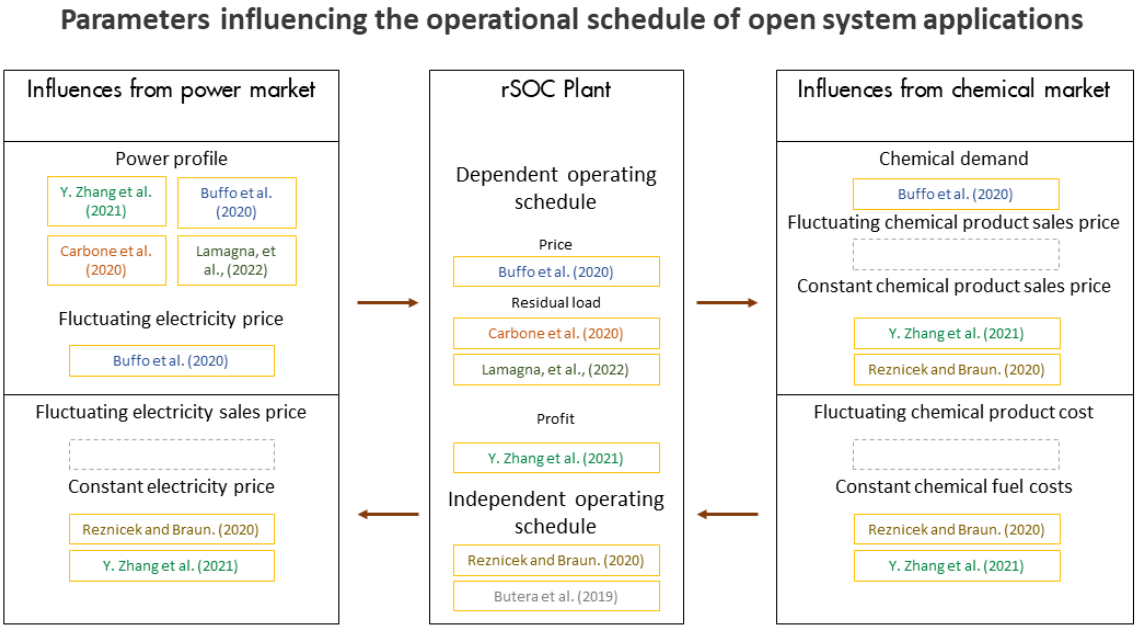


Figure A.11: A schematic to assist pointing out the application based gaps in open system applications

The operational schedule modelled by Reznicek et al. [74] is independent of both the power market and the chemical market. The study operates its rSOC in SOEC mode for half of its lifetime and SOFC mode in the other half of its lifetime. Also, the prices assumed in the economic analysis are assumed to be constant.

Zhang et al. [98] performs a techno-economic analysis of an open system application. The study, provides little transparency on its system design, as it is generated by a decomposition-based model Wang et al. [92]. The operational schedule seems to be based on a fluctuating wind profile while maximising profit. In the profit objective function, constant electricity and chemical product prices are taken into account. Little transparency in the eventual operating schedule is provided.

Lamagna et al. [44] models an offshore wind turbine connected rSOC system, to have a continuous supply of power for the wind turbine auxiliary systems. Excess hydrogen is fed to a hydrogen pipeline. The hydrogen pipeline is only used to export hydrogen and is not taken into account in the economic analysis. As the operating schedule of the small-scale rSOC is based only on the residual load, the focus of the study is on the closed electricity storage system, instead of the open system application. As a result, limited influence from the chemical and power market is modelled.

An operational schedule, influenced by the power market price, was used in the study by Buffo et al. [12]. It does so, to determine when to produce electricity to supply to the households in its district, and to cheaply produce hydrogen for a predetermined load and electricity storage load. This way the rSOC system prevents the district to purchase electricity during peak hours. An analysis of the economic performance is not included in the study. Also, both electricity and hydrogen are not sold to respectively the power and chemical markets.

Butera et al. [13] and Carbone et al. [16] are both technical studies that are not influenced by financial components of the power and chemical market. Carbone et al. [16] is operated on the basis on residual load. The model used in Butera et al. [13] has a completely independent operation schedule.

To the best of the authors knowledge, there exists a gap in modelling open system rSOC applications. This gap is the modelling of the system with an operational schedule influenced by both a dynamic power profile and dynamic power price. Additionally a gap lies in using a dynamic chemical sales en buy price.

Reducing computational time

Various studies from Table A.1 model the systems behaviour with a time resolution smaller than 1 hour [45, 44, 12, 98].

A combination of time resolution and number of calculations per time step can increase the computational time required for a model to be significant, especially when optimisation is used. As a result, one can choose to reduce the modelling time by utilising representative or typical days to represent the system's behaviour over a longer period. Three applications of such a method are described.

Buffo et al. [12] utilises MATLAB to integrate a 0D map of steady-state operating points of the combined stack and balance of plant systems with the temporal energy demand and wind power generation data. A one-minute time-resolved model plans out the operational capacity and mode for each minute. To reduce the computational work the number of days is reduced from 365 to 24 by simulating on a typical weekday and weekend day, throughout twelve months. This gives a realistic representation and can serve as an example for the overarching research.

For the same of reducing computational time, Qi et al. [71] applies a scenario reduction method using probability distance proposed by Conejo et al. [21]. The goal of the study is to optimise the capacity of a high-temperature electrolysis system with a dynamic operation strategy under volatile loading conditions. This scenario reduction method divides the year into four seasons and selects a representative day from each season that is, closest to the original data sets in terms of power rating and volatility, as shown in Figure A.12. This approach reduces the number of decision variables by reducing the time periods considered in the optimisation process, from 8760 to 96. As follows from a sensitivity analysis, it maintains the essential characteristics of the system's behaviour to make a capacity optimisation.

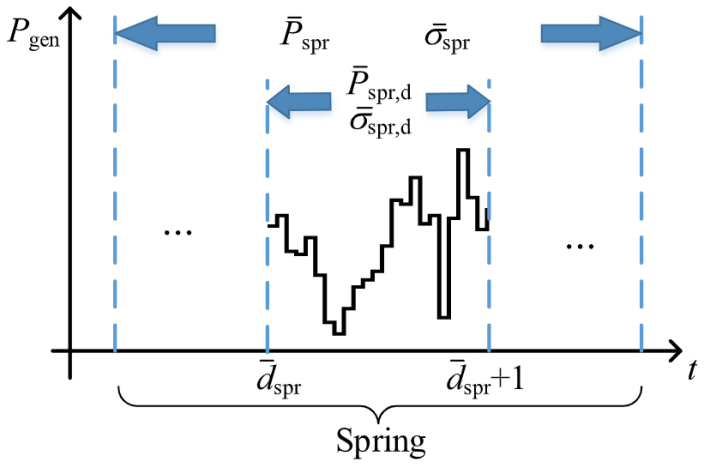


Figure A.12: The scenario reduction method, and example for the spring season [71]

The previously mentioned scenario reduction method is deducted from the k-means method developed by Fazlollahi et al. [28]. Zhang et al. [98] uses this method to cluster both wind power and power demand in 8 typical days. Despite computing only 8 typical days, a lifetime profit analysis can be done, by multiplying the profit of each typical day by the number of repetitions in a year and finally summing over all years and typical days.

Although four days might be enough for representing a year for the purpose of sizing [71], it does not mean this is enough for the purpose of determining the effect of reversible operation throughout the year. Zhang et al. [98], who chooses eight typical days, shows more resemblance to the overarching research goal. However, the model is based on a constant electricity price. The realistic operation of such a system should depend on the combined power profile and (dynamic) power prices. Therefore, to

capture the essential characteristics of this combined system, more than eight typical days are expected to be required.

System design optimisation Various tools can be used to design a system. These tools can help optimise and size the integrated system and its components. Two examples to optimise the system sizing were observed in the reviewed literature (Table A.1). The methods are mentioned, but no further analysis on these methods is performed.

Lamagna et al. [45] uses a simulation software called ConfigDym, that estimates the energy optimisation strategies for a Smart Energy Hub in real-time. The MATLAB-based tool is developed in-house by Sylfen.

Wang et al. [92] proposed a set of optimal design options for different production processes using a decomposition-based two-step optimisation method. These design options were created by adjusting key parameters in the fuel cell stack and chemical reactors, as well as optimising the use of heat energy. Zhang et al. [98] evaluates these designs based on multiple factors, such as the efficiency of energy conversion and the power output. The final designs represent the balance between these different factors, meaning that with the same size of the fuel cell stack, the plant can produce energy at different capacities and interact with the grid and energy market in various ways.

# A.5. Analysis Methods

This chapter aims to give an overview of the metrics and methods used in a selection of studies from Table A.1. The selection, as shown in Table A.2, consists of the Techno-economic studies (TEA) and two Technical analysis studies (TA). The metrics used are represented in the final column. Discussed are the techno economic methods (A.5.1), a geographic and environmental method (A.5.2) and sensitivity analysis (A.5.3).

Table A.2: An overview of the techno-economic and environmental studies on rSOC applications, including their primary performance indicators

| Author | Year | Research type | Application | Performance Indicators |
|---|---|---|---|---|
| Reznicek et al. [74] | 2020 | TEA | Open | LCOSNG , LCOE , Wobbe Index , $\eta_{LHV}$ |
| Lamagna et al. [44] | 2022 | TEA | Open/Closed | LCOH, LCOS |
| Zhang et al. [98] | 2021 | TEA | Open | CAPEX Target |
| Chadly et al. [19] | 2022 | TEA | Closed | LCOS |
| Lamagna et al. [45] | 2021 | TEA | Closed | NPV, IRR, PBP |
| Buffo et al. [12] | 2020 | TA | Open/Closed | $CO_2$ emissions, RE share, $\eta_{LHV}$ |
| Carbone et al. [16] | 2021 | TA | Open | Biomass and residual load availability |

## A.5.1. Techno-Economic Methods

This section summarises the metrics used in TEA research from Table A.2. The formulas in this section can be case specific, to give context to the application. While, some insights are gathered in this section, a more generalised discussion about the best applicable methods for the overarching research is given in subsection A.7.2

The study by Reznicek et al. [74] conducts an analysis of the system design, performance and cost implications of a 50MWe rSOC system. To analyse different system designs, decision variables include stack current density in each mode, reactant utilisation in each mode, and stack pressure. This is not required for this study.

In order to quantitatively evaluate the performance of the proposed system design, the primary performance metrics employed are the lower heating value (LHV) efficiencies for each respective operating mode.

$$\eta_{LHV,P2G} = \frac{\dot{m}_{SNG} LHV_{SNG}}{\dot{W}_{net,AC}} \tag{A.6}$$

$$\eta_{LHV,G2P} = \frac{\dot{W}_{net,AC}}{\dot{m}_{NG} LHV_{NG}} \tag{A.7}$$

where $\dot{m}_{SNG}$, $LHV_{SNG}$ and $\dot{m}_{NG}$, $LHV_{NG}$ respectively are the supplied flow rate and lower heating value of synthetic natural gas and natural gas. Likewise, $W_{net,AC}$ and $W_{net,AC}$ represent the net power input including stack power and the net system power output, deducting inverter and motor losses from the stack ago

In addition to the LHV efficiencies, the study also employs the WobbeIndex, which is not further discussed.

To evaluate the economic performance of the system the Levelised costs of Synthetic Natural Gas (LCOSNG) and the Levelised costs of energy (LCOE) are assessed. Equation A.8 is for an electrolysis only application and Equation A.9 for an equally distributed dual operation between SOEC and SOFC mode.

$$LCOSNG = \frac{C_{cap,P2X,ann} + C_{CO2,ann} + C_{H2o,ann}}{E_{SNG,ann}} + \frac{P_{elec}}{\eta_{LHV,PtG}} + C_{O\&M} \tag{A.8}$$

$$LCOE = \frac{C_{cap,ann} + C_{O2,ann} + C_{CO2,ann} + C_{H2o,ann} + C_{fuel,ann} + C_{elec,ann}}{E_{P2X,ann}} + C_{O\&M} \tag{A.9}$$

The annualized capital cost of component i is defined as

$$C_{cap,ann,i} = f_{install} C_{cap,i} (\frac{r}{1-(1+r)^{-N_t}} \tag{A.10}$$

where $f_{install}$ is the factor that accounts for the cost of installing the component, $C_{cap,i}$ is the initial cost of component i, r is the rate used to discount future costs, and $N_t$ is the number of years that component i is expected to last.

Equation A.8 can be generalised for every product produced by electrolysis, as for example hydrogen [60]. The generalised definition for a chemical X would be the LCOX, using the unit euro per kilogram of chemical X produced this would yield,

$$LCOX = \frac{CAPEX_{ann} + OPEX}{m_X} \tag{A.11}$$

The metric LCOE (Equation A.9), is also referred to as Levelised Cost of Energy Storage (LCOS) and is utilised in techno-economic analysis to compare the economic feasibility of different energy storage technologies [19].

The techno-economic study by Lamagna et al. [45] aims to simulate and analyse the economic and environmental performance of an rSOC in different scenarios on civil environment applications on an island. Three economic metrics were used to evaluate the scenarios the Net Present Value (NPV), Internal Rate of Return (IRR) and Pay Back Period (PBP). To analyse the scenarios on environmental achievements the system's primary energy savings, emission reductions and storage efficiency were studied.

The formula for Net Present Value (NPV) is:

$$NPV = \sum_{t=1}^{n} \frac{CF_t}{(1+r)^t} \tag{A.12}$$

where $CF_t$ is the cash flow at time t, r is the internal rate of return, and n is the number of time periods.

The IRR is the discount rate at which the Net Present Value (NPV) is equal to zero. The formula for the Internal Rate of Return (IRR) is:

$$0 = NPV = \sum_{t=1}^{n} \frac{CF_t}{(1+IRR)^t} \tag{A.13}$$

The payback period is defined as.

$$PBP = \frac{CAPEX}{CF_t} \tag{A.14}$$

However strong, LCOS, LCOE and PBP definitions depend on CAPEX estimations, which can rely on many uncertainties. First of all, a good CAPEX estimation requires either vendor quotations or a detailed technical design. Second, CAPEX estimations are only reliable if components from the detailed design are off-the-shelf. This makes it hard to determine reliable LCOS and LCOE definitions for technologies that are under development.

An alternate metric is the plant CAPEX target, which is proposed by Zhang et al. [98]. The plant CAPEX target is defined as the capital expenditure per reference stack for the plant to achieve a payback period equal to the plant's lifetime, $l$. The higher the plant's CAPEX target, the sooner the designed plant will become financially self-sufficient. This metric is powerful as it can be compared to industry CAPEX indications, providing insight into the feasibility of different options for a profitable energy system.

$$Plant\ CAPEX\ target\ (l) = \frac{LifetimeProfit(l)}{\#ReferenceStacks} \tag{A.15}$$

### A.5.2. Geographic and Environmental Analysis

Carbone et al. [16] performs a regional analysis to determine the best location for the studies use case. The study aims to estimate the potential deployment of a novel rSOC technology in a future power system dominated by intermittent renewables. To measure this potential at different locations the study uses two metrics. The first is the balancing need of the power grid in 2030. The second is the availability of low-grade organic waste. The study is a technical case study and does not account for the economic and political factors driving the wholesale price and the total system costs of the power grid. However, the method to asses a technological feasibility

The environmental performance indicator of a system is the amount of carbon dioxide emitted during operation. The emissions are usually calculated as the sum of the emissions of the system components and are represented in tonnes of $CO_2$ per [12]. The carbon emissions can also be represented by a carbon penalty price. That way, carbon emissions are incorporated in the LCOX (Equation A.17).

### A.5.3. Sensitivity Analysis

All techno-economic performance metrics can be augmented by a sensitivity analysis. A sensitivity analysis is conducted to assess a results dependency on various assumptions and input parameters [19, 71]. This dependency can provide a deeper understanding of the optimal operating conditions for a technology. One can, for example, asses the plant CAPEX target, for a selection of price scenarios.

## A.6. Conclusion: Research Gaps

Based on the literature analysis performed, mainly on the basis of Table A.1, several research gaps can be identified. First a broad analysis based on the applications and the system design choices was performed, then literature was analysed on the modelling approaches used, lastly methods to perform techno-economic analysis of rSOC systems were reviewed. The following research gaps were selected:

**Conclusions on research gaps**

- Techno-economic research to large scale steam rSOC in open system application
- Dynamic operational schedule, profit optimising
- Industrial rest heat integration
- Comparison of hydrogen and methane as secondary feedstock for steam rSOC

To strengthen these research gaps, their relevance and validity are shortly discussed.

As pointed out in section 2.1, the growing intermittency of the energy mix asserts a pressing need for chemical energy storage. rSOE has the potential to bring superior efficiency compared to other electrolysis technologies. Additionally, rSOEs reversible functionality could yield high capacity factors, increasing economic feasibility, compared to sole SOE plants and other electrolysis technologies. Therefore, it is relevant to assess the techno-economic feasibility of large scale steam rSOC in an open system application. As can be concluded from this literature study there exists a gap around this research interest. An rSOC-application-based literature search led to a wide range of studies, of which a selection is listed in Table A.1. Six of these applications are (partly) open system applications, that are defined as a system supplying at least a part of their chemical product, from SOEC mode to the market [16, 98, 74, 44, 13, 12]. Of these open system applications three are performing an economic analysis [98, 44, 74]. Deeper analysis shows that only Zhang et al. [98] models an open system application, but focuses on comparing different primary feedstock types. Further research gaps would bring further novelty compared Zhang et al. [98].

To assess the economic feasibility of an rSOC system a dynamic operational schedule is required. It is most realistic that this schedule is dependent on various dynamic parameters. As an example in fuel cell operation the profitability of a system can benefit from selling electricity via the spot market at a dynamic price.

To the best of the authors knowledge, there exists a gap in modelling open system rSOC applications, as shown in subsection A.4.3. This gap is the modelling of the system with an operational schedule influenced by both a dynamic power profile and dynamic power price. Additionally a gap lies in using a dynamic chemical sales and buy price.

It is interesting to study the potential of external rest heat integration, in the form of Low Pressure steam, in an rSOC system. Roughly 16% of the total energy required for producing hydrogen with SOE, consist of heat, as reported in [63]. Therefore, heat integration has the potential to increase the efficiency of the process. For large-scale applications, it becomes increasingly interesting to look at an external rest-heat source, as CAPEX of heat storage systems can scale with system capacity. At a macro and BoP system level the studies listed in Table A.1 use various heat re-use and external renewable heat generation solutions in their system designs, as described above. However, non of these studies model the use of rest-heat from industrial processes. And so, a gap remains.

Lastly, it is recommended to look at the effects of using a different secondary fuel than the electrolysis product. This would mean producing hydrogen in electrolysis mode, while using methane as secondary feedstock in fuel cell operation. A back of the envelope calculation, reveals the dependency of LCOH on the fuel cell capacity factor, the fuel price and the additional capital costs of a methane-based plant. An analysis comparing the fuels would reveal one of the two to be more favourable. A research gap exists in this research interest, as non of the studies included in this review, include this product-fuel differentiating, also this research interest lies in a gap.

# A.7. Conclusion: Research Methods

## A.7.1. Modelling Approaches

Various studies on rSOC based research were analysed on the modelling methods used. The goal was to learn what methods are most effective to fit a purpose of a research. These learnings were translated into applicable conclusion for the overarching research.

**Conclusions on modelling approaches**

- A high quality 0D model is deemed sufficient to represent stack or even balance of stack operation
- As a starting point the BoP can be modelled as 0D unit based modelbe modelled as a oD model
- A more detailed BoP design can be made in a later stage, with the purpose of improving system performance by comparing plant configurations
- Cell degradation is significant and should be taken into account
- A time dependent model is required, preferably with a profit optimisation
- Use of computational time reducing methods based on representative days is recommended.

In this literature review three dimensions of stack modelling have been proposed, of which 0D is deemed most applicable for integrated system modelling. The depth of each model should serve the purpose of the research. With respect to 0D, 1D and 0.5D models allow for a more in depth understanding of the cell performance. The use of these models can be to identify potential limitations or areas for improvement. As Stack or BoS system dynamics performance improvement is not the direct purpose of the overarching research. A high quality low fidelity 0D model is deemed sufficient to represent stack and balance of stack (module) operation. To do this a performance map from literature, or from vendor can be used.

The design of Balance of Stack (BoS) and Balance of Plant (BoP) is an important aspect of chemical process engineering, and can be achieved through the use of various chemical process design programs. The same line of reasoning holds for the BoP design, compared to just described stack modelling. It is recommended to base the depth of BoS and BoP modelling on the purpose of the research. The primary objectives of creating a detailed BoP design include improving system performance, comparing BoP designs for different plant configurations (such as the use of methane or hydrogen as secondary feedstock), and determining accurate cost estimates through precise system dimension. For undeveloped technologies such as rSOC a detailed BoP design does not necessarily lead to accurate cost estimations.

Based on the theory described in subsection 2.2.1, it can be concluded that cell degradation is a significant phenomenon that is worth taking into account. Using the degradation rate seen in [68], a full year operation results in a 7% voltage degradation. In the authors opinion, only taking into account a system lifetime does not suffice as the yearly effect is so significant. It is clear that there exists a difference in degradation for SOFC and SOEC operation (2.2.1) [35, 62]. However, further research is needed to come to a definite answer to use in a model. Therefore, taking into account a linear degradation, based on pilot experiment results, as is done by Chadly et al. [19] is deemed sufficient as a modelling starting point.

A time-dependent model, preferably with a profit optimising operational schedule is required to study the effects of reversible SOE operation over the lifetime of a system. A starting point can be to operate on the day ahead market. It can be used to generate time-dependent profiles, allowing dynamic system analysis. Throughout rSOC related literature, optimisations are used to determine operational schedules and perform system component sizing. As the focus of the overarching study is not dedicated on optimising, simplified version of these methods should be adapted.

Optimisations and time-dependent profiles can bring added perspective to a system study. In that case, reducing computational time can be a valuable endeavour as time resolution and the number of calculations per time step can significantly increase computational time. One approach to decrease computational time is to approximate parameters with a predictable time-based pattern, such as representative or typical days, as is done in the k-means method.

Literature examples show that computational time can be reduced by over 90%, using these methods. By analysing these examples, it was concluded that, more than eight typical days are expected to be required, to capture the essential characteristics of a combined fluctuating price and fluctuating power profile system.

### A.7.2. Conclusion: Techno-Economic KPI Analysis

To learn what techno economic analysis metrics and methods are most effective for rSOC based research, several techno-economic studies were reviewed in section A.5. These learnings led to a selection of applicable suggestion for the overarching research.

**Conclusions on techno economic approaches**

- A CAPEX-target metric is recommended to measure techno-economic performance
- CAPEX estimations of immature technologies can quickly become uncertain
- Other insightful metrics are LCOE, PBP, NPV, IRR and an open system specific proposed LCOH definition
- The thermodynamic performance of a system can be indicated by the LHV efficiencies, the hydrogen yield and electricity yield.
- A geographical analysis can be done on the basis of a promising starting base case location.
- A sensitivity analysis can provide a deeper understanding of the optimal operating conditions for a technology.

Using a CAPEX target as a metric is recommended to measure the techno-economic performance of an immature technology based system, as rSOC. Many TEA studies base their metrics on component based CAPEX estimations. However, these can be unreliable as the components used are not necessarily off-the-shelf. Therefore flipping this metric, by determining a CAPEX target can serve to indicate the feasibility of a system. An example is the CAPEX Target per reference stack from [98]

$$Plant\ CAPEX\ target\ (l) = \frac{LifetimeProfit(l)}{\#ReferenceStacks} \tag{A.16}$$

Keeping in mind that CAPEX estimations can be uncertain, CAPEX-based metrics can still be used. Most commonly used for P2X and P2X2P systems are respectively the LCOX and LCOS. An open system rSOC application in which the amount of chemical produced is not necessarily equal to the amount of chemicals used to make electricity, can be denoted as P2X(2P). As a P2X(2P) application falls between these two definitions an addition to the LCOH definition is proposed.

$$LCOH = \frac{CAPEX_{ann} + OPEX - CF_{e,ann}}{m_{X,ann}} \tag{A.17}$$

With $m_X, ann$ being the mass of the annually produced hydrogen. Derived from that, the LCOH is represented as Euro/kg of hydrogen produced. The variable $CAPEX_{ann}$ is defined as the annualised (discounted) capital expenditure. While OPEX is the operational expenditure, including the Costs of Good Sold (CoGS), being the electricity, secondary feedstock and CO2 penalty used for respectively electrolysis and fuel cell operation. In this way the additional revenue stream created in fuel cell operation is entwined in the LCOH definition.

Additional KPIs worth looking at are the, mass of produced Hydrogen, Net Present Value (NPV), Internal Rate of Return (IRR) and Pay Back Period (PBP).

In general, technical performance is indicated by the lower heating value (LHV) efficiencies for both operational modes (P2X and X2P).

$$\eta_{LHV,P2X} = \frac{\dot{m}_X LHV_X}{\dot{W}_{net,AC}} \tag{A.18}$$

$$\eta_{LHV,X2P} = \frac{\dot{W}_{net,AC}}{\dot{m}_X LHV_X} \tag{A.19}$$

All techno-economic performance metrics can be augmented by a sensitivity analysis. A sensitivity analysis is conducted to assess a results dependency on various assumptions and input parameters, which can provide a deeper understanding of the optimal operating conditions for a technology.

# B

# Appendix: Methodology

## B.1. Steady State Performance Map

| SOEC | 200MW | | | |
|---|---|---|---|---|
| Operating point ratio | Efficiency | Specific energy use | H2 production | Steam use |
| [-] | [-] | [kWh/kg] | [kg/h] | [kg/h] |
| 1,20 | 0,82 | 40,3 | 6473 | 71919 |
| 0,97 | 0,81 | 40,8 | 5173 | 57481 |
| 0,74 | 0,80 | 41,0 | 3924 | 43603 |
| 0,51 | 0,78 | 42,5 | 2612 | 29020 |
| 0,28 | 0,72 | 46,1 | 1324 | 14707 |

| SOFC (H2) | 50MW | | |
|---|---|---|---|
| Operating point | Efficiency | Specific energy production | H2 use |
| [-] | [-] | [kWh/kg] | [kg/h] |
| 1,48 | 0,56 | 18,4 | 4018 |
| 1,24 | 0,58 | 19,1 | 3228 |
| 0,96 | 0,58 | 19,2 | 2491 |
| 0,64 | 0,60 | 20,0 | 1594 |
| 0,27 | 0,45 | 14,9 | 893 |

| SOFC (NG) | 50MW | | |
|---|---|---|---|
| Operating point | Efficiency | Specific energy production | NG use |
| [-] | [-] | [kWh/kg] | [kg/h] |
| 1,43 | 0,58 | 7,7 | 9350 |
| 1,19 | 0,61 | 8,0 | 7490 |
| 0,92 | 0,62 | 8,2 | 5619 |
| 0,58 | 0,58 | 7,6 | 3781 |
| 0,19 | 0,33 | 4,3 | 2154 |

Figure B.1: The steady state performance map results of the SOEC and SOFC for hydrogen and natural gas as secondary feedstock.

## B.2. Specific Energy Curves

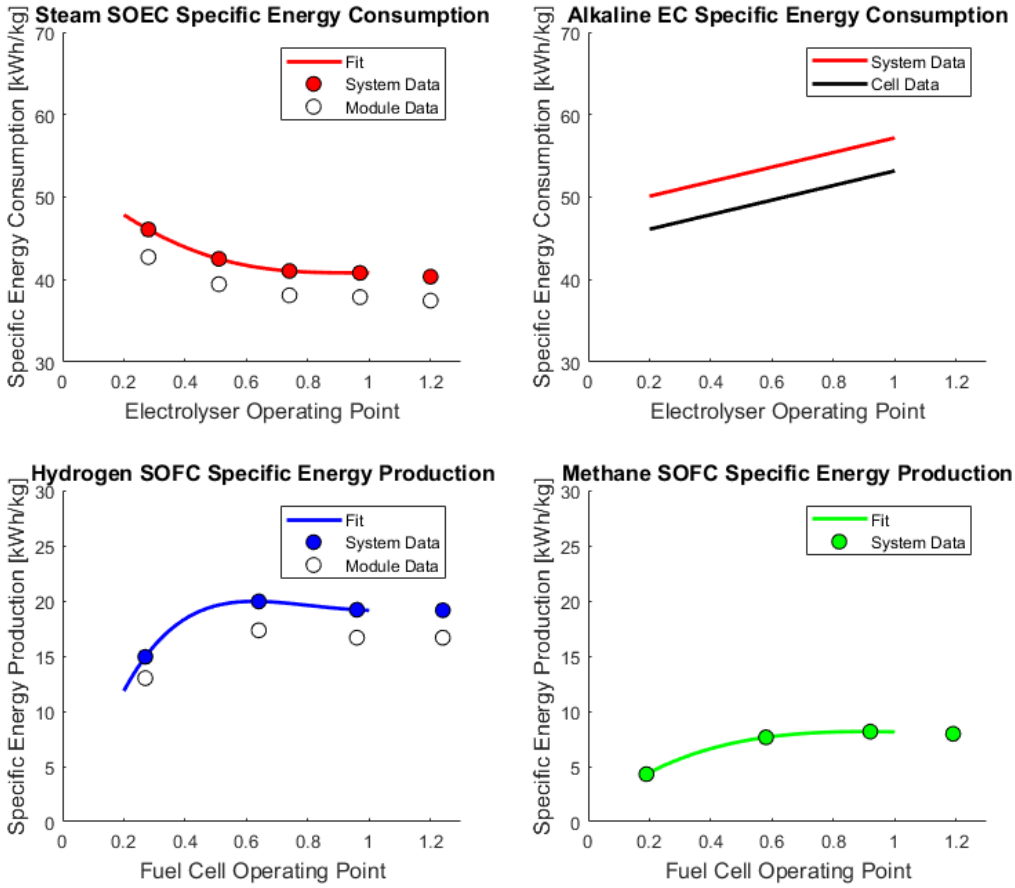


Figure B.2: Efficiency curves displayed as specific energy production and consumption for different operating modes in different configurations: steam SOEC, alkaline EC, hydrogen SOFC, methane SOFC.

## B.2.1. Alkaline Specific Energy Curve Background

**Stack Rated Values (SOL)**

| | | |
|---|---|---|
| Power = | 18233 | kW |
| Voltage = | 548 | V |
| Current = | 33296 | A |

**Output**

| | | |
|---|---|---|
| | 4121,9 | $Nm^3/hr$ |
| Production = | 4,4 | $kWh/Nm^3$ |

**Unit Dimensions**

| | | |
|---|---|---|
| Cell diameter = | 1,92 | m |
| Cell area = | 2,895 | $m^2$ |
| No of Cells = | 296 | *60* |
| Cell thickness | | cm |
| Stack height = | 0 | m |

| | | |
|---|---|---|
| F = | 9,65E+04 | C/mol |
| 1 kg H2 = | 496,03 | mol |
| | 1,11E+01 | m3 |
| Faradaic Eff = | 100% | |

I = 1,15 A/cm2

| Operating range of one module: | | | |
|---|---|---|---|
| | 20% | 100% | |
| Current | 3330 | 33296 | A |
| H2 | 412,2 | 4121,9 | Nm3/hr |

**Example, start of life**

| | Compressior | 2 | kwh/kg |
|---|---|---|---|
| | Other | 2 | kwh/kg |

| | Load % | i / A $cm^{-2}$ | $E_{cell}$ / V | $i_{stack}$ / A | $E_{stack}$ / V | P / kW | $H_2$ / kg $hr^{-1}$ | $H_2$ / $Nm^3$ $hr^{-1}$ | Specific e | Specific e+ | Eff % |
|---|---|---|---|---|---|---|---|---|---|---|---|
| 0 | 0 | 0,00 | 1,23 | 0 | 364 | 0 | 0,0 | 0,0 | 0,0 | | |
| 0,1 | 10 | 0,12 | 1,55 | 3330 | 459 | 1528 | 37,1 | 412,2 | 41,2 | 45,2 | 0,73 |
| 0,2 | 20 | 0,23 | 1,58 | 6659 | 469 | 3121 | 74,1 | 824,4 | 42,1 | 46,1 | 0,72 |
| 0,3 | 30 | 0,35 | 1,62 | 9989 | 479 | 4780 | 111,2 | 1236,6 | 43,0 | 47,0 | 0,70 |
| 0,4 | 40 | 0,46 | 1,65 | 13318 | 488 | 6505 | 148,3 | 1648,8 | 43,9 | 47,9 | 0,69 |
| 0,5 | 50 | 0,58 | 1,68 | 16648 | 498 | 8295 | 185,3 | 2060,9 | 44,8 | 48,8 | 0,68 |
| 0,6 | 60 | 0,69 | 1,72 | 19978 | 508 | 10151 | 222,4 | 2473,1 | 45,6 | 49,6 | 0,66 |
| 0,7 | 70 | 0,81 | 1,75 | 23307 | 518 | 12073 | 259,5 | 2885,3 | 46,5 | 50,5 | 0,65 |
| 0,8 | 80 | 0,92 | 1,78 | 26637 | 528 | 14061 | 296,5 | 3297,5 | 47,4 | 51,4 | 0,64 |
| 0,9 | 90 | 1,04 | 1,82 | 29966 | 538 | 16114 | 333,6 | 3709,7 | 48,3 | 52,3 | 0,63 |
| 1 | 100 | 1,15 | 1,85 | 33296 | 548 | 18233 | 370,7 | 4121,9 | 49,2 | 53,2 | 0,62 |
| | 110 | 1,27 | 1,88 | 36625 | 557 | 20417 | 407,7 | 4534,1 | 50,1 | 54,1 | 0,61 |

| Assume output is: | | |
|---|---|---|
| 99,90% | H2 | |
| 0,10% | O2 | |
| 0,5 | barg | |

**Example, end of life (8 years)**

| % | i / A $cm^{-2}$ | $E_{cell}$ / V | $i_{stack}$ / A | $E_{stack}$ / V | P / kW | $H_2$ / kg $hr^{-1}$ | $H_2$ / $Nm^3$ $hr^{-1}$ | Eff % |
|---|---|---|---|---|---|---|---|---|
| 0 | 0,00 | 1,23 | 0 | 364 | 0 | 0,0 | 0,0 | |
| 10 | 0,12 | 1,80 | 3330 | 533 | 1774 | 37,1 | 412,2 | 82% |
| 20 | 0,23 | 1,83 | 6659 | 543 | 3614 | 74,1 | 824,4 | 81% |
| 30 | 0,35 | 1,87 | 9989 | 553 | 5519 | 111,2 | 1236,6 | 79% |
| 40 | 0,46 | 1,90 | 13318 | 562 | 7490 | 148,3 | 1648,8 | 78% |
| 50 | 0,58 | 1,93 | 16648 | 572 | 9527 | 185,3 | 2060,9 | 77% |
| 60 | 0,69 | 1,97 | 19978 | 582 | 11630 | 222,4 | 2473,1 | 75% |
| 70 | 0,81 | 2,00 | 23307 | 592 | 13798 | 259,5 | 2885,3 | 74% |
| 80 | 0,92 | 2,03 | 26637 | 602 | 16032 | 296,5 | 3297,5 | 73% |
| 90 | 1,04 | 2,07 | 29966 | 612 | 18331 | 333,6 | 3709,7 | 72% |
| 100 | 1,15 | 2,10 | 33296 | 622 | 20697 | 370,7 | 4121,9 | 70% |
| 110 | 1,27 | 2,13 | 36625 | 631 | 23128 | 407,7 | 4534,1 | 69% |

Figure B.3: Alkaline Efficiency calculation sheet used to make the Specific Energy Curve Figure 3.7, assumptions based on [39].

## B.3. Flow Diagrams

In this subsection, the process flow diagrams of the rSOE ($H_2$) and rSOE (NG) are depicted. These are used to create the steady state performance map presented in section B.1.

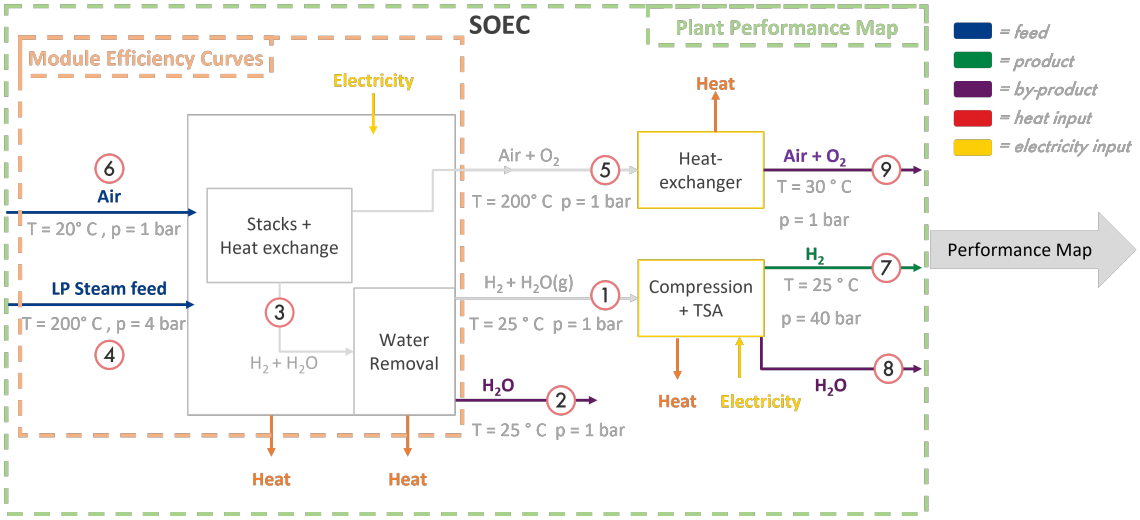


Figure B.4: Steam SOEC process flow schematic indicating the various key process points, module scope and performance map scope. Note: Heat integration through heat exchange is included in the module. Integrating remaining heat flows (Orange arrows) is an opportunity for efficiency improvement, but are left not-optimised.

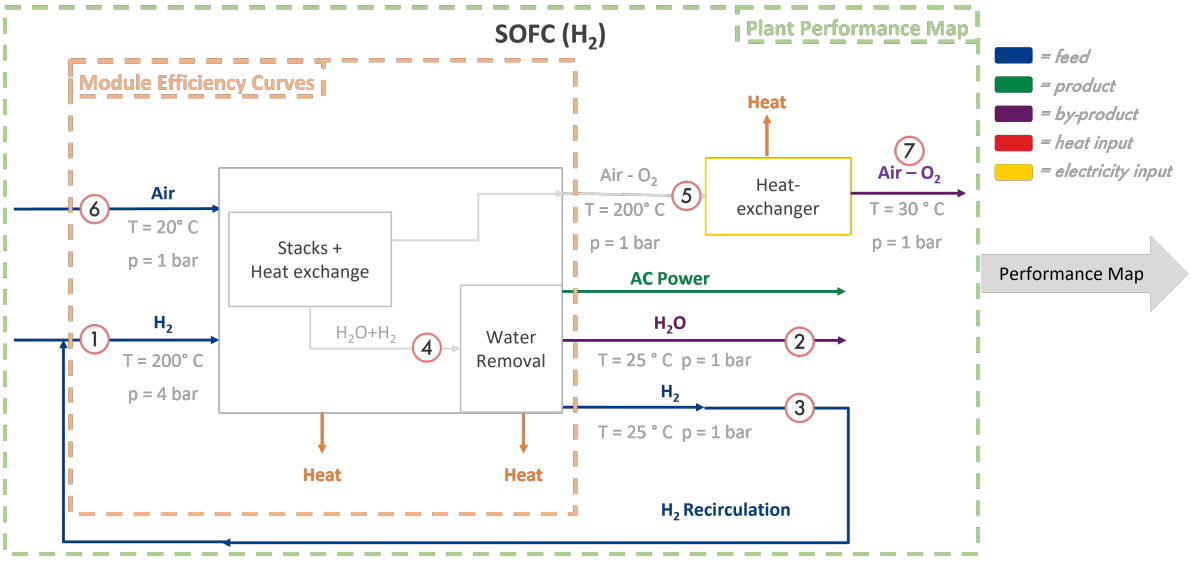


Figure B.5: Hydrogen-based SOFC process flow schematic indicating the various key process points, module scope and performance map scope. Note: Heat integration through heat exchange is included in the module. Integrating remaining heat flows (Orange arrows) is an opportunity for efficiency improvement, but are left not-optimised.

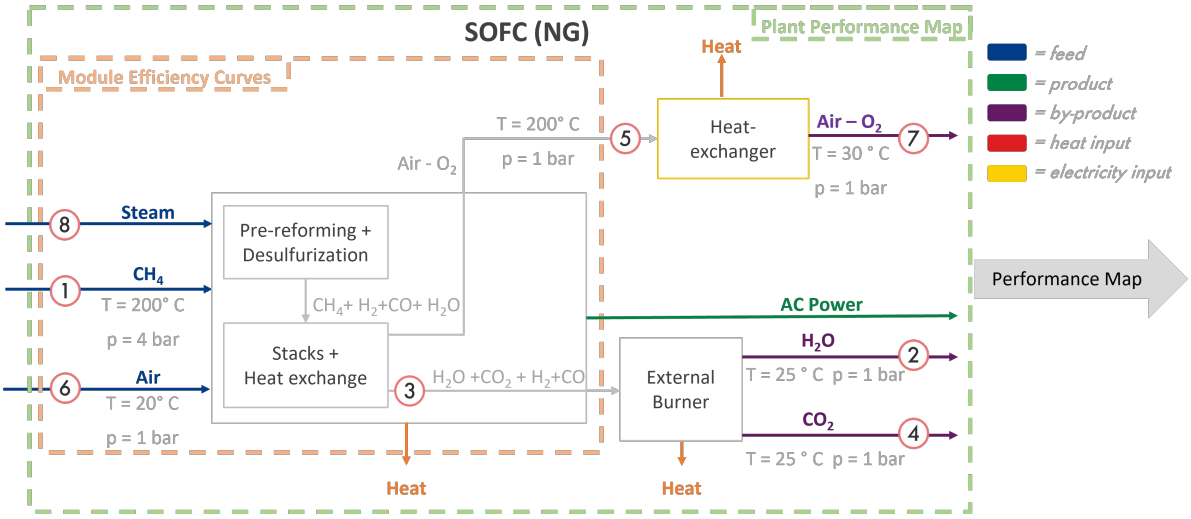


Figure B.6: NG-based SOFC process flow schematic indicating the various key process points, module scope and performance map scope. Note: Heat integration through heat exchange is included in the module. Integrating remaining heat flows (Orange arrows) is an opportunity for efficiency improvement, but are left not-optimised.

## B.4. Parameters for the Steady State Model

The required parameters are the Steam Utilization Factor $UF_{steam}$, desired molar fraction of oxygen $X_{O_2}$ in the incoming air, molar masses of all components $\mu_X$ and the amount of saturated water in hydrogen at different temperatures and pressures ($y_{H2O}$ ).

Table B.1: Parameters used in the steady state model

| Component | Parameter | Description | Unit | Value | Ref |
|---|---|---|---|---|---|
| rSOE | $e_X(p)$ | Specific energy curve of configuration X | (-) | Figure 3.7 | [83] |
| | $UF_{steam}$ | Steam Utilisation Factor | $\%_{mol}$ | 81 | [83] |
| | $UF_{H_2}$ | Fuel ($H_2$) Utilisation Factor | $\%_{mol}$ | 86 | [83] |
| | $LHV_{H_2}$ | Lower Heating Value | $kWh/kg$ | 33.33 | [83] |
| | $X_{O_2,EC}$ | Desired molar fraction of oxygen in EC out | $\%_{mol}$ | 33 | [83] |
| | $X_{O_2,FC}$ | Desired molar fraction of oxygen in FC out | $\%_{mol}$ | 18.5 | [83] |
| | $y_{H_2O}(T,P)$ | Saturated water in hydrogen | $\%_{mol}$ | Figure B.7 | [72, 10] |
| Compressor | $e_{comp}$ | Nominal energy consumption of the compressor | $kWh/kg$ | 2.68 | B.4.2 |
| | $n$ | Number of stages | $(-)$ | 3 | [83] |
| | $P_{comp}$ | Total installed compressor capacity | $MW$ | 19 | [83] |
| Hydrogen | $T_{dp}$ | Hydrogen backbone required dewpoint | °C | <-20 | [1] |
| Backbone | $DP$ | Degree of Purity of qualified grade hydrogen | % | >99 | [96] |
| General | $\Delta H$ | Electrolysis enthalpy change at 800 °C | $kJ/mol$ | 248.4 | [24] |
| | $\Delta G$ | Electrolysis gibbs energy change at 800 °C | $kJ/mol$ | 188.4 | [24] |
| | $T\Delta S$ | Electrolysis enthalpy change at 800 °C | $kJ/mol$ | 60 | [24] |

### B.4.1. Saturated Water Content

Linear interpolation is used as an estimate, to determine water content in hydrogen at flow points 1 and 8.

| Saturated water in Hydrogen at pressure P and temperature T | | | |
|---|---|---|---|
| T | P | $Y_{H2O}$ | Source |
| *[K]* | *[bar]* | *[mole $H_2O$ /mole $H_2$]* | |
| 310 | 1 | 0,0109 | Lin int |
| 310 | 40 | 0,00405 | Lin int |
| 310 | 10 | 0,0093 | |
| 310 | 50 | 0,0023 | |
| 310 | 80 | 0,0013 | |
| | | | |
| 283 | 1 | 0,0021 | Lin int |
| 283 | 40 | 0,0007 | Lin int |
| 283 | 10 | 0,0018 | |
| 283 | 50 | 0,00037 | |
| 283 | 80 | 0,00024 | |
| | | $Y_{H2O, 1}$ | |
| 310 | 1 | 0,0109 | |
| 283 | 1 | 0,0021 | |
| 298 | 1 | 0,0070 | Lin int |
| | | $Y_{H2O, 8}$ | |
| 310 | 40 | 0,00405 | |
| 283 | 40 | 0,0007 | |
| 298 | 40 | 0,0026 | Lin int |

Figure B.7: $y_{H_2O}$: Linear interpolation of saturated water content graph from [72, 10]. Blue filled cells indicates data extracted from sources.

## B.4.2. Three Stage Compression Table

Compressor energy duty is calculated according to the data in Figure B.8. Linear scaling of this energy duty with hydrogen massflow is assumed in the specific energy calculations.

| Input: | | |
|---|---|---|
| inlet pressure | 1 | bar |
| isentropic efficiency | 0,65 | - |
| input temperature | 27 | deg Celsius |

| Constants/variables: | | | |
|---|---|---|---|
| gas constant | R | 8,314 | Pa*m3/Kmol |
| molar weight H2 | M_H2 | 0,0020157 | kg/mol |
| heat capacity ratio | k | 1,42 | - |
| average compressibility factor | Z_a | 1,1381 | - |
| flow rate | Q | 1 | kg/hr |
| LHV H2 | | 33,3 | kWh/kg |
| HHV H2 | | 39,41 | kWh/kg |

sources:
http://www.jmcampbell.com/tip-of-the-month/2011/11/compressor-calculations-rigorous-using-equation-of-state-vs-shortcut-method/
https://www.industrializedcyclist.com/ulf%20bossel.pdf
https://www.youtube.com/watch?v=ZkTw8bNrshA

| | output pressure [bar] | | | | | | | | | | | |
|---|---|---|---|---|---|---|---|---|---|---|---|---|
| | 40 | 70 | 100 | 200 | 300 | 400 | 500 | 600 | 700 | 800 | 900 | 1000 |
| ISOTHERMAL | | | | | | | | | | | | |
| isothermal: [J/s] | 1268,58 | 1461,03 | 1583,69 | 1822,06 | 1961,50 | 2060,43 | 2137,16 | 2199,86 | 2252,88 | 2298,80 | 2339,30 | 2375,53 |
| isothermal: [kWh/kg] | 1,27 | 1,46 | 1,58 | 1,82 | 1,96 | 2,06 | 2,14 | 2,20 | 2,25 | 2,30 | 2,34 | 2,38 |
| percentage of HHV | 3,22% | 3,71% | 4,02% | 4,62% | 4,98% | 5,23% | 5,42% | 5,58% | 5,72% | 5,83% | 5,94% | 6,03% |
| ADIABATIC, ISENTROPIC | | | | | | | | | | | | |
| adiabatic, isentropic: [J/s] | 2616,71 | 3325,93 | 3843,20 | 5018,80 | 5826,87 | 6461,90 | 6993,05 | 7453,83 | 7863,28 | 8233,36 | 8572,15 | 8885,38 |
| adiabatic, isentropic: [kWh/kg] | 2,62 | 3,33 | 3,84 | 5,02 | 5,83 | 6,46 | 6,99 | 7,45 | 7,86 | 8,23 | 8,57 | 8,89 |
| percentage of HHV | 6,64% | 8,44% | 9,75% | 12,73% | 14,79% | 16,40% | 17,74% | 18,91% | 19,95% | 20,89% | 21,75% | 22,55% |
| 1-stage: adiabatic | | | | | | | | | | | | |
| temperature after stage [C] | 940 | 1188 | 1368 | 1778 | 2060 | 2282 | 2467 | 2628 | 2771 | 2900 | 3018 | 3128 |
| adiabatic, NOT isentropic [J/s] | 4025,71 | 5116,82 | 5912,62 | 7721,23 | 8964,41 | 9941,38 | 10758,54 | 11467,43 | 12097,35 | 12666,71 | 13187,93 | 13669,82 |
| adiabatic, NOT isentropic [kWh/kg | 4,03 | 5,12 | 5,91 | 7,72 | 8,96 | 9,94 | 10,76 | 11,47 | 12,10 | 12,67 | 13,19 | 13,67 |
| percentage of HHV | 10,21% | 12,98% | 15,00% | 19,59% | 22,75% | 25,23% | 27,30% | 29,10% | 30,70% | 32,14% | 33,46% | 34,69% |
| 2-stage: **(intercooling back to initial temperature**, equal pressure ratios between stages) | | | | | | | | | | | | |
| intercooling pressure [bar] | 6 | 8 | 10 | 14 | 17 | 20 | 22 | 24 | 26 | 28 | 30 | 32 |
| temperature after stage [C] | 362 | 431 | 478 | 576 | 639 | 685 | 723 | 754 | 782 | 806 | 828 | 848 |
| adiabatic, NOT isentropic [J/s] | 2954,07 | 3560,24 | 3973,61 | 4842,05 | 5392,89 | 5804,24 | 6135,58 | 6414,54 | 6656,33 | 6870,29 | 7062,55 | 7237,40 |
| adiabatic, NOT isentropic [kWh/kg | 2,95 | 3,56 | 3,97 | 4,84 | 5,39 | 5,80 | 6,14 | 6,41 | 6,66 | 6,87 | 7,06 | 7,24 |
| percentage of HHV | 7,50% | 9,03% | 10,08% | 12,29% | 13,68% | 14,73% | 15,57% | 16,28% | 16,89% | 17,43% | 17,92% | 18,36% |
| 3-stage: **(intercooling back to initial temperature**, equal pressure ratios between stages) | | | | | | | | | | | | |
| intercooling pressure [bar] | 3,42 | 4,12 | 4,64 | 5,85 | 6,69 | 7,37 | 7,94 | 8,43 | 8,88 | 9,28 | 9,65 | 10,00 |
| temperature after stage [C] | 230 | 267 | 292 | 344 | 376 | 399 | 417 | 433 | 446 | 458 | 468 | 478 |
| adiabatic, NOT isentropic [J/s] | 2678,87 | 3177,26 | 3509,56 | 4189,74 | 4609,71 | 4918,03 | 5163,27 | 5367,70 | 5543,43 | 5697,82 | 5835,71 | 5960,42 |
| adiabatic, NOT isentropic [kWh/kg | 2,68 | 3,18 | 3,51 | 4,19 | 4,61 | 4,92 | 5,16 | 5,37 | 5,54 | 5,70 | 5,84 | 5,96 |
| percentage of HHV | 6,80% | 8,06% | 8,91% | 10,63% | 11,70% | 12,48% | 13,10% | 13,62% | 14,07% | 14,46% | 14,81% | 15,12% |
| 4-stage: **(intercooling back to initial temperature**, equal pressure ratios between stages) | | | | | | | | | | | | |
| intercooling pressure [bar] | 2,51 | 2,89 | 3,16 | 3,76 | 4,16 | 4,47 | 4,73 | 4,95 | 5,14 | 5,32 | 5,48 | 5,62 |
| temperature after stage [C] | 172 | 197 | 214 | 248 | 269 | 284 | 296 | 306 | 315 | 322 | 329 | 335 |
| adiabatic, NOT isentropic [J/s] | 2553,66 | 3005,57 | 3303,52 | 3905,50 | 4272,21 | 4539,14 | 4750,13 | 4925,13 | 5074,94 | 5206,10 | 5322,87 | 5428,19 |
| adiabatic, NOT isentropic [kWh/kg | 2,55 | 3,01 | 3,30 | 3,91 | 4,27 | 4,54 | 4,75 | 4,93 | 5,07 | 5,21 | 5,32 | 5,43 |
| percentage of HHV | 6,48% | 7,63% | 8,38% | 9,91% | 10,84% | 11,52% | 12,05% | 12,50% | 12,88% | 13,21% | 13,51% | 13,77% |

Figure B.8: Excel calculation sheet, for the energy use of the three stage compressor [11]. Used value is marked red.

# B.5. Mass and Energy Balances

## B.5.1. Mass Balances: SOEC

For the flows indicated by the red circled numbers in Figure B.4, the mass flow diagrams were constructed. The mass balances use the parameters listed in Table B.1 and the specific energy curves from Shell [83].

$$\dot{m}_1 = \dot{m}_{1,H_2} + \dot{m}_{1,H_2O(g)} \tag{B.1}$$

$$\dot{m}_{1,H_2} = \frac{P_{ac}}{e_{ECmodule}} \tag{B.2}$$

In this equation $e_{EC,module}$ is the EC module specific energy consumption, as a function op operating capacity as represented by the black-lined circles in Figure B.2.

$$\dot{m}_{1,H_2O(g)} = \frac{\dot{m}_{1,H_2}}{\mu_{H_2}} y_{H_2O,1} \tag{B.3}$$

$$\dot{m}_2 = (1 - UF_{steam}) \frac{\dot{m}_{1,H_2}}{\mu_{H_2} UF_{steam}} \mu_{H_2O} - \dot{m}_{1,H_2O(g)} \tag{B.4}$$

$$\dot{m}_3 = \dot{m}_1 + \dot{m}_2 \tag{B.5}$$

$$\dot{m}_{5(O_2)} = \frac{1}{2} \frac{\dot{m}_{1,H_2}}{\mu_{H_2}} \mu_{O_2} \tag{B.6}$$

$$\dot{m}_5 = \frac{1}{X_{O_2}} \frac{\dot{m}_{5(O_2)}}{\mu_{O_2}} \mu_{air,5} \tag{B.7}$$

$$\dot{m}_6 = \dot{m}_5 - \dot{m}_{5(O_2)} \tag{B.8}$$

$$\dot{m}_4 = \dot{m}_3 + \dot{m}_5 - \dot{m}_6 \tag{B.9}$$

$$\dot{m}_7 = \dot{m}_1 - \dot{m}_8 \tag{B.10}$$

$$\dot{m}_8 = (y_{H_2O,1} - y_{H_2O,8}) \frac{\dot{m}_{1,H_2}}{\mu_{H_2}} \mu_{H_2O} \tag{B.11}$$

With $y_{H_2O,1}$ and $y_{H_2O,8}$ being the water concentration in hydrogen. In the validation $y_{H_2O,8}$ was set at the value according to pressure and temperature (Figure B.7). From this it was concluded an absorbing bed technology as a TSA is required. As values resulting from $\dot{m}_8$ are not used in the performance map, precise calculations of absorbing capacity of the TSA are left out of scope.

$$\dot{m}_9 = \dot{m}_5 \tag{B.12}$$

## B.5.2. Mass Balances:SOFC ($H_2$)

In this equation $e_{FCH_2,module}$ is the module specific energy production as a function op operating capacity as represented by the black-lined circles in Figure B.2.

$$\dot{m}_{1,H_2} = \frac{P_{ac}}{e_{FC,H_2,module}} \tag{B.13}$$

$$\dot{m}_{2,H_2O} = \frac{\dot{m}_{1,H_2}}{\mu_{H_2}} FUF \mu_{H_2} \tag{B.14}$$

$$\dot{m}_{3,H_2} = \dot{m}_{1,H_2} FUF \tag{B.15}$$

$$\dot{m}_{4,H_2+H_2O} = \dot{m}_{1,H_2} + \dot{m}_{2,H_2O} \tag{B.16}$$

$$\dot{m}_5 = \frac{\dot{m}_{O_2}}{\mu_{O_2}} \frac{\mu_{air,5}}{\chi_{O_2,FC}} \tag{B.17}$$

$$\dot{m}_{6,O_2} = \frac{\dot{m}_{2,H_2O}}{2\mu_{H_2O}} \mu_{O_2} \tag{B.18}$$

$$\dot{m}_6 = \dot{m}_5 + \dot{m}_{6,O_2} \tag{B.19}$$

$$\dot{m}_7 = \dot{m}_6 \tag{B.20}$$

### B.5.3. Mass Balances:SOFC (NG)

The essential information for the macro model is the feedstock consumption in NG mode,

$$\dot{m}_{1,NG} = \frac{P_{ac}}{e_{FC,NG,module}} \tag{B.21}$$

In this equation $e_{FCH_2,module}$ is the module specific energy production as a function op operating capacity as represented by the black-lined circles in Figure B.2.

### B.5.4. Energy Balances: SOEC

Energy balances where constructed to establish knowledge of where and in what form the energy flows. The energy balances were constructed for SOEC operation and served as validation of heat-integration potential. The module specific energy consumption curves were modified for the compressor energy consumption. The general equation for energy balance was used

$$Q = -(W_e + \Delta H^0_{reaction} + \Delta H_{th}) \tag{B.22}$$

,in which $Q$ is the heat released by the system, $W_e$ is the electrical power supplied to the electrolyser, $\Delta H_{reaction}$ the enthalpy of the reaction and $\Delta H_{th}$ the enthalpy change in product flow streams due to temperature and pressure changes. Unit of these variables are [kJ/hour]. As units kJ per hours are used, the name denoting electrical power consumption, $W_e$, is modified compared to the definition used for the mass balances$P_{AC}$. In this system the gravitational and kinetic internal energy are neglected. The enthalpy changes are calculated as,

$$\Delta H_{th} = \sum \dot{m}_i h_i, \tag{B.23}$$

$$\Delta h^o_{f,reaction} = \sum \Delta h^o_f(products) - \sum \Delta h^o_f(reactants), \tag{B.24}$$

$$\Delta H^o_{reaction} = \Delta h^o_{f,reaction} \frac{\dot{m}_{product}}{\mu_{product}}. \tag{B.25}$$

SOEC: Module

For the system in electrolysis mode the following energy balances hold

$$\Delta H_{th} = \dot{m}_4 h_4 + \dot{m}_6 h_6 - \dot{m}_5 h_5 - \dot{m}_2 h_2 - \dot{m}_1 h_1 \tag{B.26}$$

$$\Delta h^o_{f,reaction} = \frac{1}{2} * \Delta h^o_f(O_2) + \Delta h^o_f(H_2) - \Delta h^o_f(H_2O) \tag{B.27}$$

$$\Delta h^o_{f,reaction} = \frac{1}{2} * 0[KJ/mol] + 0[KJ/mol] - (-)248.4[KJ/mol] \tag{B.28}$$

$$\Delta H^o_{reaction} = \Delta h^o_{f,reaction} \frac{\dot{m}_1}{\mu_{H_2}} \tag{B.29}$$

$$W_e = P_{AC,SOEC} * 3600 \tag{B.30}$$

SOEC: Water separation

$$\Delta H_{th} = \dot{m}_3 h_3 - \dot{m}_1 h_1 - \dot{m}_2 h_2 \tag{B.31}$$

$$\Delta H^o_{reaction} = 0 \tag{B.32}$$

$$W_e = 0 \tag{B.33}$$

$$Q = -\Delta H_{th} \tag{B.34}$$

SOEC: Internal air heatexchange

Inside the module, heat from the sweep air, $\dot{m}_{10}$ is exchanged with incoming flows. After the heat exchange the flow is denoted $\dot{m}_5$.

$$\Delta H_{th} = \dot{m}_{10} h_{10} - \dot{m}_5 h_5 \tag{B.35}$$

$$\Delta H^o_{reaction} = 0 \tag{B.36}$$

$$W_e = 0 \tag{B.37}$$

$$Q = -\Delta H_{th} \tag{B.38}$$

SOEC: Product gas internal heatexchange

Inside the module, heat from the product gas, $\dot{m}_{11}$ is exchanged with incoming flows. After the heat exchange the flow is denoted $\dot{m}_3$.

$$\Delta H_{th} = \dot{m}_{11} h_{11} - \dot{m}_3 h_3 \tag{B.39}$$

$$\Delta H^o_{reaction} = 0 \tag{B.40}$$

$$W_e = 0 \tag{B.41}$$

$$Q = -\Delta H_{th} \tag{B.42}$$

SOEC: Outside air heatexchange

A component in the module

$$\Delta H_{th} = \dot{m}_9 h_9 - \dot{m}_5 h_5 \tag{B.43}$$

$$\Delta H^o_{reaction} = 0 \tag{B.44}$$

$$W_e = 0 \tag{B.45}$$

$$Q = -\Delta H_{th} \tag{B.46}$$

SOEC: Compressor
3compressors and 3coolers

$$\Delta H_{th} = \dot{m}_1 h_1 - \dot{m}_7 h_7 - \dot{m}_8 h_8 \tag{B.47}$$

$$\Delta H^o_{reaction} = 0 \tag{B.48}$$

$$W_e = W_{compressor} \tag{B.49}$$

$$Q = -(W_e + \Delta H_{th}) \tag{B.50}$$

## B.5.5. Heat Flow Diagram

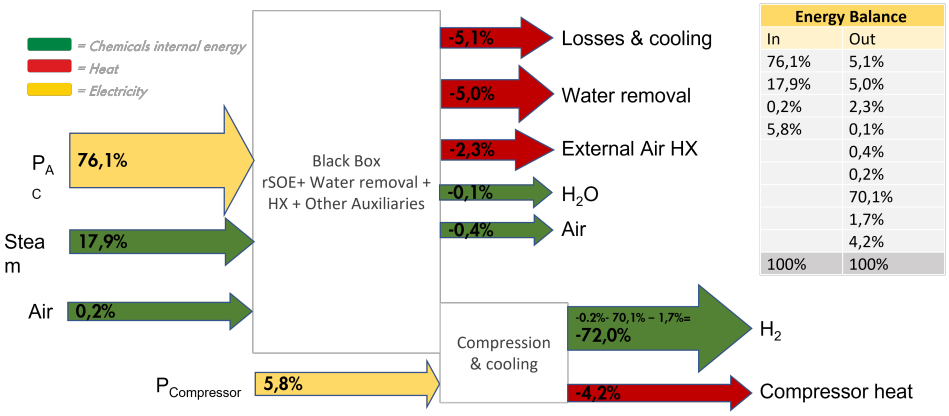


Figure B.9: Sanky Diagram indicating energy flows in the overall rSOE process.

### B.5.6. Degradation

As discussed in subsection A.1.4 stack degradation is a significant phenomena. It is clear that there exists a difference in degradation for SOFC and SOEC operation (A.1.4) [35, 62]. However, further research is needed to come to a definite answer to use in a model. Therefore, taking into account a linear voltage degradation, based on pilot experiment results, as is done by Chadly et al. [19] is deemed sufficient for the scope of this study. On a cell level the voltage degradation has a direct effect on efficiency, however on a system level the cells can be operated in such a way that the total system efficiency does not change [79]. This can be done up to a point of degradation where the system efficiency also starts to decrease, which is the moment in time to replace the stacks.

Although the stacks are operated in such a way that the efficiency does not decrease, at some point the overall system capacity does decrease. Degradation is modelled according to an end-of-lifetime (EOL) definition. The stacks are at EOL when they are degraded to 75% of their original capacity. The degradation in the model follows the profile depicted in Figure B.10. A linear capacity degradation from middle-of-lifetime (MOL) to (EOL) is assumed. The EOL parameter is taken as a sensitivity parameter in the sensitivity analysis.

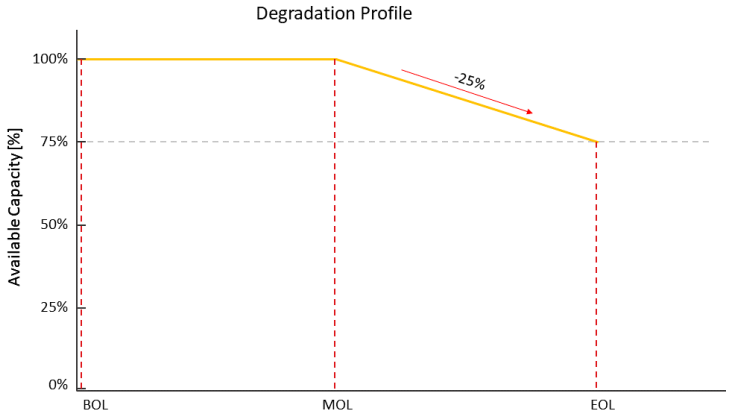


Figure B.10: The degradation profile used to model stack degradation

Table B.2: Expected deviations used for the sensitivity analysis

| Macro component | Parameter | Description | Unit | Low | Mid | High | Ref |
|---|---|---|---|---|---|---|---|
| rSOE | EC Efficiency | EC Performance | €/kW | -10% | 0% | +10% | [79] |
| | FC Efficiency | FC Performance $H_2$/ NG | €/kW | -10% | 0% | +10% | [79] |
| | $P_{min}$ | Lower operation limit | % | 10 | 20 | 30 | [83] |
| | $P_{max}$ | Upper operation limit | % | 80 | 100 | 100 | [83] |
| | $R_{up,EC}$ | Ramping-up constraint EC | $\%/min$ | 1 | 2 | 5 | [83] |
| | $R_{down,EC}$ | Ramping-down constraint EC | $\%/min$ | -5 | -2 | -1 | [83] |
| | $R_{up,FC}$ | Ramping-up constraint FC | $\%/min$ | 1 | 2 | 5 | [83] |
| | $R_{down,FC}$ | Ramping-down constraint FC | $\%/min$ | -5 | -2 | -1 | [83] |
| | $f_{HS}$ | Hot standby energy consumption | $\%/Cap_{EC}$ | 3 | 5 | 7 | [79] |
| | $t_{switch}$ | Switching time | h | 0.1 | 0.25 | 2 | [79] |
| | $P_{nom,EC}$ | Nominal capacity EC mode | MW | 180 | 200 | 220 | |
| | $Ratio_{FC/EC}$ | Ratio between nominal capacities of FC and EC mode | (-) | $\frac{1}{5}$ | $\frac{1}{4}$ | $\frac{1}{3}$ | [83] |
| | $EOL_{(r)SOE}$ | Stack End-of-Lifetime | years | 3 | 5 | 7 | [83] |
| | $EOL_{Alkaline}$ | Stack End-of-Lifetime | years | 6 | 8 | 10 | [83] |
| Economics | $CAPEX_{system}$ | Total installed system CAPEX | €/kW | -20% | 0% | +20% | [none] |
| | $Ratio_{stack/system}$ | Ratio for stack replacement | (%) | 5 | 10 | 15 | [9, 40] |
| | $Ratio_{O/C}$ | Average project OPEX share | (-) | 0.015 | 0.035 | 0.045 | [17] |
| | Inflation | Yearly Inflation Grid fee | % | 2 | 5 | 7 | [48] |
| Project | $r$ | Discount rate | % | 5 | 7 | 9 | [17] |
| Grid | $C_{Grid,month}$ | Monthly Dutch Grid Fee | €/kW/year | -20% | +0% | +20% | [48] |
| | $C_{Grid,year}$ | Yearly Dutch Grid Fee | €/kW/year | -20% | +0% | +20% | [48] |
| Hydrogen Backbone | $\theta_{H_2,sell}$ | Constant hydrogen sell price | €/kg | 1 | 3.5 | 5 | [70] |
| | $Ratio_{H_2,sell/buy}$ | Ratio between selling and buying hydrogen | (-) | $\frac{3}{5}$ | $\frac{4}{5}$ | 1 | [98] |
| Wind | $P_{nom,wind}$ | Nominal capacity of the windfarm | MW | 630 | 700 | 770 | [22] |
| | $P_{ppa}$ | Capacity of windenergy reserved for PPA | MW | 0 | 200 | 400 | [22] |
| | $\theta_{LCOE,buy}$ | Levelised Cost Of Energy Windfarm | €/MWh | 39.6 | 46.5 | 63.9 | [61] |
| Steam source | $\theta_{steam,buy}$ | Steam buy price | $€/tonne$ | 13 | 13 | 135 | [79, 31] |
| NG | $\theta_{NG,raw}$ | Price of raw natural gas | €/ $kg$ | 0.1 | 0.3 | 0.5 | [2] |
| | $\theta_{CO_2,ETS,tonne}$ | Price of raw natural gas | €/ $tonne$ | 100 | 125 | 150 | [25, 76] |
| | $t_{flush}$ | FC to EC flushing time | $h$ | 0.1 | 0.25 | 0.5 | [79] |

# B.6. Sensitivity Analysis Methodology

## B.6.1. Expected Deviations

Table Table B.2 shows the values for which different parameters were varied in the sensitivity analyses. This section shortly touches on the reasoning behind the values chosen as expected deviations.

- The rates for EC Efficiency, FC Efficiency are the writers educated guess, substantiated by the spread reported by Otto Machhammer [63], displayed in Table 2.1.
- Ramprates modeled for the mid case are based on [83] and rather small compared to [14, 58]. The high bound is therefore based on [58]. The low bound is taken to be half the mid case.
- The high bound of the hotstandby consumption is based on [88], while the mid and low are based on Santhanam [79].
- The switch time low and mid bound is recommended by Santhanam [79]. The high bound is the (unrealistically high) value at which the TEP decreases with 10%, to study the result of system design to the feasibility.

- As explained in subsection A.1.3, the $Ratio_{FC/EC}$ varies across systems. The spread mentioned in various sources is used as the minimum and maximum value for the sensitivity analysis [68, 55, 59, 66].
- The EOL bounds are based on Santhanam [79] and Luo et al. [50] and Martin [54].
- CAPEX and gridfee bounds are chosen at 20%, to see the results reaction to such a deviation. Deeper CAPEX and Gridfee analysis is done in the scenario analysis.
- The stack CAPEX to system CAPEX ratio is based on a combination of varying ratio and varying share of direct CAPEX costs to the total system CAPEX costs. These last are estimated to vary between 30-40% as mentioned in subsection 2.5.1. For ratio ratios between 20-30% of the direct CAPEX are assumed [40, 9, 90, 5].
- Discount rate, Fixed Opex share, $Ratio_{H_2,sell/buy}$, and inflation are varied educated, but arbitrarily.
- The $P_{nom,wind}$ and $P_{ppa}$ are varied from the mid-values provided by Deurvoost [22], to simulate less consistent and more volatile conditions.
- $\Theta_{LCOE,buy}$ bounds are based on a low, mid, and high wind energy penetration prediction by NREL [61] for 2035.
- The steam buy price low value is chosen to be equal to the mid-value, which is based on a project [79], but is considered low. The high deviation is based on the price of steam for dedicated steam production, which is known from experience at Pernis Refinery [31].
- The natural gas price can strongly vary as was seen in 2022-2021 Figure 3.9. The high bound is based on high bound projection from Afman [2]. The low bound is the same but a negative deviation from the mid-value, which is an arbitrary choice.
- It is assumed prices for $CO_2$ will rise, as the amount of available credits decreases. The low bound is chosen close to the current value representing minimum increase [25]. While the high value is twice the increment expected by the two sources used for the mid-value [76, 25].
- The flushtime is varied arbitrarily recommended by Santhanam [79].

# C

# Appendix: Results

The results in this chapter are referred to throughout the thesis. The chapter is built up in the same format as the results chapter, starting with results from the operational schedule (C.1), followed by findings from the scenario analysis (C.2) and the sensitivity analysis (C.3. The last section (C.4) contains the results on additional analysis.

## C.1. Operational Schedules

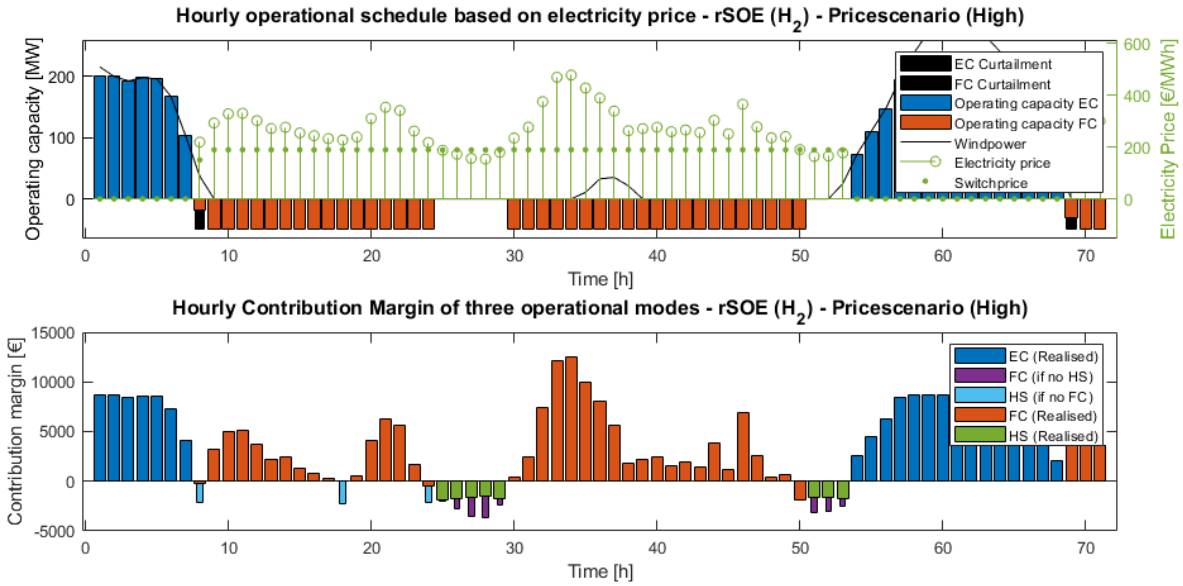


Figure C.1: The operational schedule for a randomly selected three-day period for rSOE ($H_2$) in the High power price scenario, showing a large share of FC operation. Top graph: Hourly operating point. Bottom graph: Hourly contribution margin. Power price scenario: High. Parameters: Baseline. Configuration: rSOE ($H_2$)

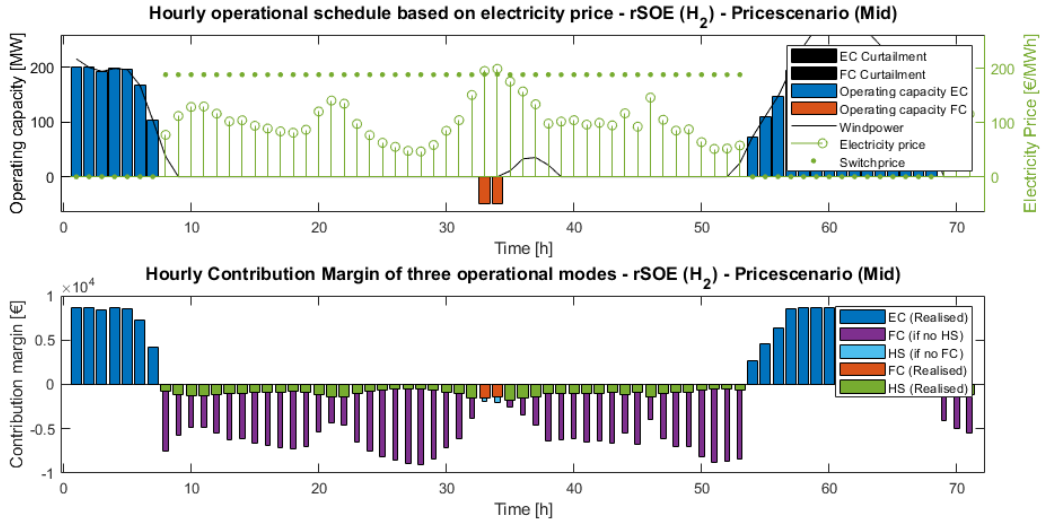


Figure C.2: The operational schedule for a randomly selected three-day period for rSOE ($H_2$) in the Mid price scenario, showing a negligible share of FC operation. Top graph: Hourly operating point. Bottom graph: Hourly contribution margin. Price scenario: Mid. Parameters: Baseline. Configuration: rSOE ($H_2$).

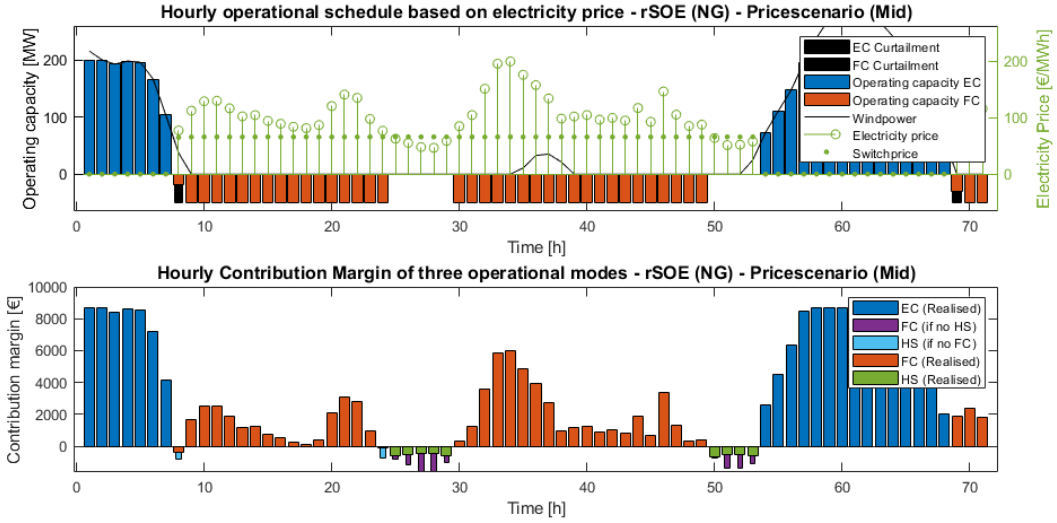


Figure C.3: The operational schedule for a randomly selected three-day period for rSOE (NG) in the Mid price scenario, showing a moderate share of FC operation. Top graph: Hourly operating point. Bottom graph: Hourly contribution margin. Price scenario: Mid , Parameters: Baseline. Configuration: rSOE (NG).

# C.2. Scenario Analysis

## C.2.1. Combined Price and CAPEX

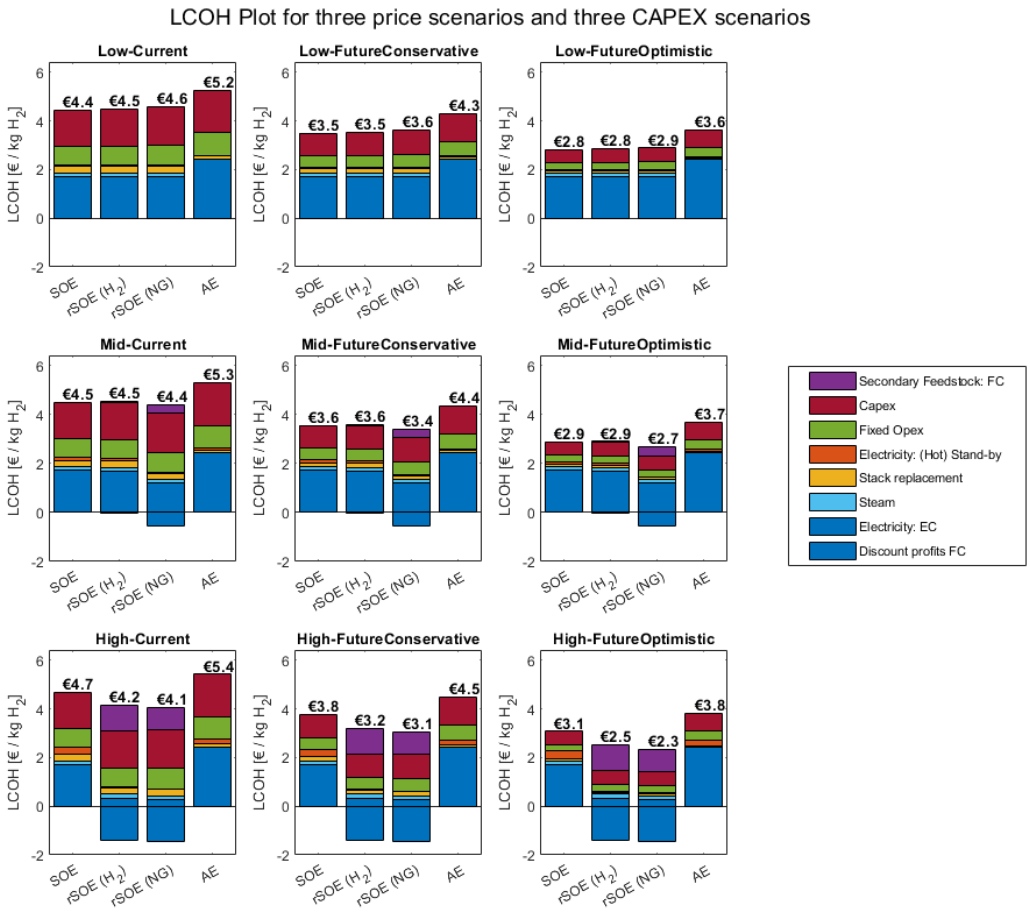


Figure C.4: The LCOH plots for all combinations of three power price scenarios and three CAPEX scenarios. The subtitles indicate the price scenario - followed by the CAPEX scenario

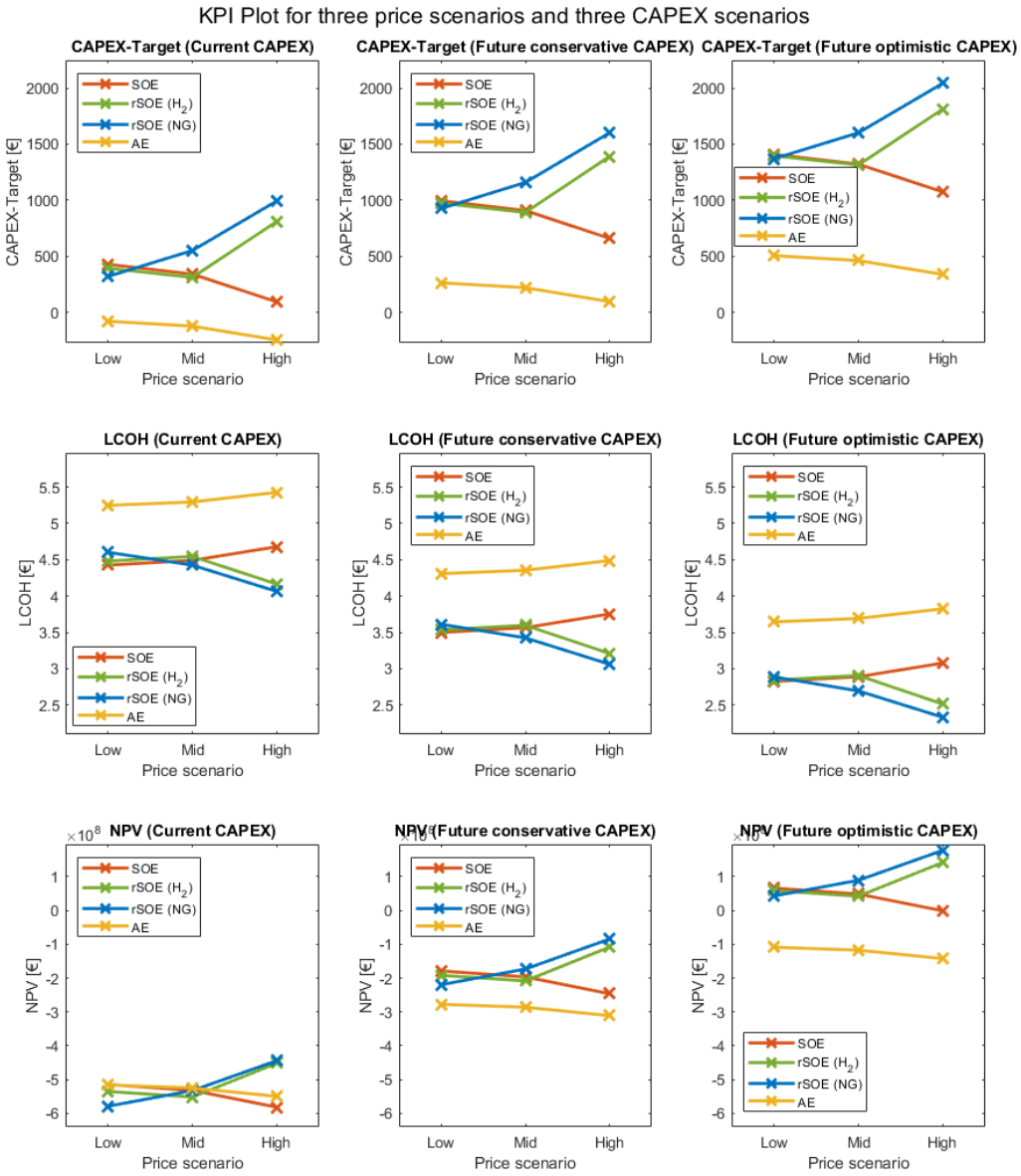


Figure C.5: The KPI plots for all combinations of three power price scenarios and three CAPEX scenarios. The subtitles indicate the KPI name - followed by the CAPEX scenario

## C.2.2. CAPEX Scenarios

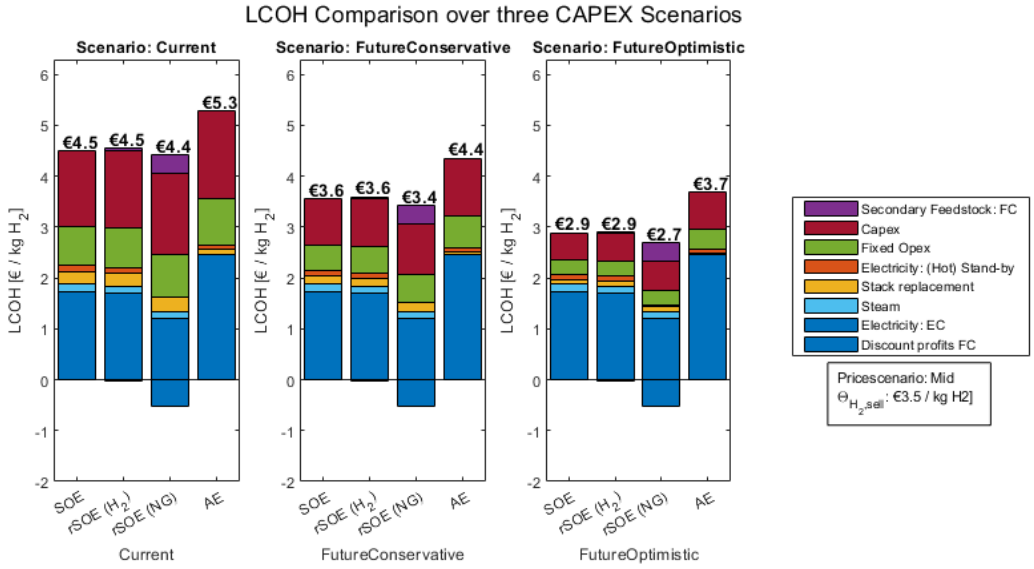


(a) Not-Normalised

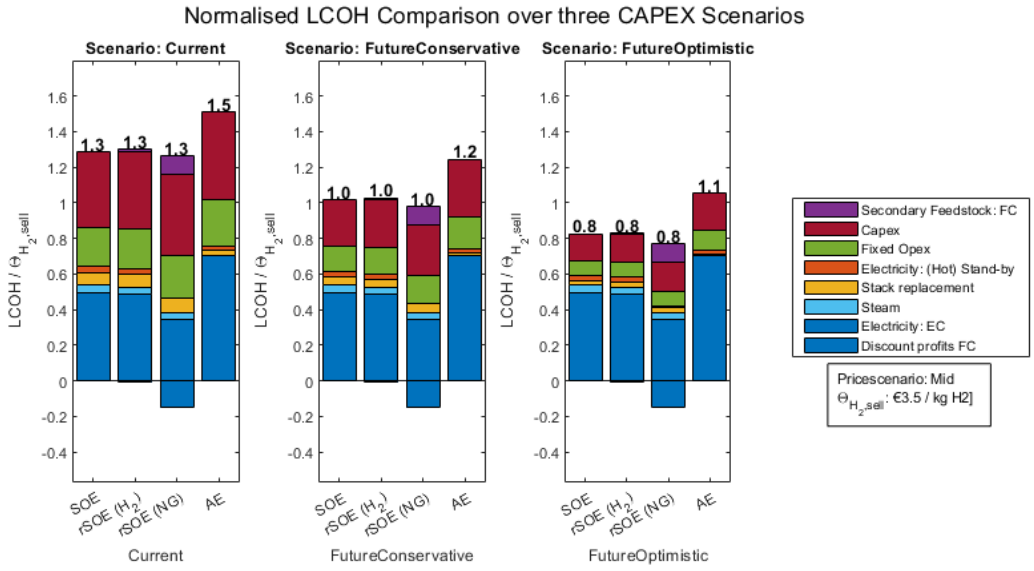


(b) Normalised

Figure C.6: Not-Normalised (a) and Normalised (b) LCOH comparison for three CAPEX scenarios, showing a decrease to sub-one levelised LCOH due to CAPEX and OPEX decrease.

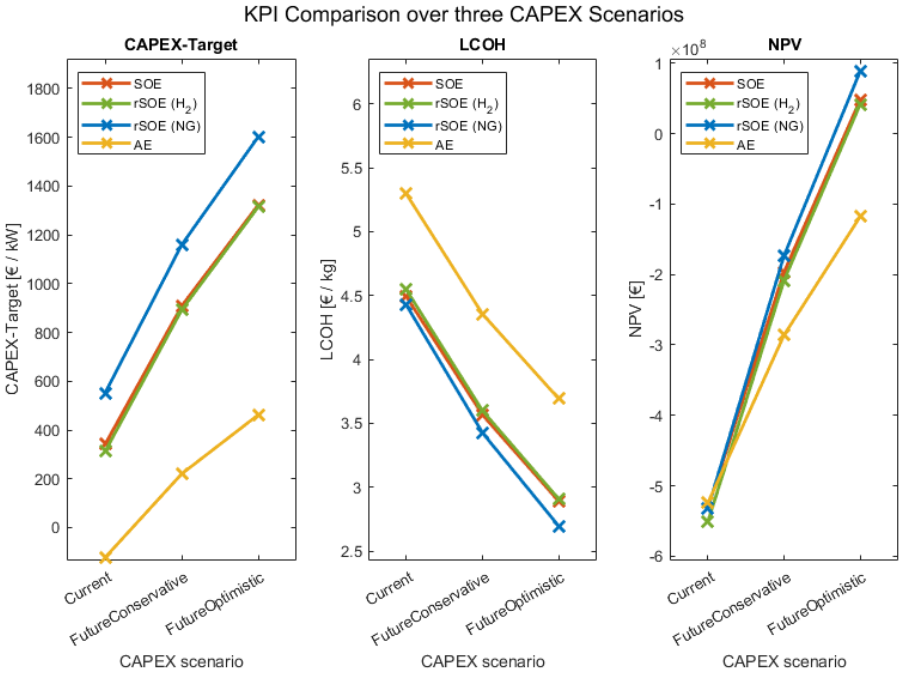


Figure C.7: KPI based configuration comparison for three CAPEX scenarios

### C.2.3. Power Price Scenario

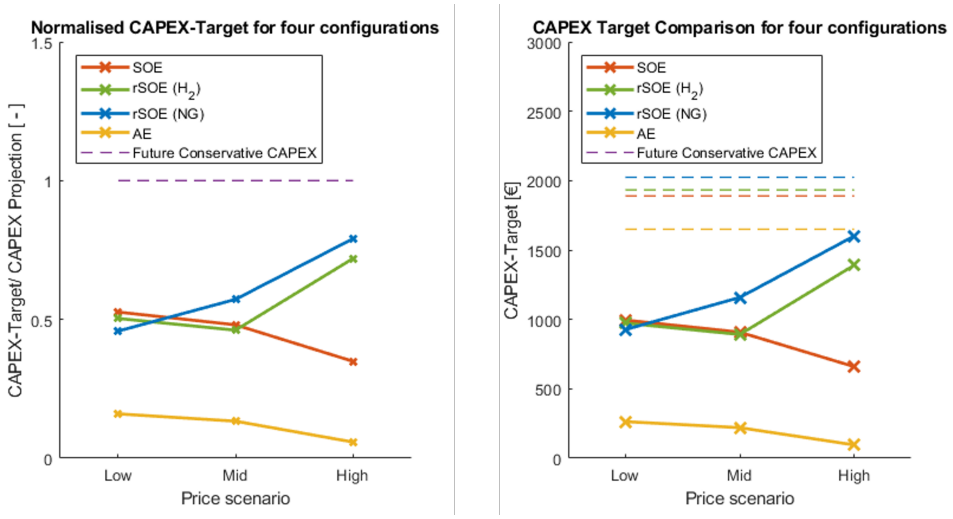


Figure C.8: CAPEX-Target Comparison for four configurations and three pricescenarios. Normalised (Left) Not normalised (Right)

Figure C.9 shows a mix of scenarios. It combines the three pricescenarios, three CAPEX scenarios and 4 configurations. It shows that under the Current and Future Conservative CAPEX scenarios the CAPEX-Target does not reach the expected CAPEX, under any of the price scenarios. It can be observed that the CAPEX-Target does reach the expected CAPEX scenario for the Future Optimistic scenario, under the extreme low and mid price scenarios.

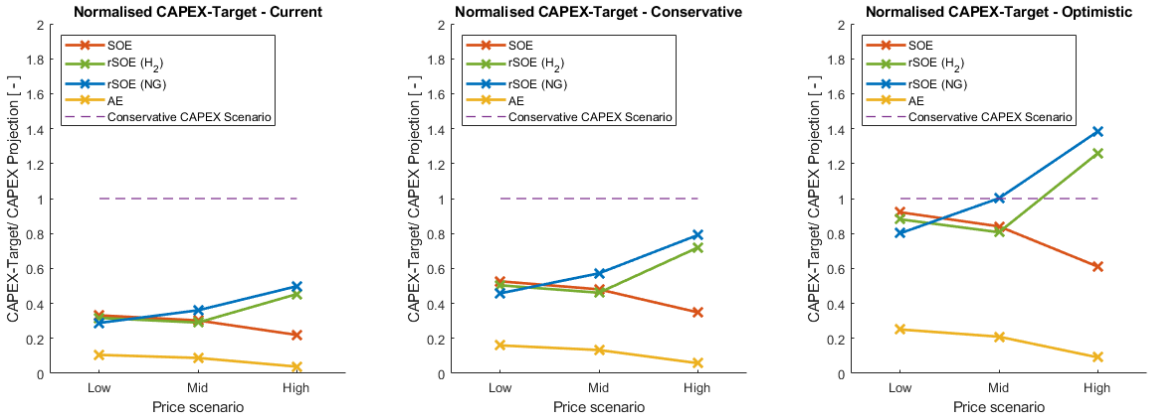


(a) /Current CAPEX (b) /Future Conservative Scenario (c) /Future Optimistic Scenario

Figure C.9: CAPEX-Target Comparison for four configurations and three pricescenarios, normalised by the three different CAPEX Scenarios

## C.2.4. Grid Fee Scenario

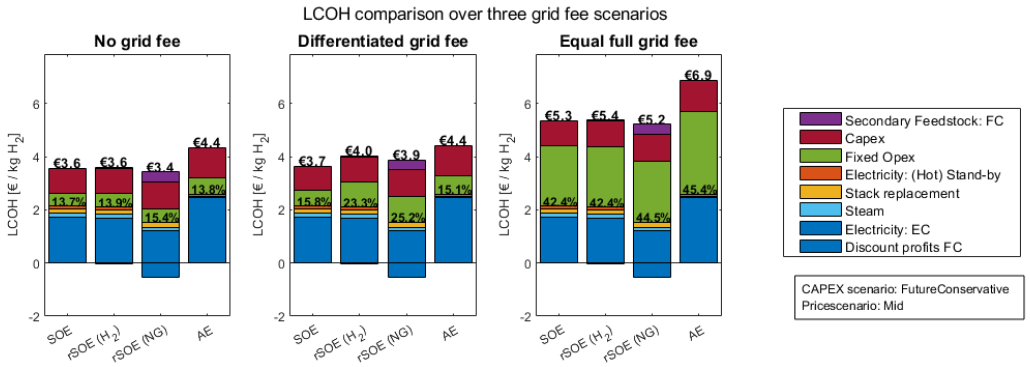


Figure C.10: LCOH Comparison for three grid fee scenarios

# C.3. Sensitivity Analysis

## C.3.1. Tornado Charts

The Torando charts for all configurations and price scenarios.

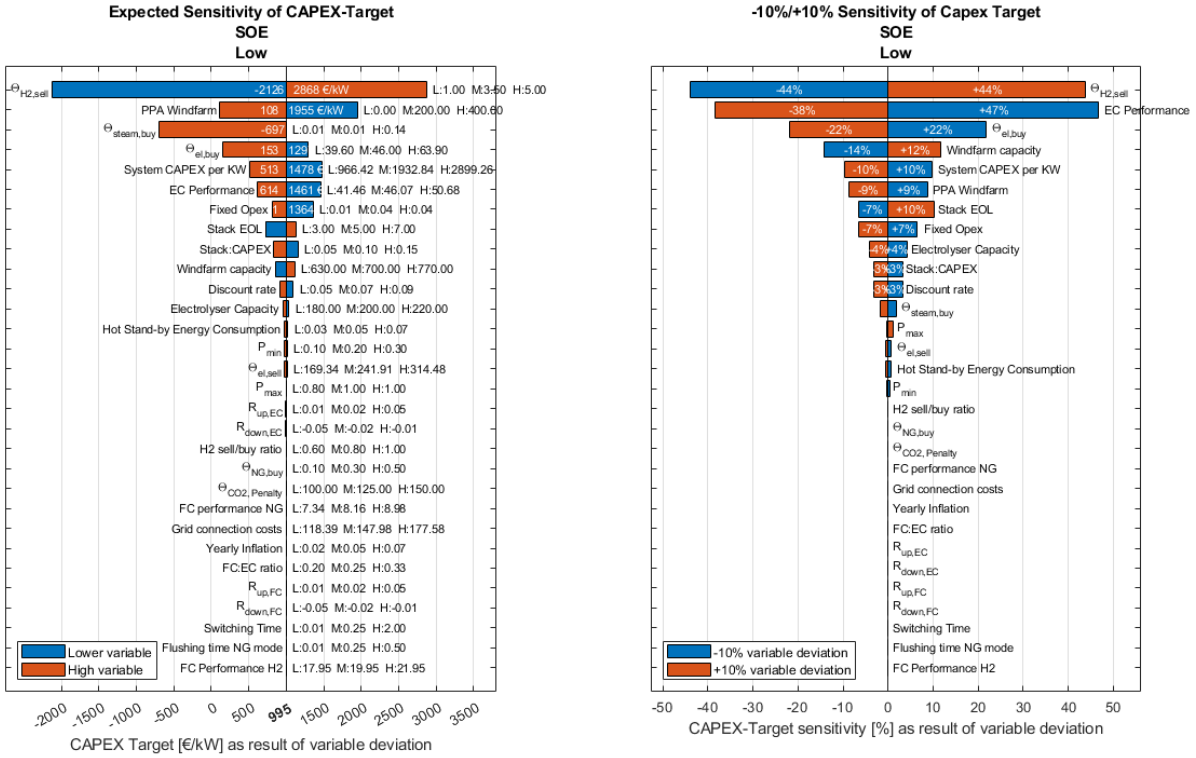


Figure C.11: Sensitivity Analysis SOE / Low

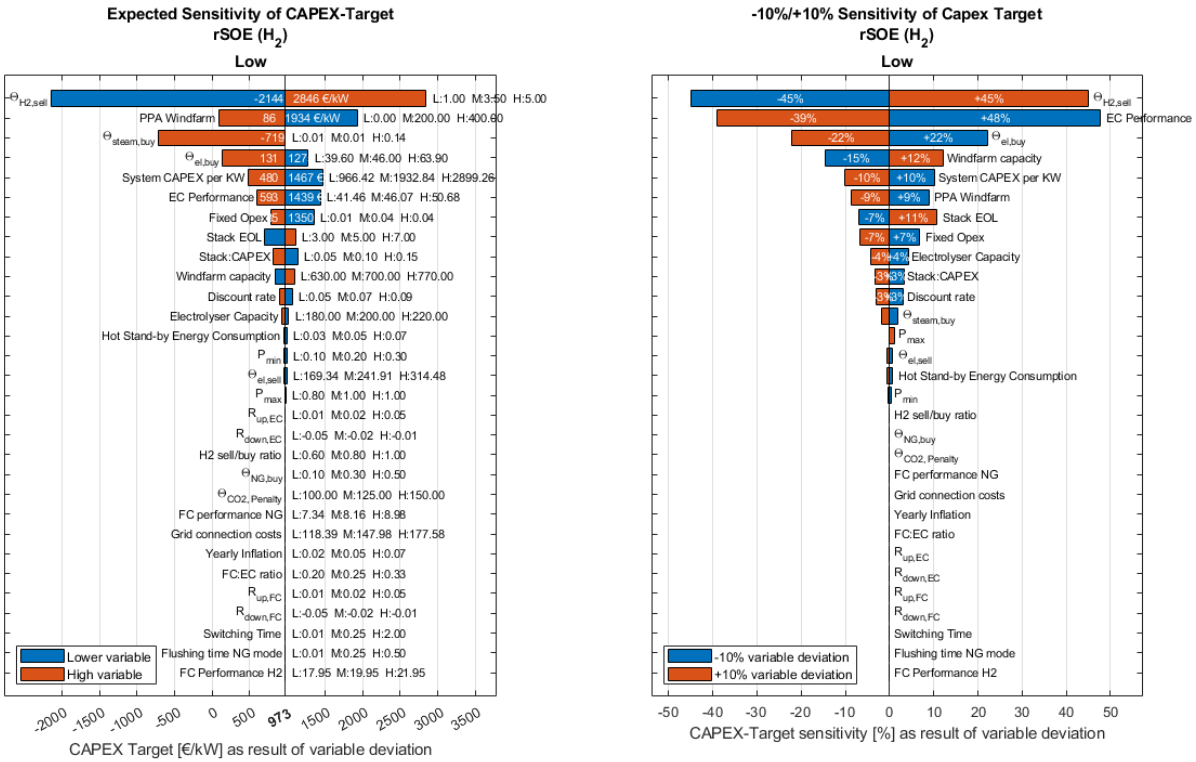


Figure C.12: Sensitivity Analysis rSOE ($H_2$) / Low

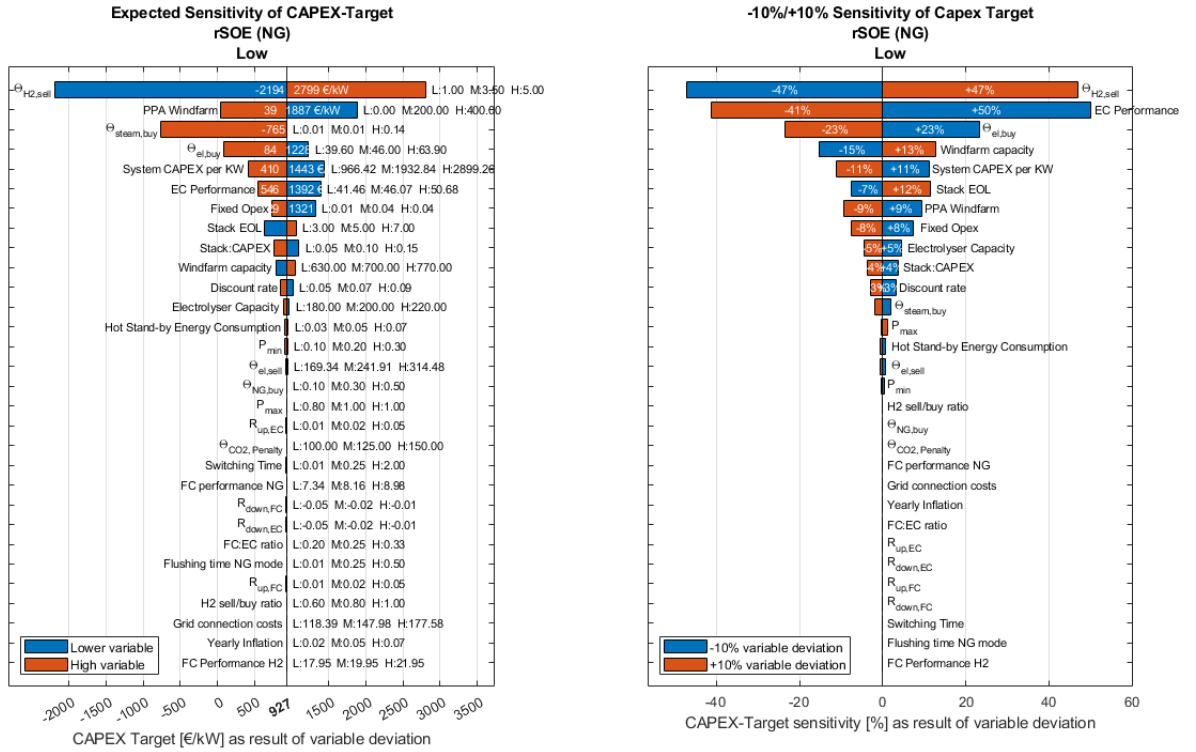


Figure C.13: Sensitivity Analysis rSOE (NG) / Low

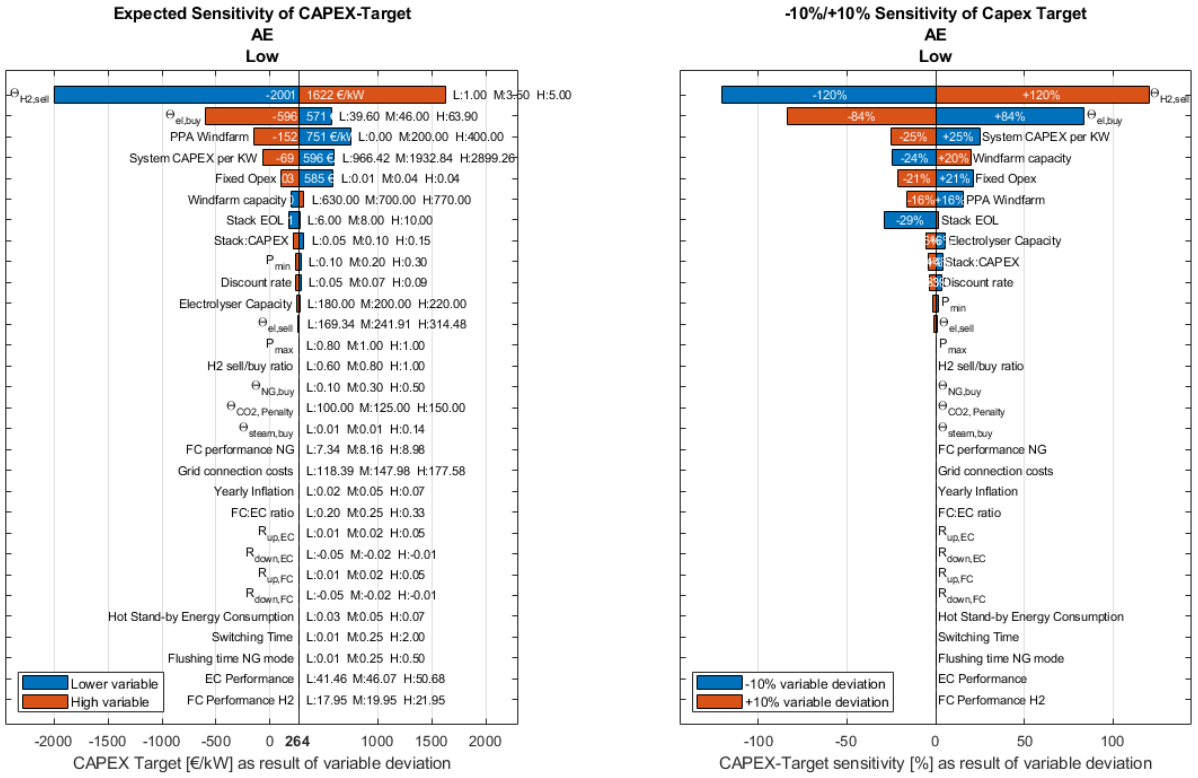


Figure C.14: Sensitivity Analysis AE / Low

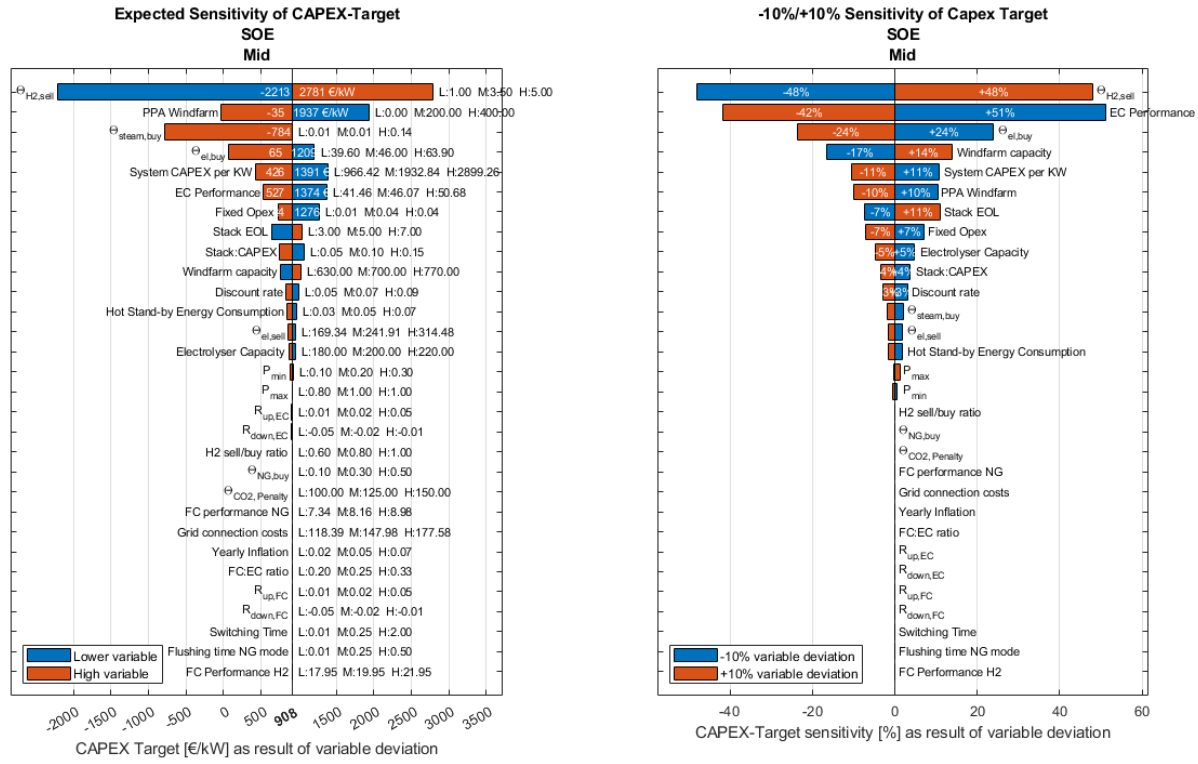


Figure C.15: Sensitivity Analysis SOE / Mid

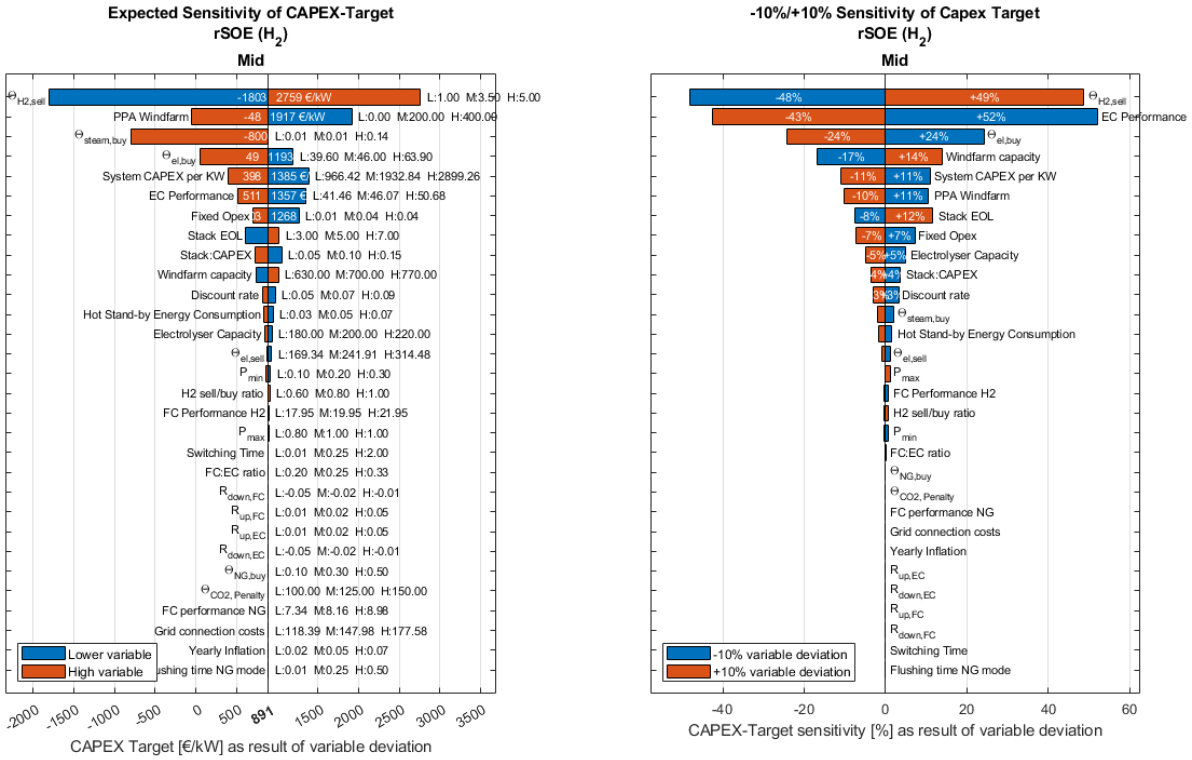


Figure C.16: Sensitivity Analysis rSOE ($H_2$) / Mid

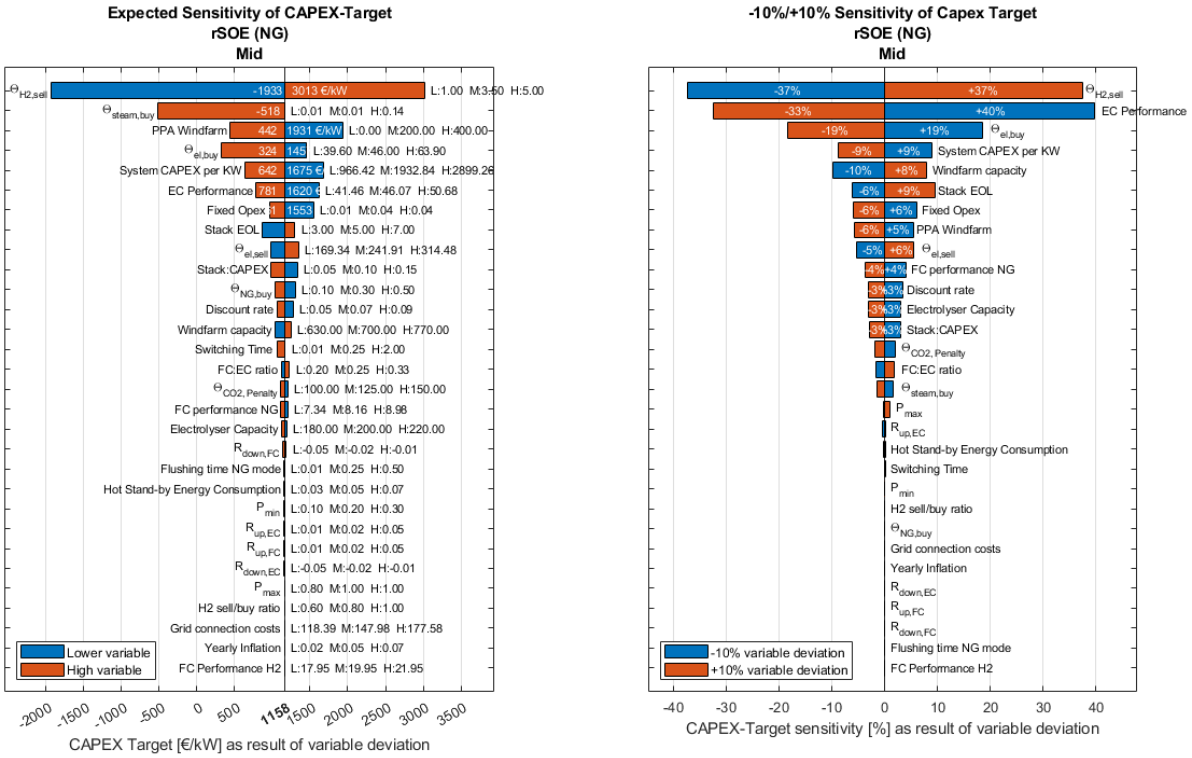


Figure C.17: Sensitivity Analysis rSOE (NG) / Mid

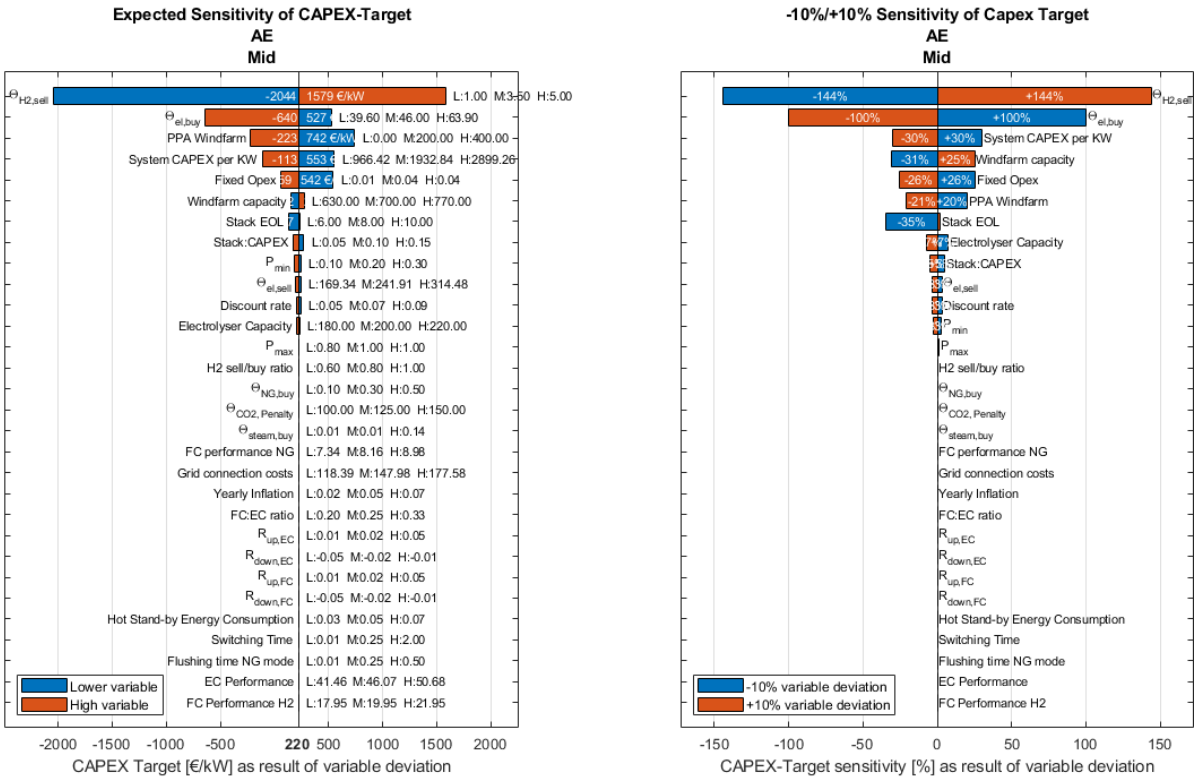


Figure C.18: Sensitivity Analysis AE / Mid

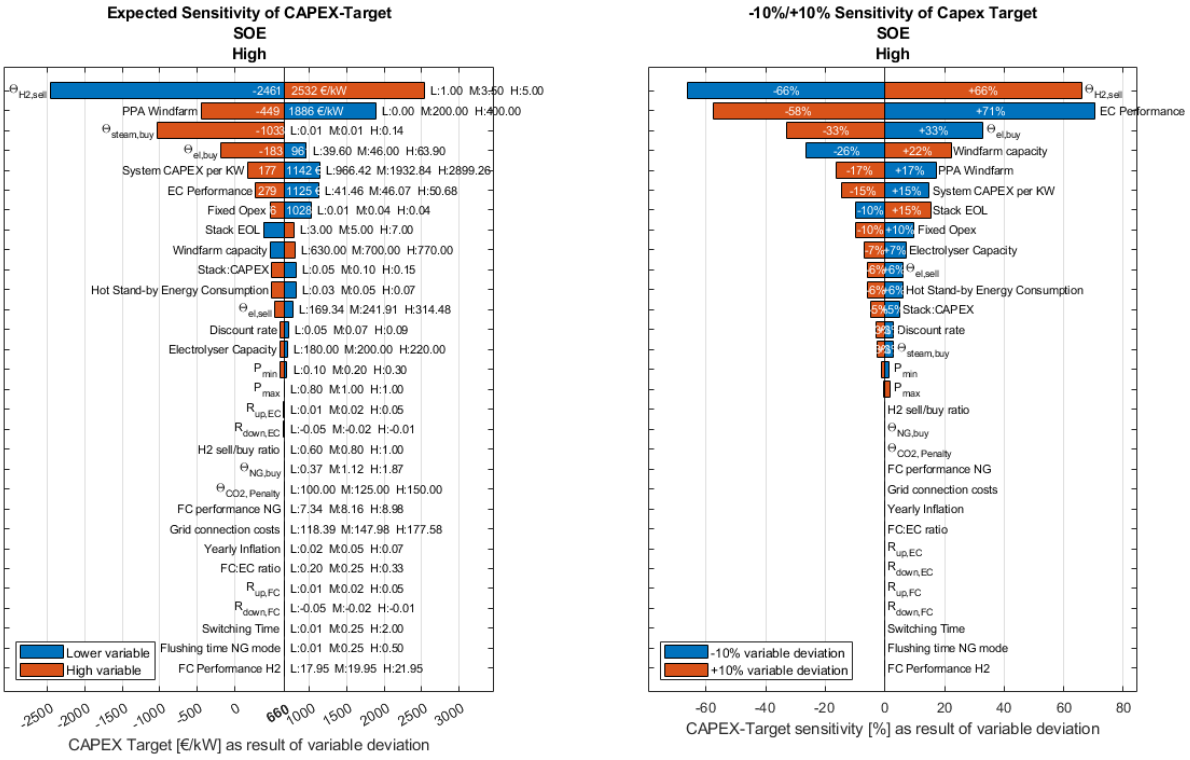


Figure C.19: Sensitivity Analysis SOE / High

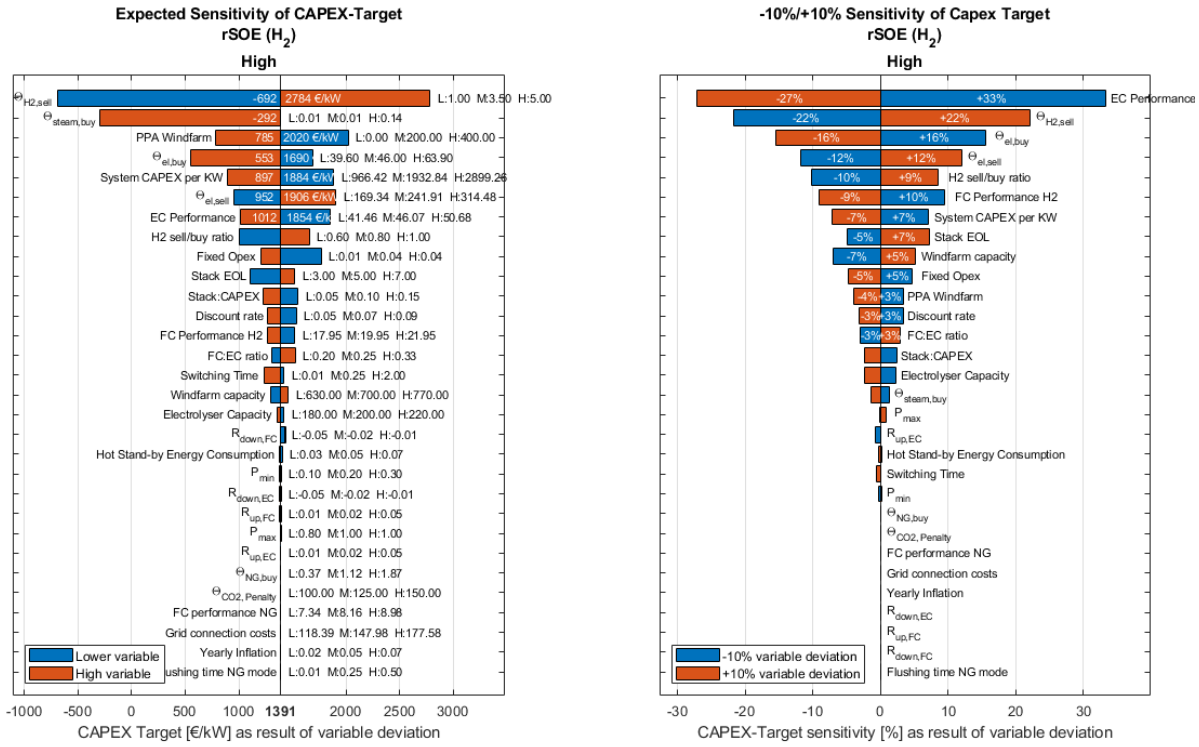


Figure C.20: Sensitivity Analysis rSOE ($H_2$) / High

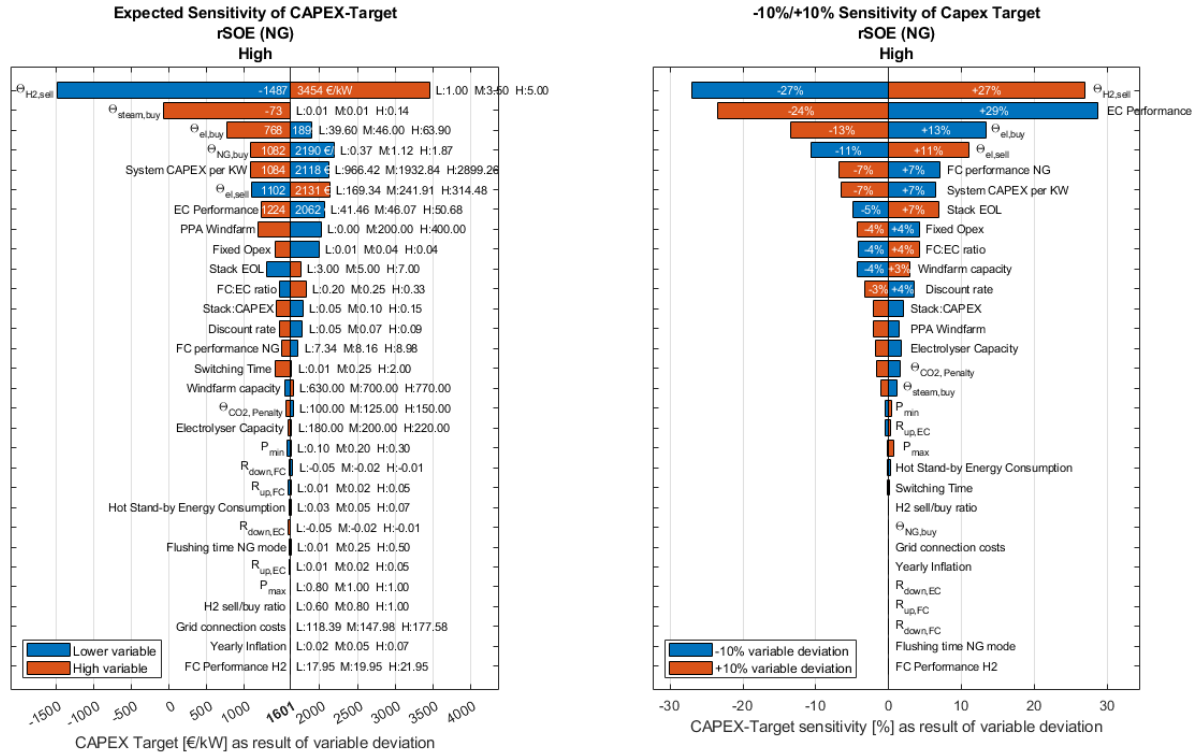


Figure C.21: Sensitivity Analysis rSOE (NG) / High

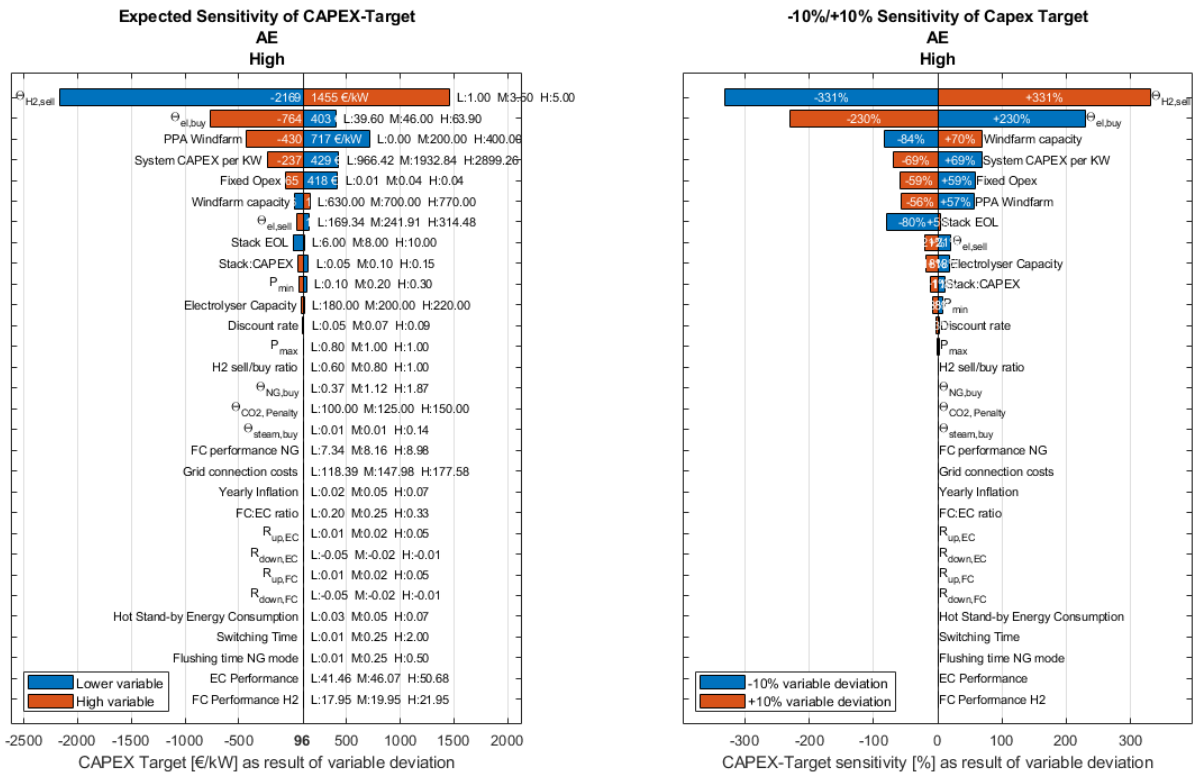


Figure C.22: Sensitivity Analysis AE / High

### C.3.2. Observations from Sensitivity Results

Some parameters that were analysed, did not bring forward findings relevant to relative feasibility improvement by reversibility. These were left out of the results chapter and placed in this Appendix subsection.

#### Power Buy Price

From the windprofile related parameters, the CAPEX-Target is also sensitive to $\theta_{el,buy}$. The proportional sensitivity to the expected deviations in this parameter are equal for all solid oxide configurations. This is caused by the prioritisation of hydrogen production when windpower is available. This causes the hours of EC operation to be equal for all configurations. Equal efficiencies among the solid oxide configurations result in equal costs for electricity consumption. Electricity costs for AE operation would higher at the same hydrogen production rate, due to lower efficiencies. The AE configuration would therefor be proportionally more sensitive to a changing electricity buy price.

#### Steam Price

In the high deviation case, the CAPEX-Target of all the Solid Oxide Configurations goes below that of the AE configuration. This can be seen in the sensitivity diagrams of the mid power price scenarios: Figure C.18 vs Figure C.15,Figure C.16 and Figure C.17).

In it self the TEP has a low sensitivity for the steam buy price. However, there is a large spread in the expected deviation of this parameter. The middle price is based on buying rest steam, while the high price is based on producing steam dedicated to the system.

#### EC Performance

The strongest general sensitivity lies in EC Performance, however as the expected deviation is small the expected sensitivity is smaller. Also by comparing Figure C.19 and Figure C.20 it can be concluded EC performance does not cuase relative feasibility improvement for reversible systems. EC Performance is defined as the total system specific energy consumption. A 10% deviation results in a deviation more then two times as high to the CAPEX-Target. It pays off to put effort into increasing the EC Performance. Specific energy consumption for the system, as displayed in Figure 3.7 is already low compared to referenced values in Table 2.1. Taking into account the educated guess variation the effect of efficiency on the CAPEX-Target becomes smaller, but still significant.

#### CAPEX

CAPEX is partly determined by system design, but has a high external uncertainty to it. Resulting from the CAPEX scenario analysis it can be concluded that the Future Optimistic CAPEX scenario would lead to profitable KPIs, for all configurations.

Specifically on reversibility, future CAPEX scenarios are slightly beneficial as can be seen from the KPIs in Figure C.7. This results from the higher system CAPEX, which proportionally also has a higher absolute decrease with the future cAPEX scenarios.

#### Parameters with Limited Relative Feasibility Effect

Stack EOL, Electricity buy price from the windfarm, Fixed Opex, Stack:CAPEX, Discount Rate and Steam Buy price do not influence the relative feasibility of reversible systems compared to non reversible systems. However, they do influence the overall feasibility.

The electricity buy price from the windfarm is an important and limiting factor in EC operation. It is the main cost factor in the LCOH of hydrogen, as was seen in Figure 4.3. This parameter puts a minimum to the price at which hydrogen can be sold, profitably. Minimizing this factor is crucial to the feasibility of all configurations.

Ramprates and Switchtimes

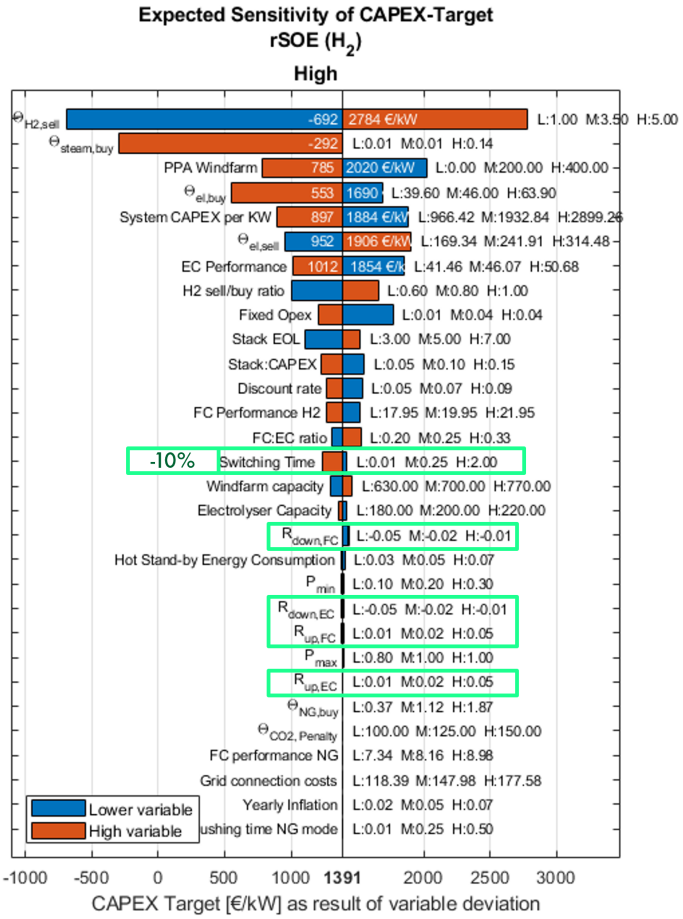


Figure C.23: Sensitivity study result, highlighting the ramprate and switchtime sensitivity.

# C.4. Additional Analysis

## C.4.1. Balancing Market Potential

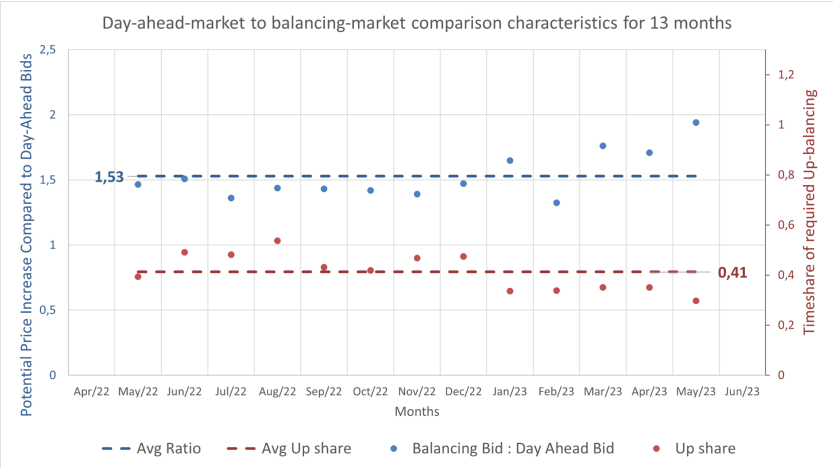


Figure C.24: The balancing market potential analysis for thirteen months in the period May 2022 to May 2023. On the left axis the potential price increase compared to the day-ahead bids. And on the right axis is the Timeshare of required Up-Balancing.

## C.4.2. View on Future Power Prices

This study makes use of modified historic datasets to study the relation between the power price and feasibility improvement by reversibility. A view on future power price developments is provided to give background to the results.

Table C.1: Historic electricity prices and standard deviation

| Year | 2018 | 2019 | 2020 | 2021 | 2022 |
|---|---|---|---|---|---|
| Average Electricity Price [Euro/MWh] | 52.54 | 41.19 | 32.19 | 102.97 | 241.91 |
| Standard Deviation [-] | 0.29 | 0.27 | 0.47 | 0.73 | 0.54 |

In the future average power prices and volatility could have several outcomes, which was simulated by the High, Mid and Low scenario. Excluding 2021 and 2022 the average power price was between 32.19 and 52.54 euro per MWh. At the time of writing this thesis, May 2023, power prices have declined from the 2022 peak to the 2021 level. The high price scenario was based on 2022 average prices. The rise in average power prices in 2021 and 2022 can be accounted to COVID and the war in Ukrain, and are probably not a good indicator for the future. As a result of low cost renewable energy, it is possible that future average prices decrease to or below the pre-COVID level. On the other, it is likely that average prices remain above pre-COVID price points as is seen the last couple of months [26]. Apart from RES profiles, the power price level depends on natural gas prices, which currently have taken on values almost in line with 2018,2019,2020 gas prices [89]. The Emission Trading Scheme, forces gas-fired plants to include the carbon price in their bids, resulting in higher bids. This price increase, due to carbon prices, was confirmed by Tennets 2021 Annual report [86]. For this reason, among others, it is not self-evident that average power prices will decrease to or below pre-COVID levels.

Qualitatively a higher RES penetration in the energy mix results in increased volatility due to the intermittent character of these sources. Historically the normalised standard deviation was between 0.27-0.73. An increased normalised standard deviation is observed in Table C.1. Partly, this can originate from increased installed RES capacity. However, a large share can also be contributed to a highly volatile gas price in 2021 and 2022 as can be seen in Figure C.25. As increased RES capacity is believed to increase power price volatility, this is included in the Mid scenario.


Figure C.25: Historic Natural Gas EU Dutch TTF Prices [89]

More radically, there is also a possibility for the power system to be completely redesigned. Pieter Bots hints at a power market based on bilateral contracts and grid balancing by a few Gas Fired Assets, which are paid for keeping their capacity available [67]. In such a case the day-ahead market as we know it today will radically change and so will the hourly price structure. A different business model and operational strategy would need to be considered in such a case.

# Bibliography


[1] Roscam Abbing. Personal Communications. Pernis, Mar. 2023.

[2] Maarten Afman. Energy and electricity price scenarios. Tech. rep. 2020.

[3] Régis Anghilante et al. "Bottom-up cost evaluation of SOEC systems in the range of 10100ăMW". In: International Journal of Hydrogen Energy 43.45 (Nov. 2018), pp. 20309–20322. ISSN: 0360-3199. DOI: 10.1016/J.IJHYDENE.2018.08.161.

[4] Juede Austine. Personal Communications. Bangalore, Apr. 2023.

[5] Battelle Memorial Institute. Manufacturing Cost Analysis of 100 and 250 kW Fuel Cell Systems for Primary Power and Combined Heat and Power Applications. Tech. rep. 2016.

[6] David E. Bell. "Regret in Decision Making under Uncertainty". In: Operations Research 30.5 (Oct. 1982), pp. 961–981.

[7] Eddy Binneveld. Personal Communications. Rotterdam, July 2023.

[8] Saheli Biswas et al. "A theoretical study on reversible solid oxide cells as key enablers of cyclic conversion between electrical energy and fuel". In: Energies 14.15 (Aug. 2021). ISSN: 19961073. DOI: 10.3390/en14154517.

[9] Hans Böhm et al. "Estimating future costs of power-to-gas  a component-based approach for technological learning". In: International Journal of Hydrogen Energy 44.59 (Nov. 2019), pp. 30789–30805. ISSN: 03603199. DOI: 10.1016/j.ijhydene.2019.09.230.

[10] J C B Brenkman. High Pressure Hydrogen Dehydration Using Ionic Liquids. Tech. rep. URL: http://repository.tudelft.nl/..

[11] Jeroen Brenkman. Personal Communications. Amsterdam, Mar. 2023.

[12] Giulio Buffo et al. "Energy and environmental analysis of a flexible Power-to-X plant based on Reversible Solid Oxide Cells (rSOCs) for an urban district". In: Journal of Energy Storage 29 (June 2020). ISSN: 2352152X. DOI: 10.1016/j.est.2020.101314.

[13] Giacomo Butera et al. "A novel system for large-scale storage of electricity as synthetic natural gas using reversible pressurized solid oxide cells". In: Energy 166 (Jan. 2019), pp. 738–754. ISSN: 03605442. DOI: 10.1016/j.energy.2018.10.079.

[14] Alexander Buttler et al. Current status of water electrolysis for energy storage, grid balancing and sector coupling via power-to-gas and power-to-liquids: A review. Feb. 2018. DOI: 10.1016/j.rser.2017.09.003.

[15] Stefano Campanari. Techno-economic Analysis of a Low Fuel Utilization Factor Solid Oxide Fuel Cell System for Hydrogen Production and Carbon Capture in Oil Refinery Applications. Tech. rep. 2018.

[16] Claudio Carbone et al. "Potential Deployment of Reversible Solid-Oxide Cell Systems to Valorise Organic Waste, Balance the Power Grid and Produce Renewable Methane: A Case Study in the Southern Italian Peninsula". In: Frontiers in Energy Research 9 (Feb. 2021). ISSN: 2296598X. DOI: 10.3389/fenrg.2021.618229.

[17] Luis Fernando Castro. Personal Communications. Amsterdam, Mar. 2023.

[18] Simonas Cerniauskas et al. "Options of natural gas pipeline reassignment for hydrogen: Cost assessment for a Germany case study". In: International Journal of Hydrogen Energy 45.21 (Apr. 2020), pp. 12095–12107. ISSN: 03603199. DOI: 10.1016/j.ijhydene.2020.02.121.

[19] Assia Chadly et al. "Techno-economic analysis of energy storage systems using reversible fuel cells and rechargeable batteries in green buildings". In: Energy 247 (May 2022). ISSN: 03605442. DOI: 10.1016/j.energy.2022.123466.

[20] Hans Cleijne et al. North sea energy outlook(NEO). Tech. rep.

[21] Antonio J Conejo et al. INTERNATIONAL SERIES IN OPERATIONS RESEARCH AND MANAGEMENT SCIENCE Decision Making Under Uncertainty in Electricity Markets. Tech. rep. URL: www.springer.com/series/6161.

[22] Taco Deurvoost. Personal Communications. Amsterdam, Mar. 2023.

[23] Dutch Government. Government Strategy on Hydrogen. Tech. rep. URL: https://www.tno.nl/nl/aandachtsgebieden/energietransitie/roadmaps/naar-co2-neutrale-.

[24] Sune Dalgaard Ebbesen et al. High temperature electrolysis in alkaline cells, solid proton conducting cells, and solid oxide cells. Nov. 2014. DOI: 10.1021/cr5000865.

[25] EMBER. Carbon Price Tracker. June 2023. URL: Carbon%20Price%20Tracker.

[26] EMBER. EMBER-Climate. 2023. URL: https://ember-climate.org/data/data-tools/carbon-price-viewer/.

[27] EPEX. "Basics of the power market". In: (Feb. 2023). URL: https://www.epexspot.com/en/basicspowermarket.

[28] Samira Fazlollahi et al. "Multi-objectives, multi-period optimization of district energy systems: I. Selection of typical operating periods". In: Computers & Chemical Engineering 65 (June 2014), pp. 54–66. ISSN: 0098-1354. DOI: 10.1016/J.COMPCHEMENG.2014.03.005.

[29] Earl Goetheer. Personal Communications. Delft, 2023.

[30] Government of the Netherlands. "Offshore Windenergy". In: (). URL: https://www.government.nl/topics/renewable-energy/offshore-wind-energy.

[31] Thijs Groenendijk. Personal Communications. Pernis, Feb. 2023.

[32] Dries Haeseldonckx et al. "The use of the natural-gas pipeline infrastructure for hydrogen transport in a changing market structure". In: International Journal of Hydrogen Energy 32.10-11 (July 2007), pp. 1381–1386. ISSN: 03603199. DOI: 10.1016/j.ijhydene.2006.10.018.

[33] S. Harboe et al. "Manufacturing cost model for planar 5 kWel SOFC stacks at Forschungszentrum Jülich". In: International Journal of Hydrogen Energy 45.15 (Mar. 2020), pp. 8015–8030. ISSN: 03603199. DOI: 10.1016/j.ijhydene.2020.01.082.

[34] Huub Hillen. Personal Communications. Amsterdam, Feb. 2023.

[35] Timothy D. Hutty et al. "Suitability of energy storage with reversible solid oxide cells for microgrid applications". In: Energy Conversion and Management 226 (Dec. 2020). ISSN: 01968904. DOI: 10.1016/j.enconman.2020.113499.

[36] IEA. Renewables- Energy System Overview. Sept. 2022. URL: https://www.iea.org/reports/renewables.

[37] The International Renewable Energy Agency. GREEN HYDROGEN COST REDUCTION SCALING UP ELECTROLYSERS TO MEET THE 1.5°C CLIMATE GOAL H 2 O 2. 2020. ISBN: 9789292602956. URL: www.irena.org/publications.

[38] ISPT. Gigawatt green hydrogen plant. Tech. rep. 2020. URL: https://ec.europa.eu/commission/presscorner/detail/en/ip_20_1259.

[39] J.B. Martin. Water Electrolysis Technology Technology Landscaping for Electrolytic Hydrogen Production Restricted. Tech. rep. 2017.

[40] Brian D James et al. Final Report: Hydrogen Production Pathways Cost Analysis (2013-2016). Tech. rep. 2016. URL: www.sainc.com.

[41] S H Jensen et al. "Large-scale electricity storage utilizing reversible solid oxide cells combined with underground storage of CO2 and CH4". In: Energy Environ. Sci. 8.8 (2015), pp. 2471–2479. DOI: 10.1039/C5EE01485A. URL: http://dx.doi.org/10.1039/C5EE01485A.

[42] Ozgur Kacar. Personal Communications. London, May 2023.

[43] Søren Krohn et al. The Economics of Wind Energy A report by the European Wind Energy Association. Tech. rep. URL: https://www.ewea.org/fileadmin/files/library/publications/reports/Economics_of_Wind_Energy.pdf.

[44] Mario Lamagna et al. “Reversible solid oxide cell coupled to an offshore wind turbine as a poly-generation energy system for auxiliary backup generation and hydrogen production”. In: Energy Reports 8 (Nov. 2022), pp. 14259–14273. ISSN: 23524847. DOI: 10.1016/j.egyr.2022.10.355.

[45] Mario Lamagna et al. “Techno-economic assessment of reversible Solid Oxide Cell integration to renewable energy systems at building and district scale”. In: Energy Conversion and Management 235 (May 2021). ISSN: 01968904. DOI: 10.1016/j.enconman.2021.113993.

[46] Sander Lensink et al. EINDADVIES BASISBEDRAGEN SDE++ 2021. Tech. rep. URL: https://www.pbl.nl/publicaties/eindad-.

[47] Graham Loomes et al. “Regret Theory: An Alternative Theory of Ratinal Choice Under Uncertainty”. In: The Economic Journal 92.368 (Dec. 1982), pp. 805–824.

[48] Martijn Lunshof. Personal Communications. Amsterdam, Mar. 2023.

[49] Yu Luo et al. “Bridging a bi-directional connection between electricity and fuels in hybrid multienergy systems”. In: Hybrid Systems and Multi-energy Networks for the Future Energy Internet. Elsevier, 2021, pp. 41–84. DOI: 10.1016/b978-0-12-819184-2.00003-1.

[50] Yu Luo et al. “Bridging a bi-directional connection between electricity and fuels in hybrid multienergy systems”. In: Hybrid Systems and Multi-energy Networks for the Future Energy Internet. Elsevier, 2021, pp. 41–84. DOI: 10.1016/b978-0-12-819184-2.00003-1.

[51] Nikolaos Lymperopoulos. Commercialisation of Energy Storage in Europe. Tech. rep.

[52] Macrofici. Reversible solid oxide cell. Feb. 2023. URL: https://en.wikipedia.org/wiki/Reversible_solid_oxide_cell#/media/File:RSOC_working_principle.svg.

[53] Marcofici. WikiMediaCommons. Feb. 2023. URL: https://commons.wikimedia.org/wiki/File:RSOC_polarization.jpg.

[54] Jeff Martin. Personal Communications. Amsterdam, Mar. 2023.

[55] Joshua Mermelstein et al. “Development and Demonstration of a Novel Reversible SOFC System for Utility and Micro Grid Energy Storage”. In: Fuel Cells 17.4 (Aug. 2017), pp. 562–570. ISSN: 16156854. DOI: 10.1002/fuce.201600185.

[56] M. B. Mogensen et al. Reversible solid-oxide cells for clean and sustainable energy. Tech. rep. 3. Nov. 2019, pp. 175–201. DOI: 10.1093/ce/zkz023.

[57] Arrigo Monti et al. “Energy Dense Storage Using Intermediate Temperature Reversible Solid Oxide Cells”. In: ECS Transactions 68.1 (June 2015), pp. 3289–3300. ISSN: 1938-5862. DOI: 10.1149/06801.3289ecst. URL: https://iopscience.iop.org/article/10.1149/06801.3289ecst.

[58] Konrad Motylinski et al. “Dynamic modelling of reversible solid oxide cells for grid stabilization applications”. In: Energy Conversion and Management 228 (Jan. 2021). ISSN: 01968904. DOI: 10.1016/j.enconman.2020.113674.

[59] Julie Mouginn et al. “Development of an Efficient rSOC Based Renewable Energy Storage System”. In: ECS Transactions 103.1 (July 2021), pp. 337–350. ISSN: 1938-5862. DOI: 10.1149/10301.0337ecst.

[60] Hossein Nami et al. “Techno-economic analysis of current and emerging electrolysis technologies for green hydrogen production”. In: Energy Conversion and Management 269 (Oct. 2022). ISSN: 01968904. DOI: 10.1016/j.enconman.2022.116162.

[61] NREL. NREL Annual Technology Baseline. July 2022. URL: https://atb.nrel.gov/electricity/2022/offshore_wind.

[62] Suhas Nuggehalli Sampathkumar et al. “Degradation study of a reversible solid oxide cell (rSOC) short stack using distribution of relaxation times (DRT) analysis”. In: International Journal of Hydrogen Energy 47.18 (Feb. 2022), pp. 10175–10193. ISSN: 0360-3199. DOI: 10.1016/J.IJHYDENE.2022.01.104.

[63] Otto Machhammer. “Energiespeicherung un trasport”. In: Chem. Ing. Tech 93.4 (2021), pp. 1–12.

[64] Alessandra Perna et al. “Designing and analyzing an electric energy storage system based on reversible solid oxide cells”. In: Energy Conversion and Management 159 (Mar. 2018), pp. 381–395. ISSN: 01968904. DOI: 10.1016/j.enconman.2017.12.082.

[65] Ro. Peters et al. “Long-Term Experience with a 5/15kW-Class Reversible Solid Oxide Cell System”. In: Journal of The Electrochemical Society 168.1 (Jan. 2021), p. 014508. ISSN: 0013-4651. DOI: 10.1149/1945-7111/abdc79.

[66] Roland Peters et al. “Efficiency analysis of a hydrogen-fueled solid oxide fuel cell system with anode off-gas recirculation”. In: Journal of Power Sources 328 (Oct. 2016), pp. 105–113. ISSN: 03787753. DOI: 10.1016/j.jpowsour.2016.08.002.

[67] Pieter Bots. Personal Communications. Apr. 2023.

[68] Oliver Posdziech et al. “System Development and Demonstration of Large-Scale High-Temperature Electrolysis”. In: ECS Transactions 91.1 (July 2019), pp. 2537–2546. ISSN: 1938-6737. DOI: 10.1149/09101.2537ecst.

[69] Bob Prinsen et al. Policy options offshore wind 2040 Final report Prepared for: Ministerie van Economische Zaken en Klimaat. Tech. rep. 2022.

[70] PWC. Green Hydrogen Costs. June 2023. URL: https://www.pwc.com/gx/en/industries/energy-utilities-resources/future-energy/green-hydrogen-cost.html.

[71] Ruomei Qi et al. “Two-stage stochastic programming-based capacity optimization for a high-temperature electrolysis system considering dynamic operation strategies”. In: Journal of Energy Storage 40 (Aug. 2021). ISSN: 2352152X. DOI: 10.1016/j.est.2021.102733.

[72] Ahmadreza Rahbari et al. “Solubility of water in hydrogen at high pressures: A molecular simulation study”. In: Journal of Chemical and Engineering Data 64.9 (Sept. 2019), pp. 4103–4115. ISSN: 15205134. DOI: 10.1021/acs.jced.9b00513.

[73] Renewable Ninja. Winddata: Renewables Ninja. May 2023. URL: https://renewables.ninja/.

[74] Evan P. Reznicek et al. “Reversible solid oxide cell systems for integration with natural gas pipeline and carbon capture infrastructure for grid energy management”. In: Applied Energy 259 (Feb. 2020). ISSN: 03062619. DOI: 10.1016/j.apenergy.2019.114118.

[75] Marvin M. Rokni. “Power to hydrogen through polygeneration systems based on solid oxide cell systems”. In: Energies 12.24 (Dec. 2019). ISSN: 19961073. DOI: 10.3390/en12244793.

[76] Paul Rudenko. Personal Communications. Amsterdam, Apr. 2023.

[77] Tyler H. Ruggles et al. “Opportunities for flexible electricity loads such as hydrogen production from curtailed generation”. In: Advances in Applied Energy 3 (Aug. 2021). ISSN: 26667924. DOI: 10.1016/j.adapen.2021.100051.

[78] RVO. Plans 2030-2050. May 2023. URL: https://english.rvo.nl/information/offshore-wind-energy/offshore-wind-energy-plans-2030-2050#:~:text=In%202022%2C%20the%20Government%20raised,of%20our%20current%20electricity%20consumption..

[79] Srikanth Santhanam. Personal Communication. Amsterdam, Mar. 2023.

[80] Leonard Savage. The Foundations of Statistics. New York: Wiley, 1954.

[81] Roberto Scataglini et al. A Total Cost of Ownership Model for Solid Oxide Fuel Cells in Combined Heat and Power and Power-Only Applications. Tech. rep. 2015.

[82] O. Schmidt et al. “Future cost and performance of water electrolysis: An expert elicitation study”. In: International Journal of Hydrogen Energy 42.52 (Dec. 2017), pp. 30470–30492. ISSN: 03603199. DOI: 10.1016/j.ijhydene.2017.10.045.

[83] Shell. Internal shell report on SOEC and SOFC. Tech. rep. Amsterdam: Shell, Dec. 2022.

[84] Tennet. “Balanceringsmarkten”. In: (Feb. 2023). URL: https://www.tennet.eu/nl/balanceringsmarkten.

[85] Tennet. BalansdeltaPrices. May 2023. URL: https://www.tennet.org/bedrijfsvoering/ExporteerData.aspx?exporttype=BalansdeltaPrices.

[86] Tennet. Electricity market insights. Tech. rep. Tennet, Apr. 2022.

[87] Tennet. "TenneT expects further increase in transmission tariffs in 2024". In: (). URL: https://www.tennet.eu/news/tennet-expects-further-increase-transmission-tariffs-2024.

[88] Marius Tomberg et al. "Operation strategies for a flexible megawatt scale electrolysis system for synthesis gas and hydrogen production with direct air capture of carbon dioxide". In: Sustainable Energy and Fuels 7.2 (Dec. 2022), pp. 471–484. ISSN: 23984902. DOI: 10.1039/d2se01473d.

[89] Trading Ecnomics. EU Natural Gas. May 2023. URL: https://tradingeconomics.com/commodity/eu-natural-gas.

[90] A. A. Trendewicz et al. "Techno-economic analysis of solid oxide fuel cell-based combined heat and power systems for biogas utilization at wastewater treatment facilities". In: Journal of Power Sources 233 (2013), pp. 380–393. ISSN: 03787753. DOI: 10.1016/j.jpowsour.2013.01.017.

[91] Tennet Tso. 2030). Tech. rep. 2025, p. 2022. URL: www.tennet.eu.

[92] Ligang Wang et al. "Reversible solid-oxide cell stack based power-to-x-to-power systems: Comparison of thermodynamic performance". In: Applied Energy 275 (Oct. 2020). ISSN: 03062619. DOI: 10.1016/j.apenergy.2020.115330.

[93] Christopher H. Wendel et al. "Design and techno-economic analysis of high efficiency reversible solid oxide cell systems for distributed energy storage". In: Applied Energy 172 (June 2016), pp. 118–131. ISSN: 03062619. DOI: 10.1016/j.apenergy.2016.03.054.

[94] Christopher H. Wendel et al. "Modeling and experimental performance of an intermediate temperature reversible solid oxide cell for high-efficiency, distributed-scale electrical energy storage". In: Journal of Power Sources 283 (June 2015), pp. 329–342. ISSN: 0378-7753. DOI: 10.1016/J.JPOWSOUR.2015.02.113.

[95] Yahoo Finance. Dutch TTF Natural Gas Calendar. May 2023. URL: https://finance.yahoo.com/quote/TTF%3DF/history?period1=1640995200&period2=1672444800&interval=1d&filter=history&frequency=1d&includeAdjustedClose=true.

[96] Yanmei Yang et al. "Comparison of Hydrogen Specification in National Standards for China". In: E3S Web of Conferences. Vol. 118. EDP Sciences, Oct. 2019. DOI: 10.1051/e3sconf/201911803042.

[97] Xiaoyu Zhang et al. "Improved durability of SOEC stacks for high temperature electrolysis". In: International Journal of Hydrogen Energy 38.1 (Jan. 2013), pp. 20–28. ISSN: 0360-3199. DOI: 10.1016/J.IJHYDENE.2012.09.176.

[98] Yumeng Zhang et al. "Reversible solid-oxide cell stack based power-to-x-to-power systems: Economic potential evaluated via plant capital-cost target". In: Applied Energy 290 (May 2021). ISSN: 03062619. DOI: 10.1016/j.apenergy.2021.116700.